# Upper Air Studies in the El Paso-Juarez Airshed

Grant Number: 582-20-11967

Rosa Fitzgerald[1], Nakul Karle[1,2], Suhail Mahmud[3], Dave Sullivan[4] and William Stockwell[1]

[1]Department of Physics, The University of Texas at El Paso (UTEP)

[2]Environmental Science and Engineering, UTEP

[3]Computational Sciences, UTEP

[4]UT Austin

Final Report prepared for the Texas Commission on Environmental Quality (TCEQ)

August 2021

**Summary**

The Planetary Boundary Layer (PBL) is the lowest one or two kilometers of the troposphere. The temperature of PBL is most strongly affected during the daylight hours by solar insolation and during the night by radiative cooling. Winds within the PBL are affected by friction with the Earth's surface. Solar insolation, radiative cooling and surface winds strongly affect the top of the planetary boundary layer, also known as the PBL height (PBLH). The volume available for pollutant dispersion and mixing (mixing boundary layer height MBLH) is directly related to PBLH. PBLH and MBLH are closely related, but not identical, because pollutant mixing might or might not extend throughout the PBL. Since the majority of pollutants are trapped within the PBL, extensive and accurate measurements of the PBLH can assist in improving air quality model simulations and their forecasting applications. In this project, backscattering aerosol profiles from the ceilometer located at the University of Texas at El Paso (UTEP) campus were used to obtain PBLHs for different seasons of the year. This data was processed using Vaisala's proprietary software BL-view and a regional database was created on a server hosted by UTEP. The experimental PBLH was compared with the modeled PBLH obtained from the trajectory model HYSPLIT. Data from the years 2015-17 was processed and analyzed extensively throughout this study. The results summarized in this report include the diurnal pattern of the PBL and its seasonal structure for this region, intercomparisons between the modeled and experimental PBLH and PBL analysis during the selected high and low ozone events.

In addition, in this report the upper air data from the Texas Commission on Environmental Quality's (TCEQ) radar wind profiler in Socorro, TX has been characterized by season, time of day, ozone levels, and altitude.

## Table of Contents

## List of Tables

## List of Figures

## Chapter 1: Introduction

Human health is adversely affected by pollutants such as ozone and particulate matter. There are two common classifications of particulate matter, $PM_{2.5}$ and $PM_{10}$, where $PM_{2.5}$ is particulate matter with an aerodynamic diameter of 2.5 μm or less and $PM_{10}$ is particulate matter with an aerodynamic diameter of 10 μm or less [1]. High ozone and particulate matter concentrations affect many major metropolitan cities in the United States, and the El Paso–Juarez airshed is one example. El Paso is a city in the far west corner of Texas, separated only by the Rio Grande River from the Mexican city of Juarez, Mexico. Juarez is one of the most populous cities in the Mexican state of Chihuahua and is surrounded by the Chihuahua desert. Both cities share the same airshed known as the El Paso–Juarez airshed, and both have a history of violating ground-level ozone air quality standards. El Paso has a very dry climate that is typical of the southwestern U.S. urban regions. El Paso's air quality problem is known to be partially due to emissions from regional industrial activities and from motor vehicles caught in prolonged traffic congestion as they cross the international bridges between the United States and Mexico [2]–[5]. In addition, the geopolitical region of El Paso–Juarez exhibits exceptional meteorological conditions [5], such as higher planetary boundary layer heights (PBLHs), than any other Texas city, influenced by the local terrain.

Accurate weather and air quality forecasting rely on the correct knowledge of PBLHs. Natural and manmade emissions are mixed during the daytime due to strong turbulence caused by atmospheric instability. A stable boundary layer (SBL), on the other hand, can cause emissions to collect and grow in concentration near the Earth's surface. Because of the resulting high pollution concentrations, vulnerable groups in the local community may become ill and possibly die.

Pollutants emitted within the PBL at ground level and near the ground have a significant impact on society and the environment.

The goal of this project is to analyze the PBLH for the El Paso-Juarez region comprehensively and study its seasonal diurnal pattern. While studying the seasonal patterns, the PBLHs obtained using the ceilometer backscatter profiles are to be compared with the PBLHs calculated by the HYSPLIT model. This experimental-model PBLH intercomparison will provide a greater understanding of the PBLH structure for this region and help in improving future air quality model simulations.

### 1.1 Planetary Boundary Layer

The Planetary Boundary Layer (PBL) is the lowest part of the troposphere which is directly influenced by the Earth's surface. It is the only part of the atmosphere where frictional forces, affecting surface winds, play an essential role and where the temperature exhibits a diurnal cycle due to daytime solar insolation and nighttime radiative cooling [6]. The mixing layer height is an essential quantity in modeling air pollution and its transport since it determines the adequate volume in which pollutants are mixed and dispersed [7], [8]. If the surface emissions are consistent, ozone concentrations do respond to the changes in the PBL height (PBLH) depending on the volume available for mixing (mixing boundary layer height, MBLH) and dispersion. Many of the chemical reactions that produce ozone are concentration dependent. Emission concentrations decrease as mixing heights increase and this reduces many reaction rates. Furthermore, ozone from the previous day can remain in the residual layer and it can be entrained when the convective boundary layer starts rising the following day, depending on the concentration within the PBL. The relationship between the PBLH and ozone is complicated and has not been studied in this region before us. Since ozone episodes are frequent during the summer, continuous monitoring of

the PBLH, especially in a region like the El Paso-Juarez, can provide relevant, necessary, information for a comprehensive regional air-quality assessment [9], [10].

Diurnal variations refer to changes in the planetary boundary layer that occur during a day-nighttime period. When the Earth's surface is heated by solar insolation, warm air rise thermals from the surface raising the PBLH. Radiative cooling from the surface during the nighttime along with radiative cooling from clouds at the top of the planetary boundary layer create cool air thermals that fall downwards. Horizontal winds affect also the rise and fall of the PBLH. When winds shear over the top of a convective boundary layer, turbulence is created. All of these phenomena affect the formation of the PBL component layers.

### 1.2 DIFFERENT LAYERS OF THE PBL

The PBL can be categorized into three main layers based on surface heating and cooling: the convective boundary layer (CBL), the nocturnal boundary layer (NBL), and the residual layer (R.L.). The convective boundary layer develops during the daytime when surface heating following sunrise produces convection. Maximum turbulence is observed during the daytime in CBL; this layer is also called the mixing boundary layer (MBL) with a mixing boundary layer height (MBLH). MBLH are higher on days with strong convection. On days with strong convection emissions enter greater volumes, therefore their concentrations are lower. Dispersion will be greater across a region on these days too. However, the production of secondary pollutants such as ozone may be more ‘efficient’ when NOx concentrations are lower. (Ozone production is highly non-linear, analogous to the human body and losing weight. When a person tries to diet, their body uses food more efficiently and weight loss becomes more difficult. Reduction in NOx and ozone concentrations are similar).

A persistent layer of air forms at night when there is a temperature inversion due to radiative cooling from a surface's infrared radiation. Pollutants tend to accumulate in layers near the Earth's surface at night when no strong breezes are blowing. This occurs when solar heating creates unstable convective conditions in the morning and afternoon that cause the CBL to form the next day, after dawn. In the daytime, the CBL tends to be turbulent, with an entrainment zone on top of it. Because of insufficient solar heating on overcast days, the nighttime boundary layer might remain during the day, resulting in poor air quality. The R.L. is the layer which is disconnected during the transition from daytime CBL to the development of the NBL. Sometimes this is known as "carryover".

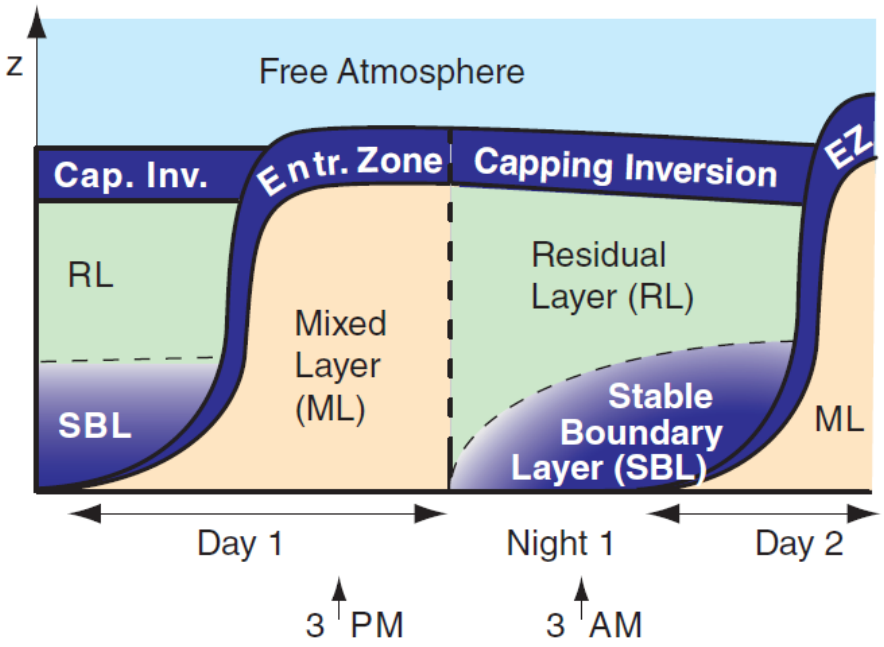


Figure 1. A typical boundary layer structure over the day clear day. The figure is taken from [11], page no. 692

# Chapter 2: Methodology

This research study involved calculation of the PBLH using aerosol backscatter profile from a ceilometer and the HYSPLIT model.

## 2.1 CEILOMETER

The Vaisala ceilometer CL31 is an eye-safe single-lens mini-lidar system, used to detect cloud base heights and vertical visibility by continuously monitoring the aerosol backscatter profiles at a wavelength of 910 nm. These profiles can also be used for determining the convective mixing layer height (MLH) [12]. The laser is an InGaAs MOCVD diode with a pulse frequency of 10 kHz, and the measurement range is from 0 - 7.7 km. The typical uncertainty of the attenuation of the backscatter coefficient for ~ 30 mins average duration is ± 20% and the changeover aerosol backscattering MLH determination for ~ 30 mins is ± 200 m [13]. A ceilometer CL31 located at the UTEP campus has been used to estimate the aerosol MLH, that which can be used as a proxy of PBLH [14], [15]. It performs well even in situations such as dust storms, and shallow nocturnal layers. The UTEP instrument has been operational and collecting data since 2015. Details of the instrument and its functionality can be found in [12].

### 2.1.1 Ceilometer PBLH calculation

A ceilometer emits brief, strong laser pulses that travel in a vertical or near-vertical direction. Backscatter is the reflection of the laser pulses generated by haze, fog, mist, virga, precipitation, aerosols, and clouds. The backscatter profile, or the signal intensity as a function of height, is saved and analyzed, and the data is used to determine cloud bases and the structure of the planetary boundary layer.

The quantity of backscattered light is identified using configurable temporal and range resolutions. Our instrument is set to the standard ceilometer operational resolution of 15 s and 10 m for a single vertical profile capture, which allows measurements of heights up to 7.5 km but we restricted our instrument to a range of 4 km above the ground level as the PBLHs over the study area are mostly within this height range.

Vaisala's electronic-noise reduction function is applied to all raw aerosol backscatter intensity profile data. Absorption and multiple scattering are not considered. For CL31, Vaisala defines a 250-m overlap between the whole field of vision of the signal's receiver and the diverging laser beam [12, 16].

Backscatter signals are generally stronger in the planetary boundary layer, where particle concentrations are higher, and weaker than in the open atmosphere, where particles are normally lower. The backscatter gradient between the planetary boundary layer and the open atmosphere (the mixing height) is detected by BL-View (a proprietary software of Vaisala). The software can identify other atmospheric structures that may create significant backscatter gradients such as residual boundary layers and high smoke or aerosol plumes. BL-View conducts vertical and temporal averaging of ceilometer data to minimize susceptibility to noise and transitory features in atmospheric structure.

### 2.2 Hybrid Single Particle Lagrangian Integrated Trajectory Model (HYSPLIT)

WRF and HYSPLIT version 4 were used to calculate PBLH [30]. The HYSPLIT model is a widely used trajectory model consisting of routines that calculate pollutant transport and dispersion taking place within a well-mixed PBLH. HYSPLIT uses potential temperature data to find the height of the inversion and its potential temperature. In HYSPLIT the PBLH is the altitude above the inversion height where the potential temperature exceeds the initial inversion

temperature by 2 Kelvin. The National Centers for Environmental Prediction's (NCEP) archive meteorological files with EDAS (Eta Data Assimilation System). The meteorological files have a spatial resolution of 40 km and a time resolution of 3-hour. These were used as the meteorological data input for the modeling [31]. UTEP was chosen as the source location, and the hourly PBLH values were obtained together with the trajectory.

### 2.3 Regional Ceilometer Database

Attenuated backscatter profile raw data was recorded by the instrument for every 16 s and saved in the form of a .DAT file. Vaisala Cloud View or CL-view was the default software used for the raw data collection. It was configured to produce a raw data file every 6 hours during a day. So, a total of 4 raw .DAT files consisting of the aerosol backscattering profiles were generated in a day. All the data throughout this project is recorded in UTC. BL-view was used comprehensively to process these raw datasets and the output provided us the PBLH values along with the 24-hour duration of backscatter intensity profile graphs. After all the processing, the raw data files along with the processed PBL files were saved on a local data server maintained by UTEP. User credentials to this server was provided to the TCEQ agency for data retrieval.

## Chapter 3: Statistical Tests

Statistical analysis is the method that identifies patterns or differences in data sets. There are mainly two types of analysis available: descriptive statistics that deal with summarizing the data from a sample using indexes such as mean or standard deviation and inferential statistics that deal with probability. In this study, we conduct descriptive statistics and exploratory data analysis for PBLH.

### PERFORMANCE, ANALYSIS AND ERROR CALCULATION:

Different tests to evaluate the performance and resemblance between HYSPLIT and the ceilometer have been computed. Among those tests, Pearson Correlation Coefficient, Refined Index of Agreement of model performance, mean absolute error, Root mean square error, and P-values are calculated to compare the performance.

Alongside with these tests, several statistical measurements were computed and compared such as mean, median, standard deviation, skewness, kurtosis, and maximum/minimum values. All the units are in meters. The statistical measurements are defined in the Appendix.

For visualization, we have used diurnal cycle plots, Box plots and linear regression plots to show the relation between the ceilometer and HYSPLIT PBLH values. In the regression plots, we take ceilometer value as an independent variable and HYSPLIT as a dependent variable with confidence bounds. Box plots are used for finding the maximum, minimum and the mean values along with outlier values. We set up the outlier values as (Q1-1.5*IQR) or (Q3+1.5*IQR) where IQR stand for interquartile range and Q1 and Q3 are first quartile and third quartile respectively.

A box or whiskers plot is a convenient visual representation of the data distribution in terms of its quartiles, medians, and outlier points. The "whiskers," are the parallel lines extending from the boxes or the candles, which illustrate variability outside the top and lower quartiles. Individual

dots in line with whiskers are occasionally used to represent outliers. Box plots can be drawn horizontally or vertically depending on the dataset. Although Box Plots appear rudimentary when compared to a Histogram or Density Plot, they have the advantage of taking up less space, which is beneficial for comparing distributions across several groups or datasets.

**YEAR 2015**

**April 2015:**

Table 1: Descriptive Statistical tests for the April 2015 data retrieved from UTEP location

| | Tests | Ceilometer | HYSPLIT |
|---|---|---|---|
| **Month: April 2015**<br>**Location: UTEP**<br>**Lat and Lon: 31.76 N and -106.5 W** | Mean | 906.033 | 1011.7 |
| | Median | 700 | 601 |
| | Standard Deviation | 578.19 | 1028.1 |
| | Skewness | 0.81 | 0.81 |
| | Maximum | 2610 | 4262 |
| | Minimum | 175 | 28.4 |
| | Kurtosis | 2.62 | 2.49 |
| | Variance | 3.34e05 | 1.05e06 |

This table shows different statistical information derived using HYSPLIT and the ceilometer. Calculated statistics include Skewness and Kurtosis values, which are closer to each other, suggesting the datasets are distributed similarly. The mean PBLH during the spring season is around 1000 meters, and the median is around 700 meters.

Table 2: Performance and Error calculation tests for the April 2015 using UTEP data

| Test | Values |
|---|---|
| Correlation Coefficient (Pearson) | 0.70 |
| Index of Agreement | 0.69 |
| Mean Absolute Error | 543.45 |
| RMSE | 748.45 |

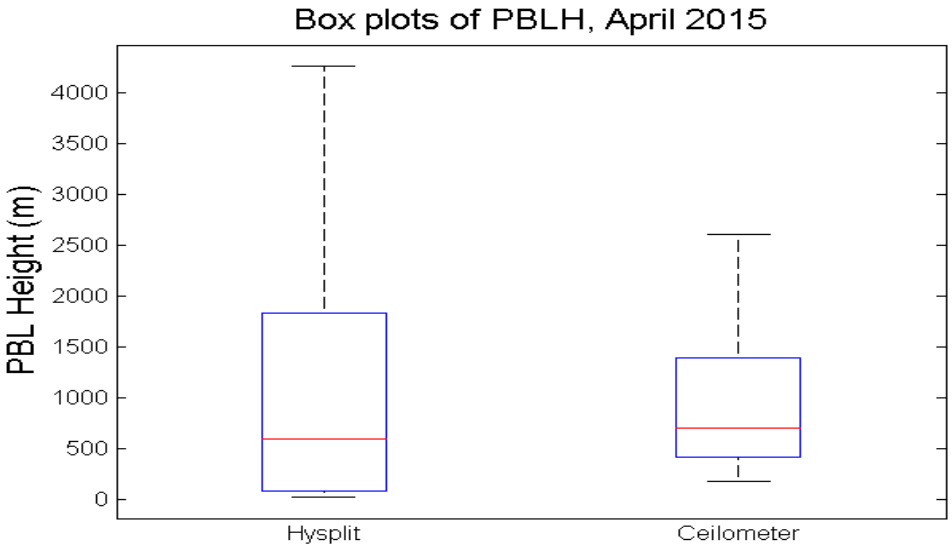


(a)

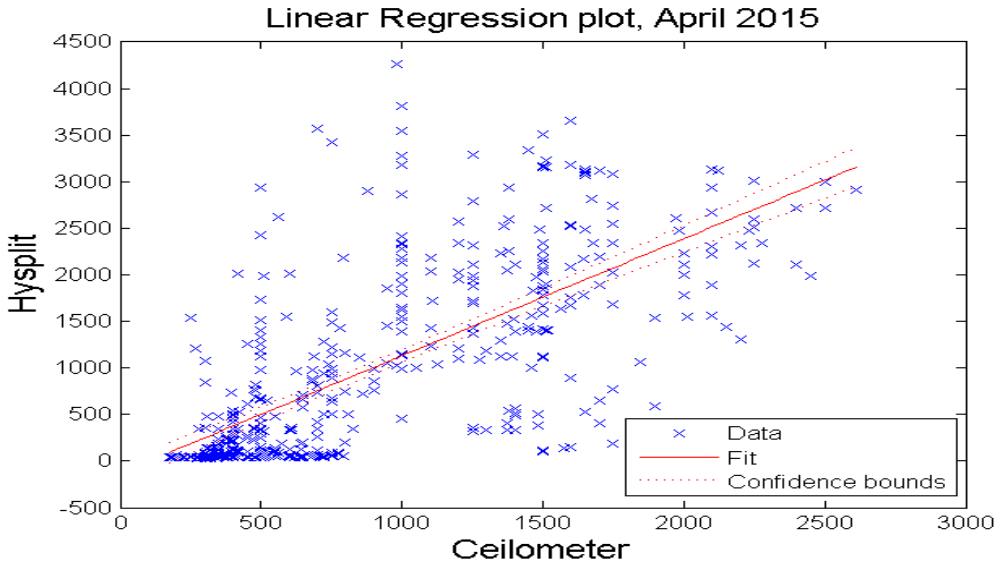

(b)

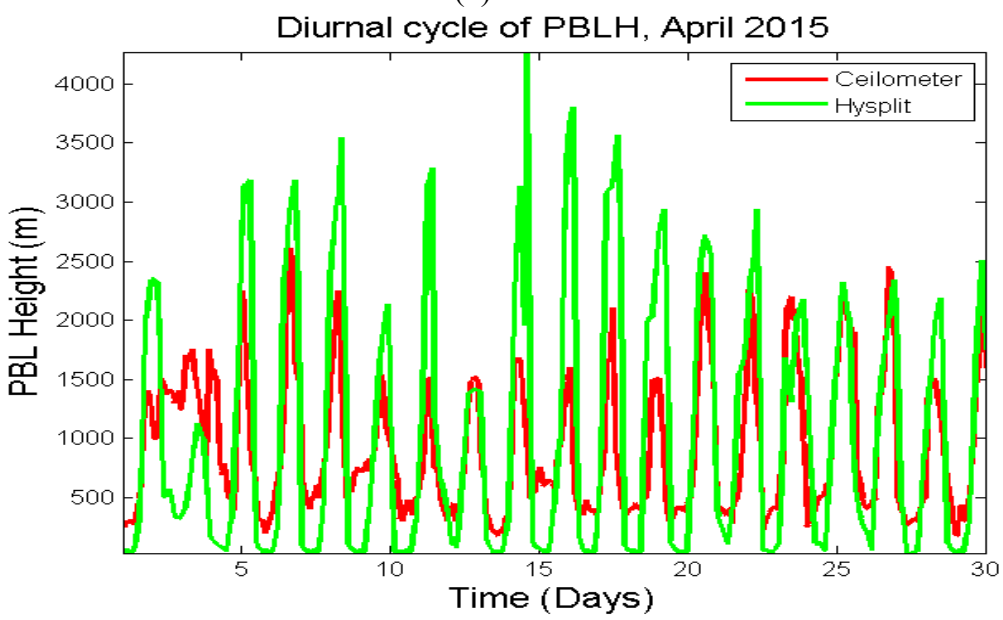


(c)

Figure 2. The statistics of the PBLH diurnal cycles over UTEP location: (a) Box plots of the data showing outliers for HYSPLIT; (b) Linear regression plots; (c) Diurnal cycle of the PBLH values throughout the month of April 2015.

Reasonable agreement was observed between the experimental and modeled PBLH with medians of both the datasets as seen in Figure 1 (a) are close to each other. The lower quartile of the ceilometer measured PBLH dataset mostly represents the nocturnal boundary layer values. The nocturnal boundary layer was observed to be in the range of 250 m or lower. Nighttime PBL recorded by the model was way too low. The height of the PBL (convective boundary layer) recorded throughout the day is marked by the upper quartile of the box. The ceilometer dataset box is a subset of the HYSPLIT obtained PBLH box. Nighttime PBL recorded by the model is on the lower side throughout the season. However, the overall correlation coefficient is 0.70 along with the index of agreement showing reasonable agreement between the two datasets.

**June 2015:**

Table 3: Descriptive Statistical tests for the June 2015 data retrieved from UTEP location.

| | Tests | Ceilometer | HYSPLIT |
|---|---|---|---|
| **Month: June 2015**<br><br>**Location: UTEP**<br><br>**Lat and Lon: 31.76 N and -106.5 W** | Mean | 832.08 | 1185.9 |
| | Median | 680 | 775.48 |
| | Standard Deviation | 491.24 | 1152.4 |
| | Skewness | 0.9591 | 0.7275 |
| | Maximum | 3000 | 4037.4 |
| | Minimum | 85 | 44.85 |
| | Kurtosis | 3.49 | 2.27 |
| | Variance | 2.417e05 | 1.328e06 |

The mean or average values of the PBLH using Ceilometer and HYSPLIT is around 900 and 1200 meters which is very common in a month of summer season. The median values are also close to each other.

Table 4: Performance and Error calculation tests for the June, 2015 using UTEP data

| **Test** | **Values** |
|---|---|
| Correlation Coefficient (Pearson) | 0.60 |
| Index of Agreement | 0.49 |
| Mean Absolute Error | 865.4 |
| RMSE | 458.7 |

The mean absolute error is somewhere around 900 meters, and the root mean square error is somewhere around 500 meters between those values.

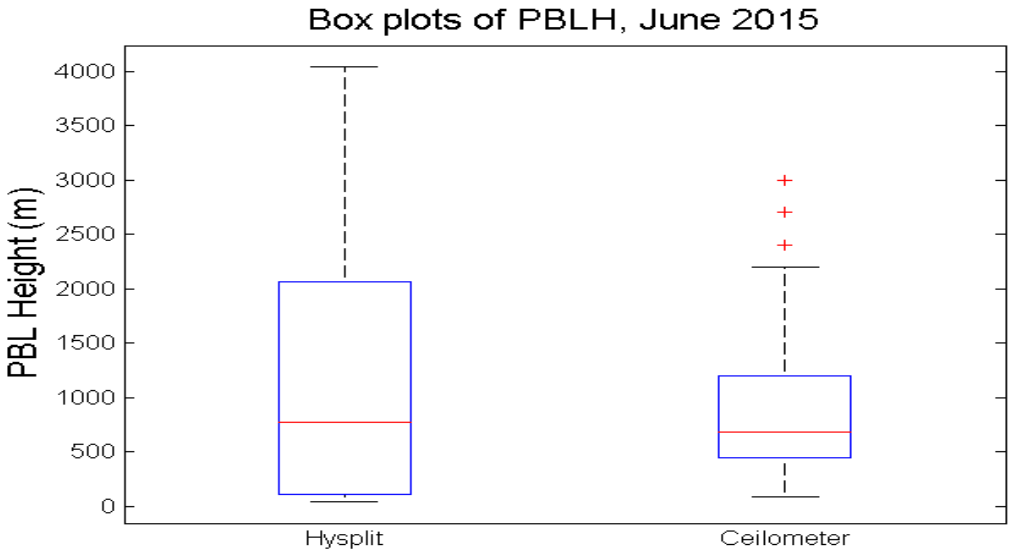
Box plots of PBLH, June 2015
PBL Height (m)
4000
3500
3000
2500
2000
1500
1000
500
0
Hysplit
Ceilometer

(a)

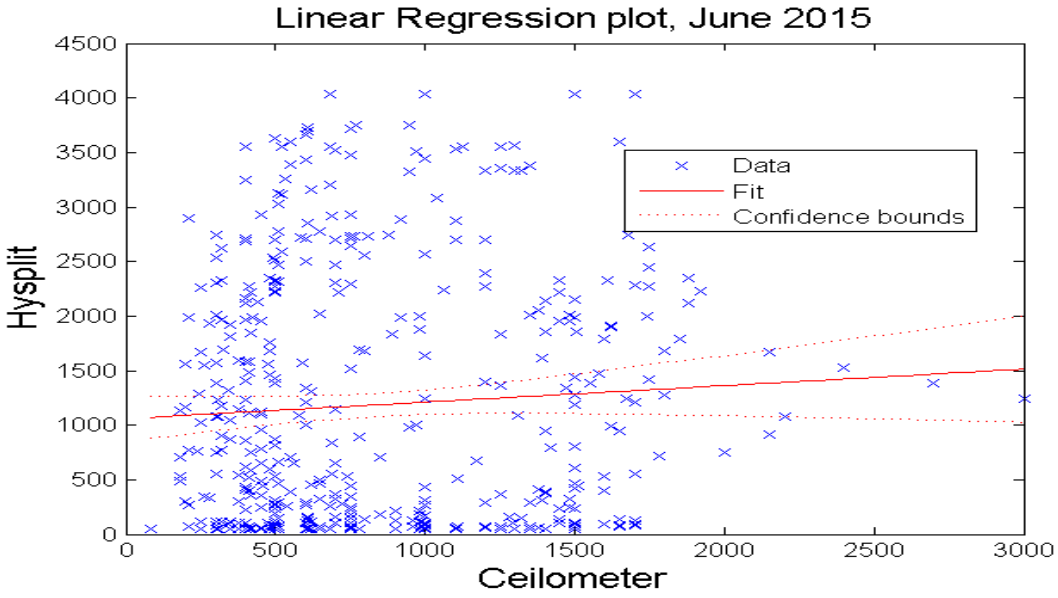
Linear Regression plot, June 2015
Hysplit
Ceilometer
Data
Fit
Confidence bounds
4500
4000
3500
3000
2500
2000
1500
1000
500
0
0
500
1000
1500
2000
2500
3000

(b)

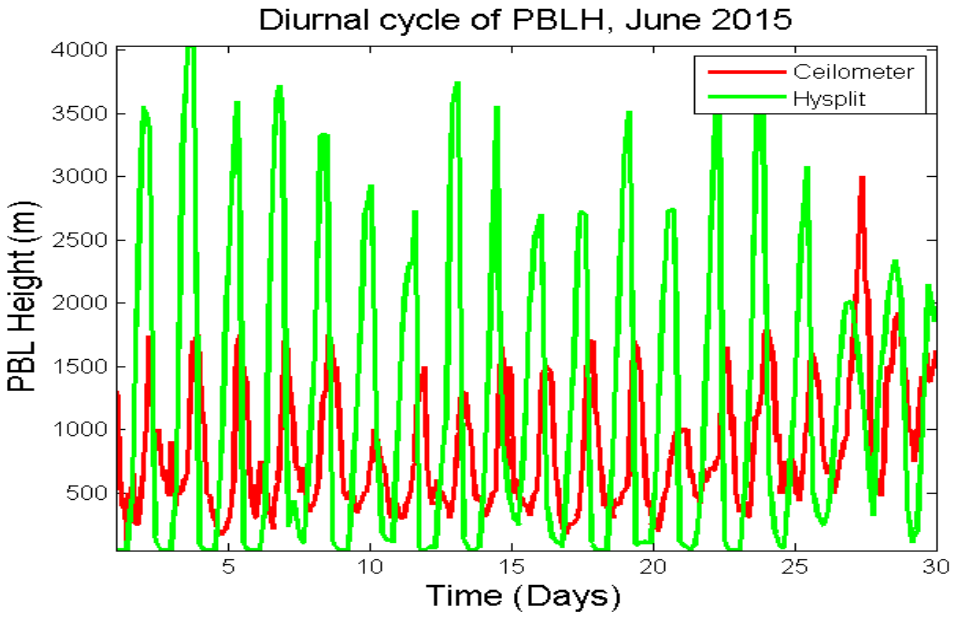


(c)

Figure 3. The statistics of the PBLH diurnal cycles over UTEP location: (a) Box plots of the data showing outliers for HYSPLIT; (b) Linear regression plots; (c) Diurnal cycle of the PBLH values throughout the month of June 2015.

The median of both the model and the experimental PBLH are close to each other. The ceilometer consistently recorded a PBL on the lower end with the maximum experimental PBLH recorded during this month that was around 3 km. In contrast the model calculated PBLH was consistently above 2.5 km. The ceilometer PBLH diurnal pattern indicated a substantial increase of the PBLH by the end of the month. The nighttime PBL calculated by the model was much too low and theoretically impossible. The correlation coefficient between the two datasets for this month was low (0.60) and index of agreement even lower, indicating relatively poor agreement between the measurements and modeling.

**September 2015:**

Table 5: Descriptive Statistical tests for the September 2015 data retrieved from UTEP

| | Tests | Ceilometer | HYSPLIT |
|---|---|---|---|
| **Month: September 2015**<br><br>**Location: UTEP**<br><br>**Lat and Lon: 31.76 N and -106.5 W** | Mean | 652.40 | 938.54 |
| | Median | 500 | 545.35 |
| | Standard Deviation | 461.24 | 951.71 |
| | Skewness | 1.1835 | 0.9235 |
| | Maximum | 2300 | 3328 |
| | Minimum | 150 | 45.1 |
| | Kurtosis | 3.6121 | 2.7192 |
| | Variance | 9.057e05 | 2.12e05 |

Based on HYSPLIT and Ceilometer data, the maximum and minimum PBLH values are 3,328 and 2,300 meters. In both cases, skewness is flattering, so we are dealing with right-skewed data distribution.

Table 6: Performance and Error calculation tests for the September 2015 using UTEP data

| **Test** | **Values** |
|---|---|
| Correlation Coefficient (Pearson) | 0.77 |
| Index of Agreement | 0.68 |
| Mean Absolute Error | 505.21 |
| RMSE | 718.65 |

There is evidence of better agreement between the two sets of PBLH values when the index of agreement and Pearson correlation coefficient are closer to 0.8 and 0.7, respectively, according to this study.

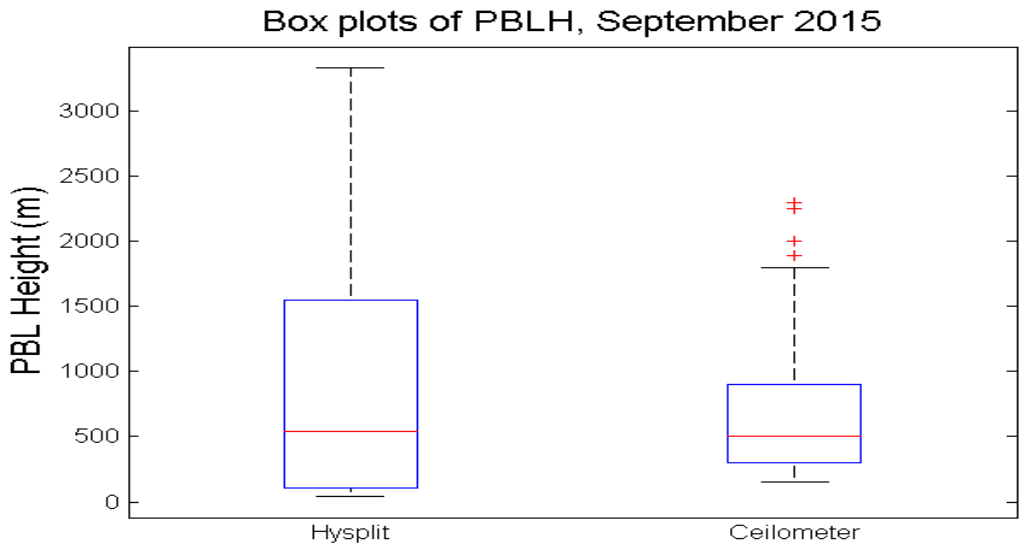
Box plots of PBLH, September 2015
PBL Height (m)
3000
2500
2000
1500
1000
500
0
Hysplit
Ceilometer

(a)

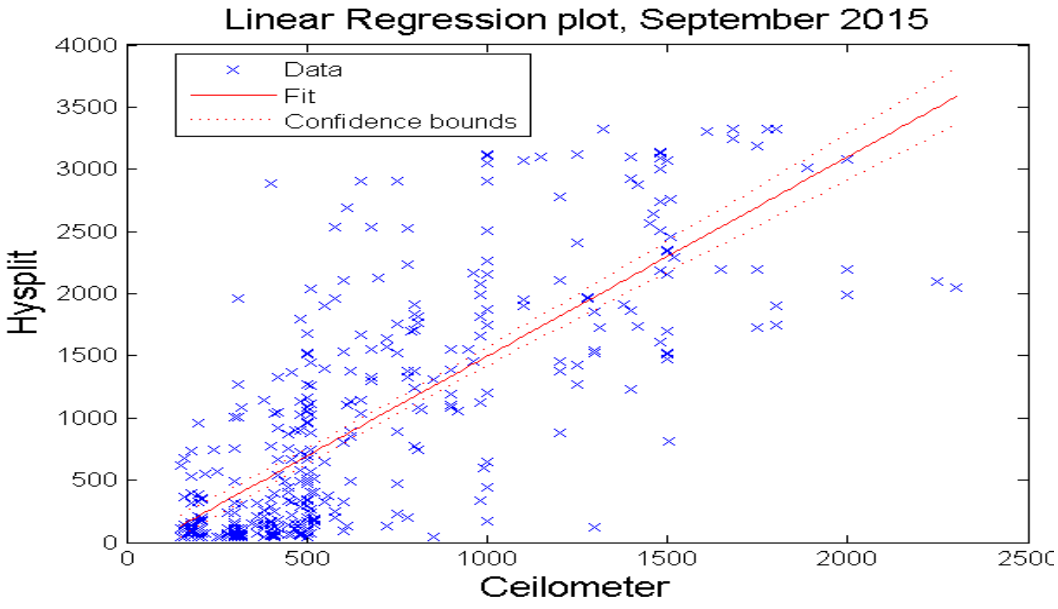
Linear Regression plot, September 2015
Data
Fit
Confidence bounds
Hysplit
4000
3500
3000
2500
2000
1500
1000
500
0
0
500
1000
1500
2000
Ceilometer

(b)

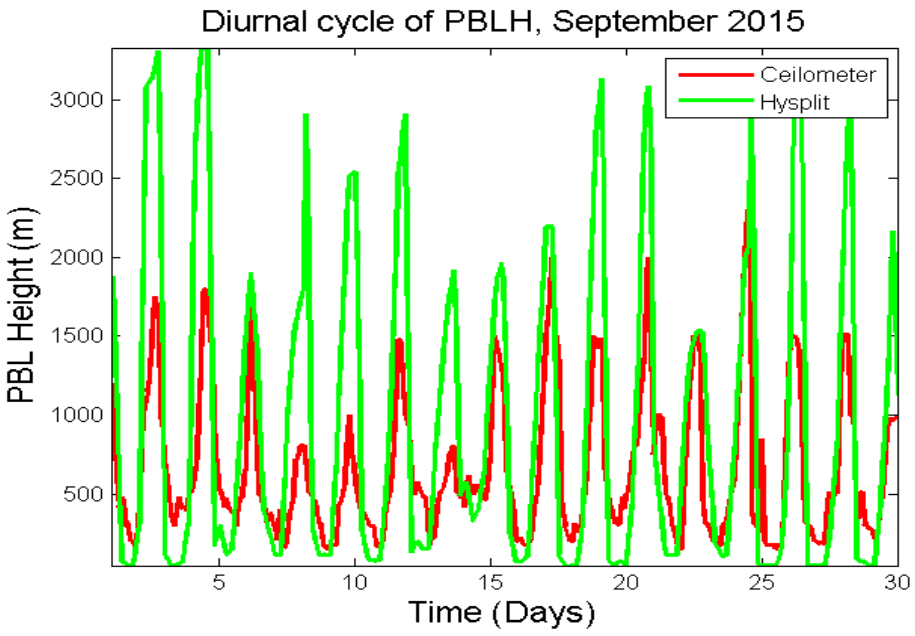


(c)

Figure 4. The statistics of the PBLH diurnal cycles over UTEP location: (a) Box plots of the data showing outliers for HYSPLIT; (b) Linear regression plots; (c) Diurnal cycle of the PBLH values throughout the month of September 2015.

The median of the experimental dataset is 500 m whereas the modeled PBLH median is slightly higher. There is a vast difference between the max PBLH recorded by the two methods. Max PBLH recorded by the ceilometer is 2300 ± 250 m whereas modeled PBLH is 3328 ± 250 m. The correlation coefficient comes out to be 0.72 which indicates a reasonable agreement between the two methods. Both the PBLH follows diurnal pattern with modeled PBLH overestimating during the daytime and underestimating at night.

**October 2015:**

Table 7: Descriptive Statistical tests for the October 2015 data retrieved from UTEP location.

| | Tests | Ceilometer | HYSPLIT |
|---|---|---|---|
| **Month: October 2015**<br>**Location: UTEP**<br>**Lat and Lon: 31.76 N and -106.5 W** | Mean | 659.04 | 660.08 |
| | Median | 550 | 404 |
| | Standard Deviation | 410.92 | 697.89 |
| | Skewness | 0.99 | 1.28 |
| | Maximum | 2290 | 3489 |
| | Minimum | 125 | 26.5 |
| | Kurtosis | 3.63 | 4.49 |
| | Variance | 1.68e05 | 4.97e05 |

In the El Paso-Juarez region, October belongs to the fall season, and the mean and median PBLH values are considerably lower than the summer month's PBLH.

Table 8: Performance and Error calculation tests for the October 2015 using UTEP data

| **Test** | **Values** |
|---|---|
| Correlation Coefficient (Pearson) | 0.72 |
| Index of Agreement | 0.69 |
| Mean Absolute Error | 352.90 |
| RMSE | 487.39 |

The correlation coefficient and the IOA values for this month are much closer to each other. In addition, the error rates are lower than in the summer months.

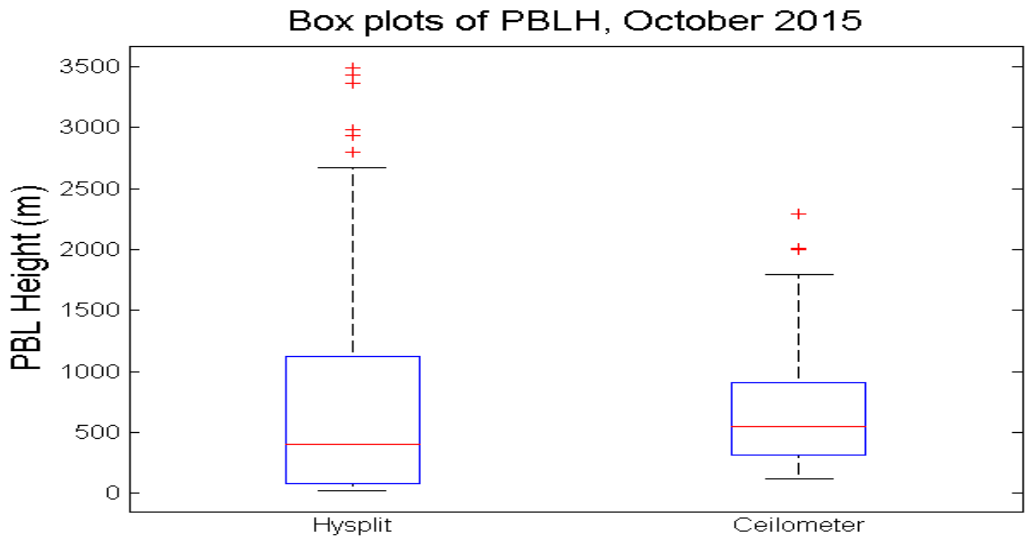
Box plots of PBLH, October 2015
PBL Height (m)
3500
3000
2500
2000
1500
1000
500
0
Hysplit
Ceilometer

(a)

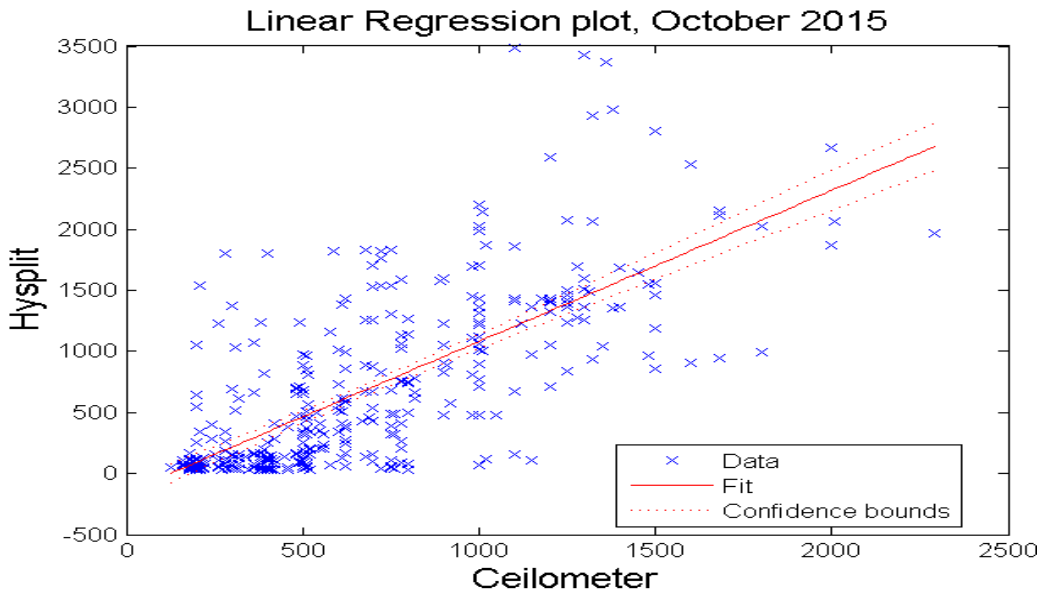
Linear Regression plot, October 2015
Hysplit
Ceilometer
3500
3000
2500
2000
1500
1000
500
0
-500
0
500
1000
1500
2000
2500
Data
Fit
Confidence bounds

(b)

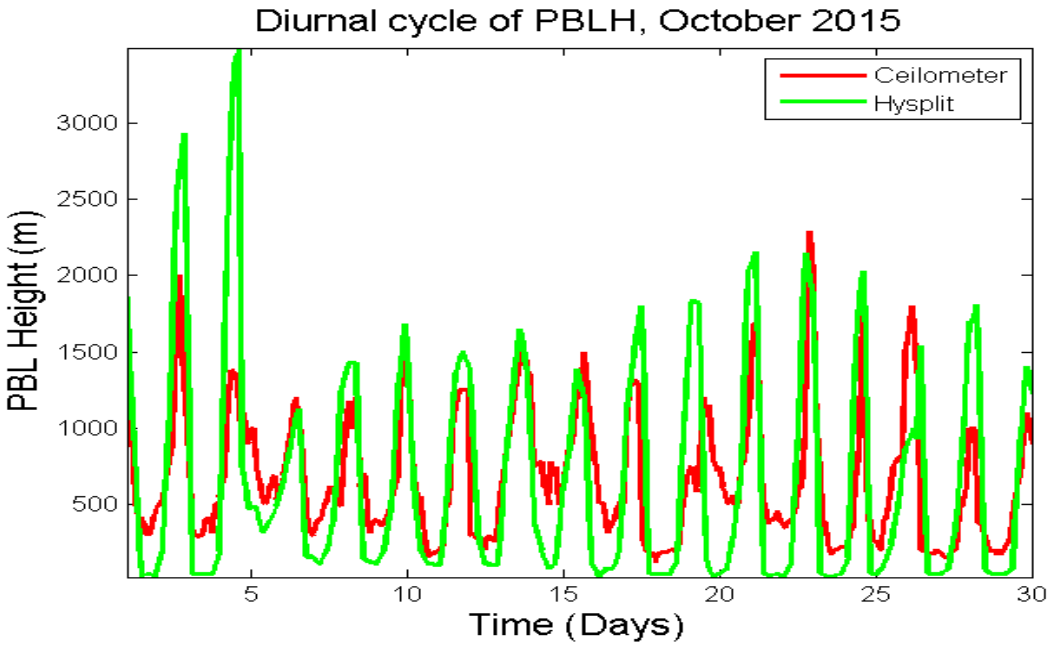


(c)

Figure 5. The statistics of the PBLH diurnal cycles over UTEP location: (a) Box plots of the data showing outliers for HYSPLIT; (b) Linear regression plots; (c) Diurnal cycle of the PBLH values throughout the month of October 2015.

**November 2015:**

Table 9: Descriptive Statistical tests for the November 2015 data retrieved from UTEP

| | Tests | Ceilometer | HYSPLIT |
|---|---|---|---|
| **Month: November 2015**<br><br>**Location: UTEP**<br><br>**Lat and Lon: 31.76 N and -106.5 W** | Mean | 519.73 | 329.12 |
| | Median | 385 | 208.9 |
| | Standard Deviation | 430.94 | 336.40 |
| | Skewness | 1.72 | 1.22 |
| | Maximum | 2000 | 1526 |
| | Minimum | 20 | 14.1 |
| | Kurtosis | 5.81 | 3.79 |
| | Variance | 1.85e05 | 1.13e05 |

The above table shows that the median and mean values of Ceilometer and HYSPLIT differed by around 200 meters. Skewness and Kurtosis, which show the symmetry of the datasets, are closer to each other.

Table 10: Performance and Error calculation tests for the November 2015 using UTEP data.

| Test | Values |
|---|---|
| Correlation Coefficient (Pearson) | 0.56 |
| Index of Agreement | 0.50 |
| Mean Absolute Error | 266.57 |
| RMSE | 414.92 |

The correlation coefficient and index of the agreement show a numerical value closer to 0.5, which indicates a mediocre resemblance between those data.

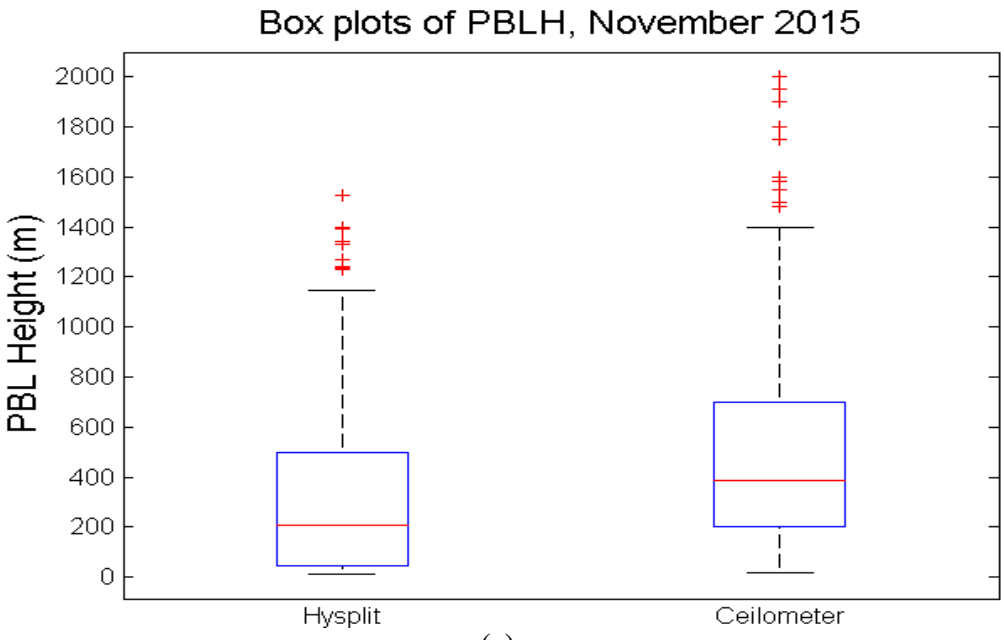


(a)

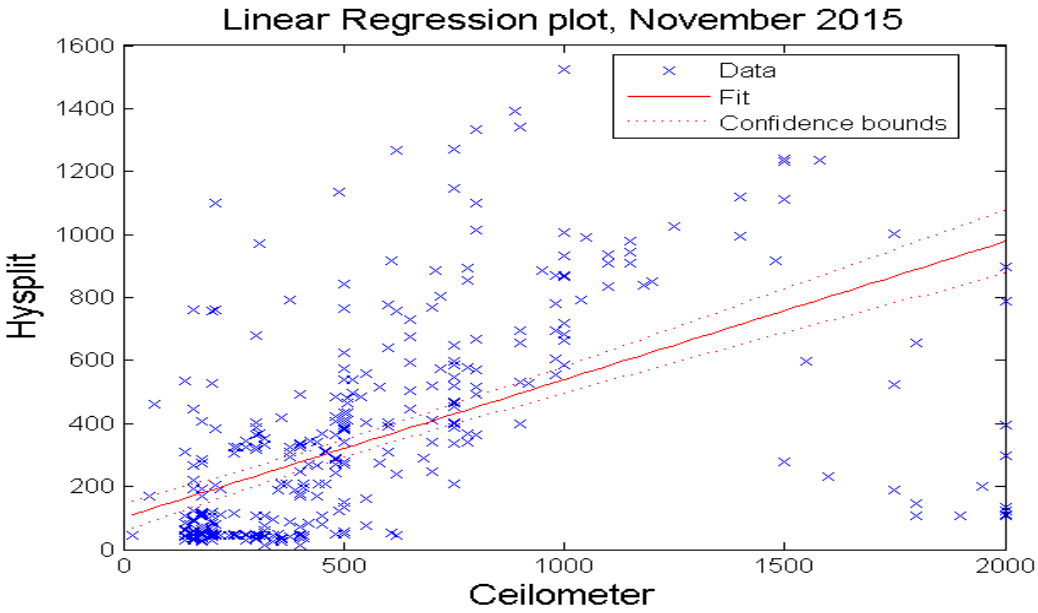


(b)

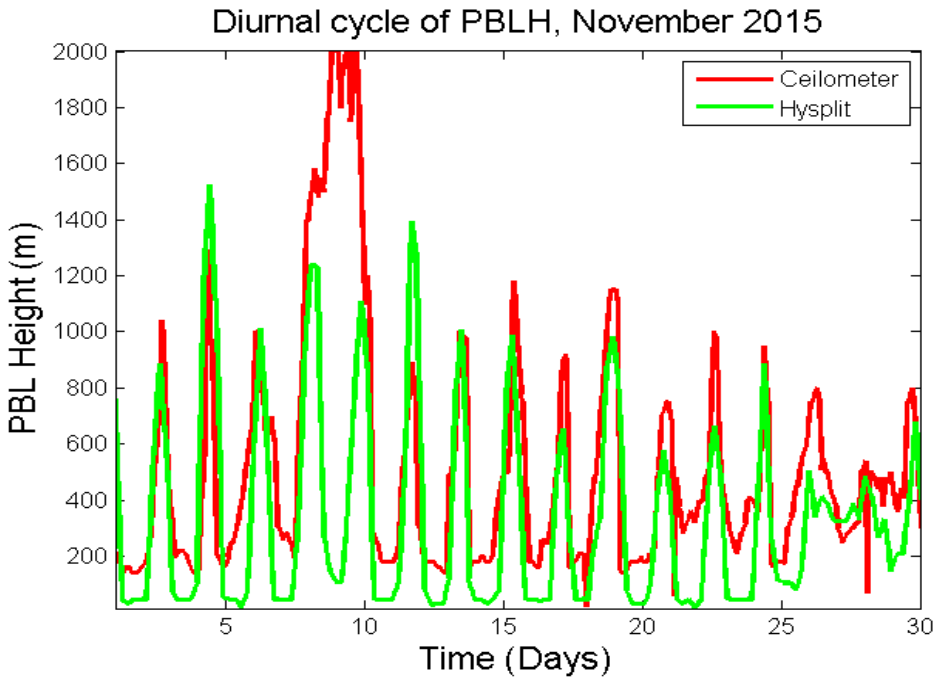


(c)

Figure 6. The statistics of the PBLH diurnal cycles over UTEP location: (a) Box plots of the data showing outliers for HYSPLIT; (b) Linear regression plots; (c) Diurnal cycle of the PBLH values throughout the month of November 2015.

**YEAR:2016**

**January 2016:**

Table 11: Descriptive Statistical tests for the January 2016 data retrieved from UTEP.

| | Tests | Ceilometer | HYSPLIT |
|---|---|---|---|
| **Month: January 2016**<br>**Location: UTEP**<br>**Lat and Lon : 31.76 N and -106.5 W** | Mean | 488.91 | 376.96 |
| | Median | 440 | 292 |
| | Standard Deviation | 290.96 | 361.33 |
| | Skewness | 0.87 | 1.05 |
| | Maximum | 1490 | 1668.03 |
| | Minimum | 120 | 11.5 |
| | Kurtosis | 3.3177 | 3.7138 |
| | Variance | 8.466e04 | 1.305e05 |

The above table shows that the median and mean values of ceilometer and HYSPLIT differed by about 100 meters. The maximum value is around 1500 meters for both cases which is a common maximum height in a winter month for this region.

Table 12: Performance and Error calculation tests for the January 2016 using UTEP data.

| **Test** | **Values** |
|---|---|
| Correlation Coefficient (Pearson) | 0.59 |
| Index of Agreement | 0.58 |
| Mean Absolute Error | 249.17 |
| RMSE | 320.17 |

Mean absolute error and root mean square error are 250 and 350 meters between the ceilometer and HYSPLIT ceilometer.

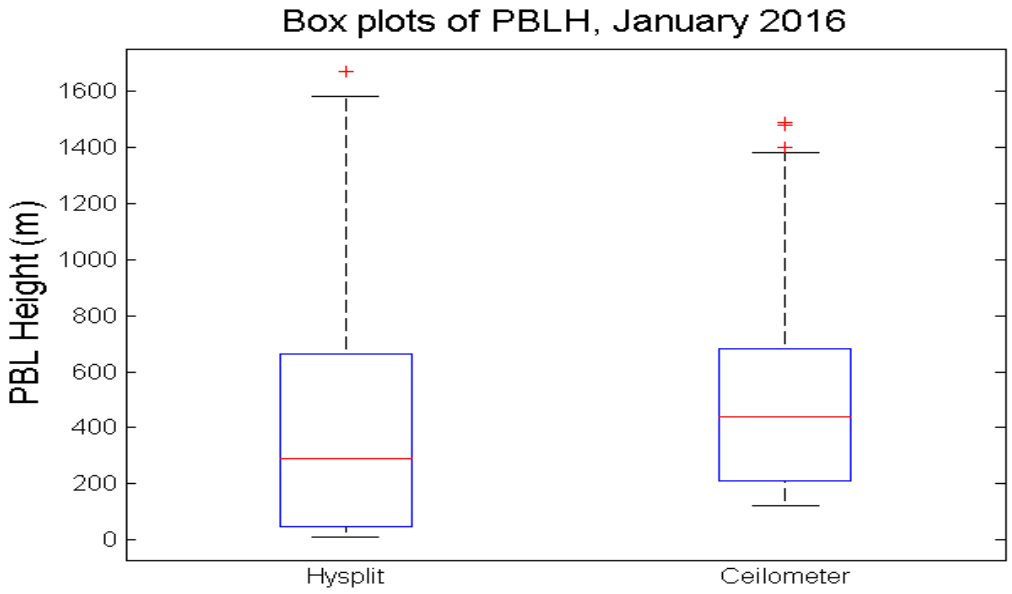
Box plots of PBLH, January 2016
PBL Height (m)
1600
1400
1200
1000
800
600
400
200
0
Hysplit
Ceilometer

(a)

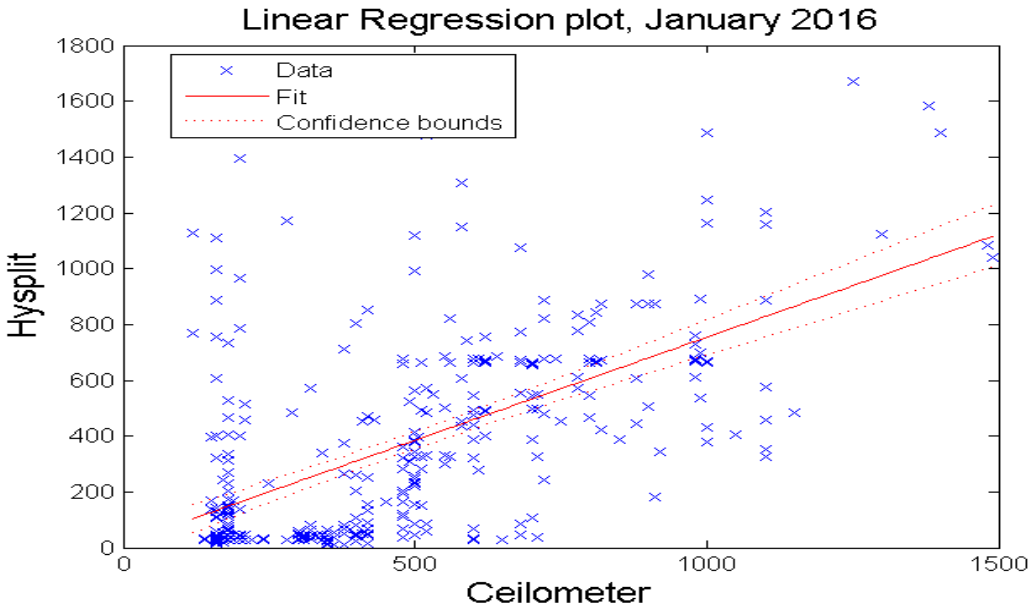
Linear Regression plot, January 2016
Data
Fit
Confidence bounds
Hysplit
1800
1600
1400
1200
1000
800
600
400
200
0
0
500
1000
1500
Ceilometer

(b)

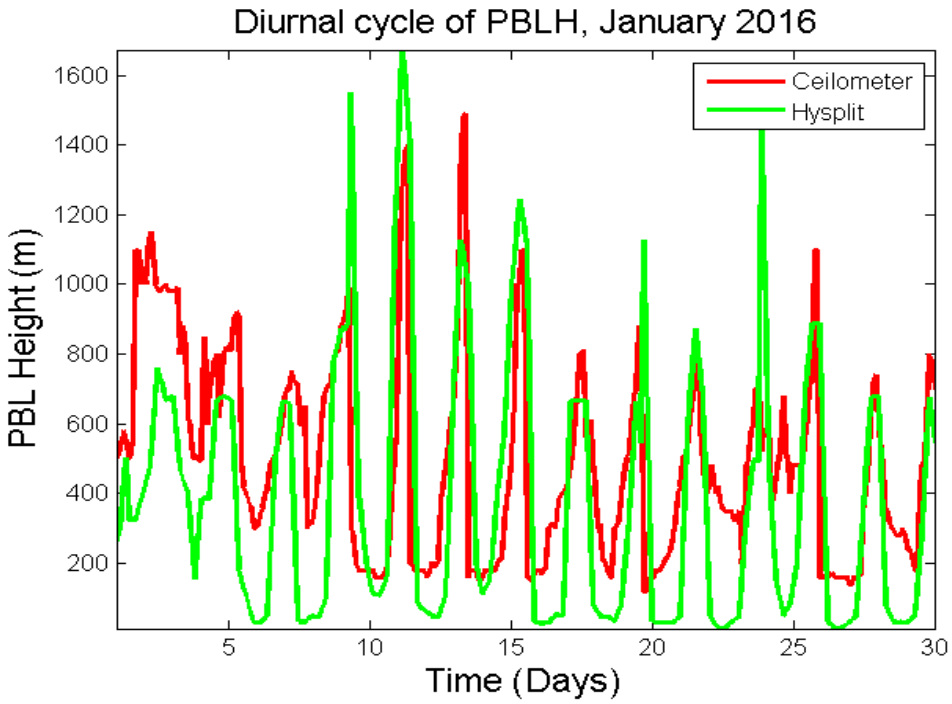


(c)

Figure 7. The statistics of the PBLH diurnal cycles over UTEP location: (a) Box plots of the data showing outliers for HYSPLIT; (b) Linear regression plots; (c) Diurnal cycle of the PBLH values throughout the month of January 2016.

**February 2016:**

Table 13: Descriptive Statistical tests for the January 2016 data retrieved from UTEP.

| | Tests | Ceilometer | HYSPLIT |
|---|---|---|---|
| **Month: February 2016**<br><br>**Location: UTEP**<br><br>**Lat and Lon: 31.76 N and -106.5 W** | Mean | 448.77 | 421.24 |
| | Median | 320 | 116.6 |
| | Standard Deviation | 362.53 | 546.77 |
| | Skewness | 2.60 | 1.67 |
| | Maximum | 3000 | 3242.2 |
| | Minimum | 100 | 9.5 |
| | Kurtosis | 13.53 | 6.12 |
| | Variance | 1.31e05 | 2.98e05 |

Mean values of ceilometer and HYSPLIT are 448.77 and 421.24 meters correspondingly. The skewness of ceilometer is higher than the HYSPLIT. The minimum PBLH value of experimental and simulation part is 100 and 9.5 meters.

Table 14: Performance and Error calculation tests for the February 2016 using UTEP data.

| Test | Values |
|---|---|
| Correlation Coefficient (Pearson) | 0.75 |
| Index of Agreement | 0.69 |
| Mean Absolute Error | 262.51 |
| RMSE | 360.96 |

The correlation coefficient and Index of agreement is high as its described on the above table.

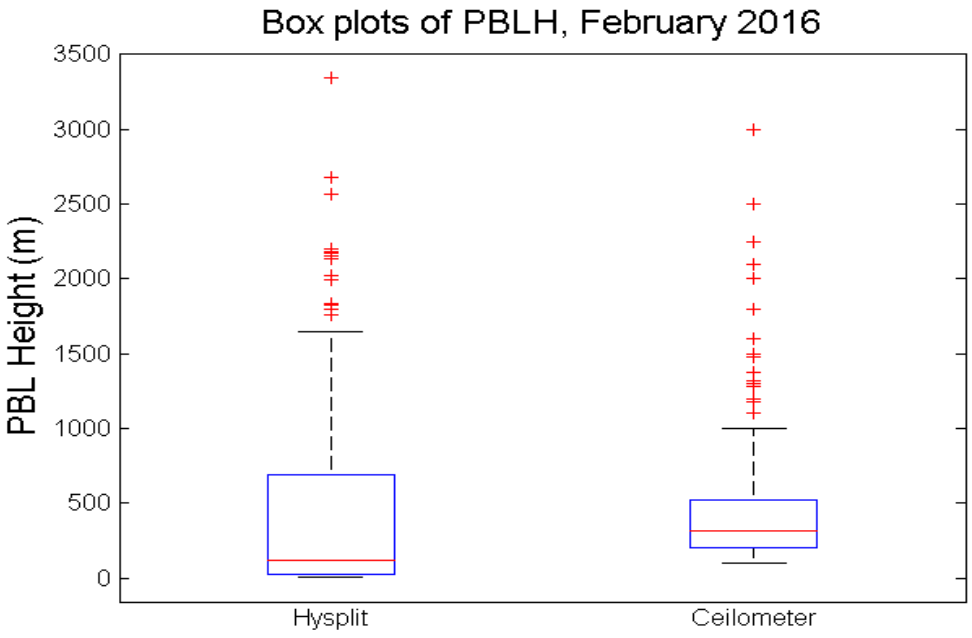


(a)

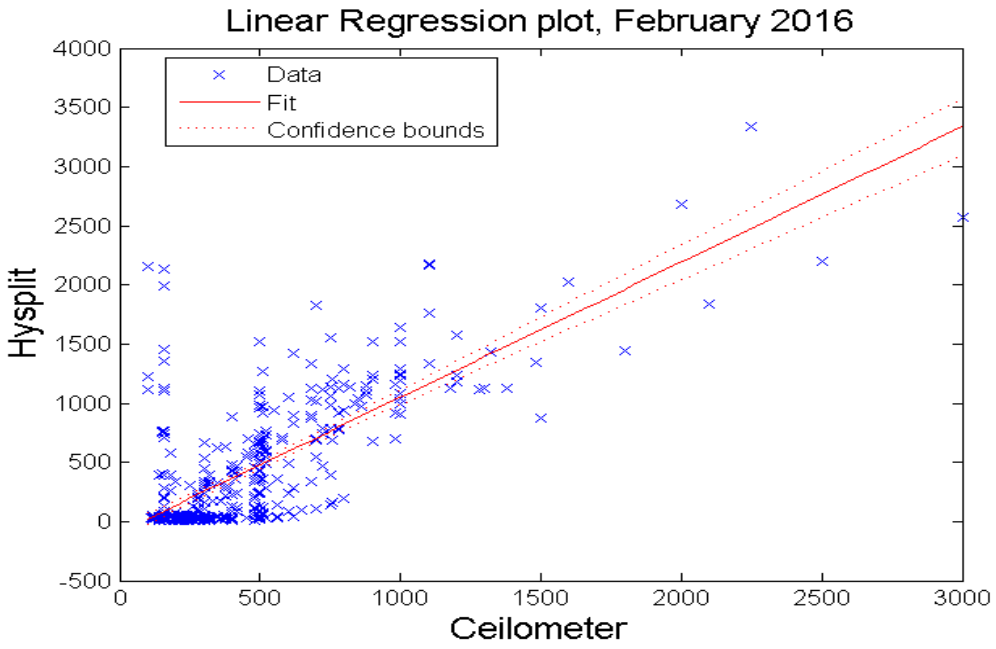


(c)

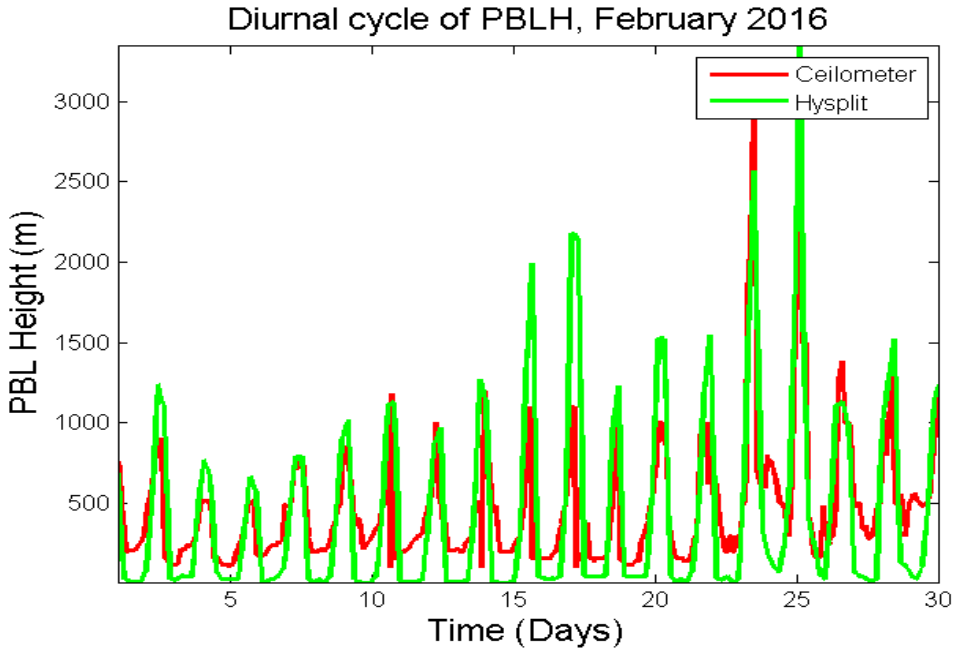


(c)

Figure 8. The statistics of the PBLH diurnal cycles over UTEP location: (a) Box plots of the data showing outliers for HYSPLIT; (b) Linear regression plots; (c) Diurnal cycle of the PBLH values throughout the month of February 2016.

**March 2016:**

Table 15: Descriptive Statistical tests for the March 2016 data retrieved from UTEP.

| | Tests | Ceilometer | HYSPLIT |
|---|---|---|---|
| **Month: March 2016**<br><br>**Location: UTEP**<br><br>**Lat and Lon : 31.76 N and -106.5 W** | Mean | 631.72 | 746.20 |
| | Median | 380 | 362.3 |
| | Standard Deviation | 631.20 | 828.88 |
| | Skewness | 1.66 | 0.88 |
| | Maximum | 3000 | 3334.9 |
| | Minimum | 120 | 27.6 |
| | Kurtosis | 5.40 | 2.51 |
| | Variance | 3.984e05 | 6.87e05 |

Mean and median values of the PBLH are around 650 meters and 370 meters respectively for both cases. Maximum value is around 3000 meters which is very prevailing in the spring season.

Table 16: Performance and Error calculation tests for the March 2016 using UTEP data.

| **Test** | **Values** |
|---|---|
| Correlation Coefficient (Pearson) | 0.67 |
| Index of Agreement | 0.71 |
| Mean Absolute Error | 414.60 |
| RMSE | 627.33 |

The Pearson correlation coefficient and the IOA are around 0.7 which shows a very strong agreement with the experimental and simulation values.

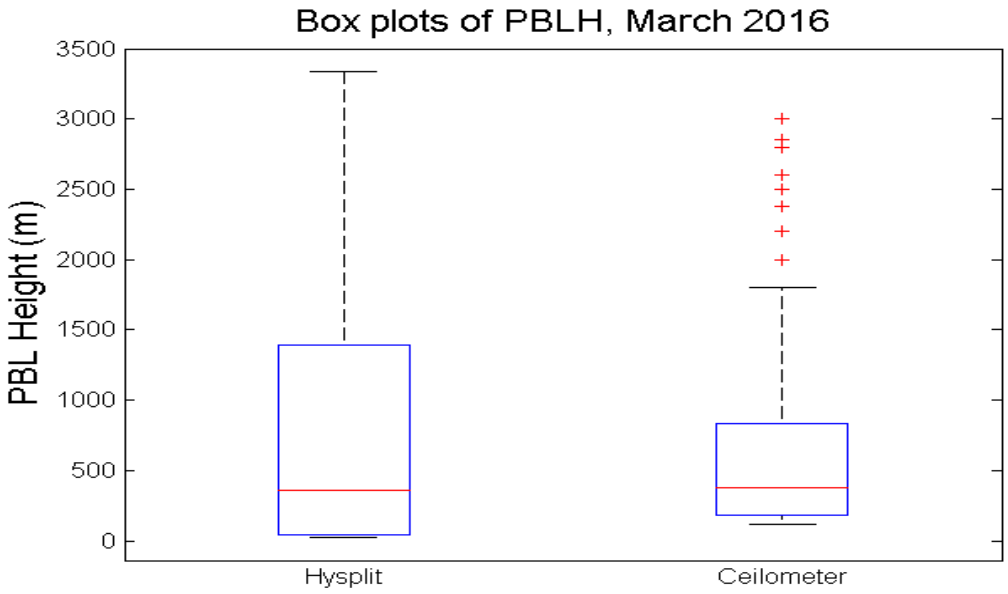
Box plots of PBLH, March 2016
PBL Height (m)
3500
3000
2500
2000
1500
1000
500
0
Hysplit
Ceilometer

(a)

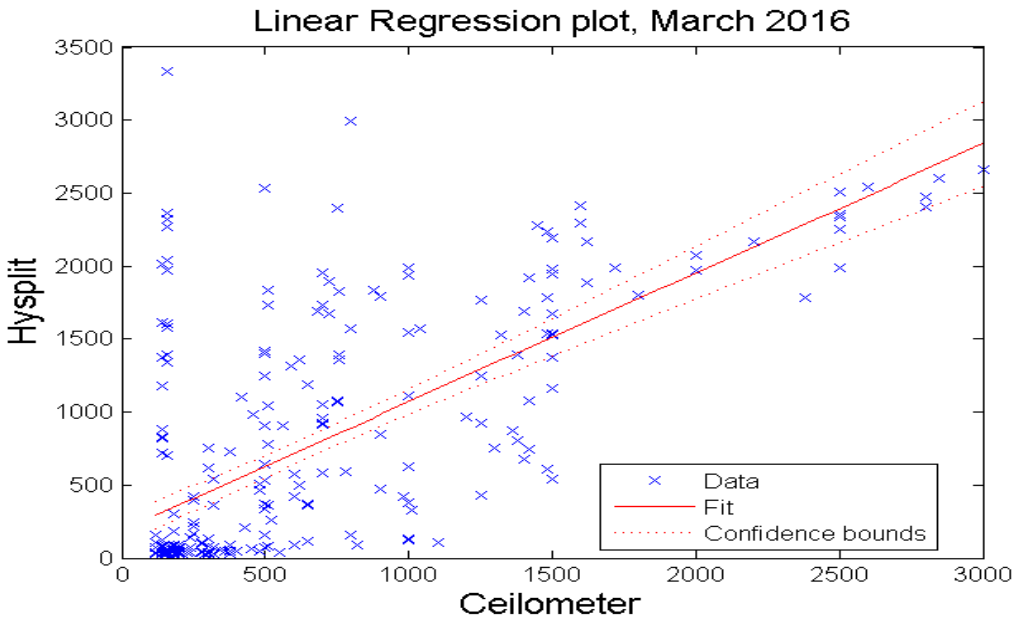
Linear Regression plot, March 2016
Hysplit
Ceilometer
0
500
1000
1500
2000
2500
3000
Data
Fit
Confidence bounds

(b)

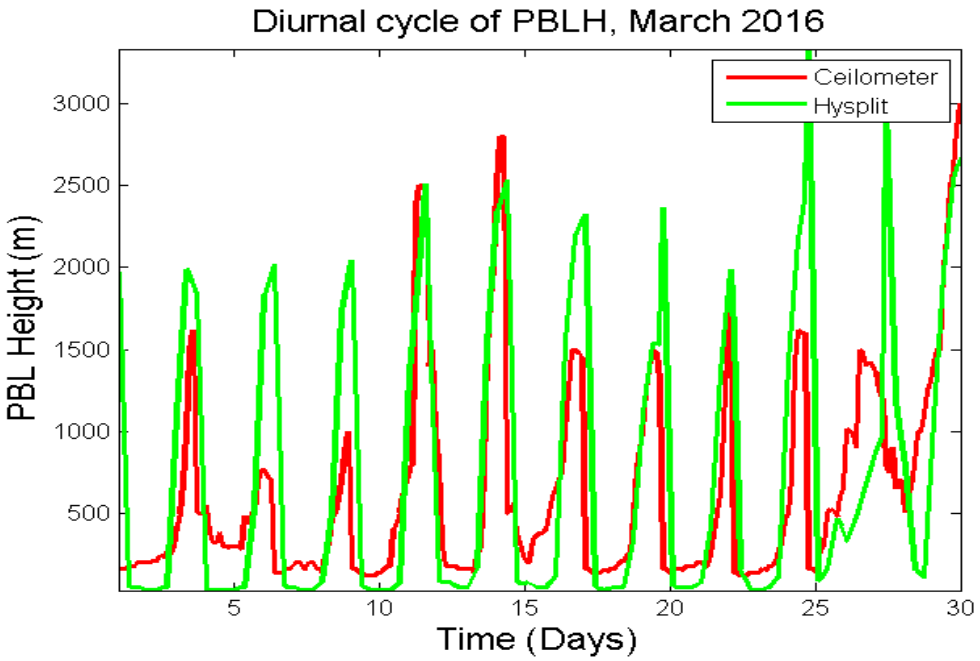


(c)

Figure 9. The statistics of the PBLH diurnal cycles over UTEP location: (a) Box plots of the data showing outliers for HYSPLIT; (b) Linear regression plots; (c) Diurnal cycle of the PBLH values throughout the month of March 2016.

**June 2016:**

Table 17: Descriptive Statistical tests for the January 2016 data retrieved from UTEP.

| | Tests | Ceilometer | HYSPLIT |
|---|---|---|---|
| **Month: June 2016** | Mean | 861.45 | 1178.3 |
| | Median | 680 | 599.3 |
| **Location: UTEP** | Standard Deviation | 576.30 | 1228.5 |
| | Skewness | 0.5281 | 0.7816 |
| **Lat and Lon : 31.76 N and -106.5 W** | Maximum | 2500 | 4280.3 |
| | Minimum | 140 | 30.2 |
| | Kurtosis | 2.11 | 2.19 |
| | Variance | 3.32e05 | 1.50e06 |

Because the PBLH varies according to temperature, it is always at its highest levels in June. Experiments and simulations show relatively similar skewness and kurtosis values.

Table 18: Performance and Error calculation tests for the June 2016 using UTEP data.

| Test | Values |
|---|---|
| Correlation Coefficient (Pearson) | 0.73 |
| Index of Agreement | 0.68 |
| Mean Absolute Error | 666.15 |
| RMSE | 947.72 |

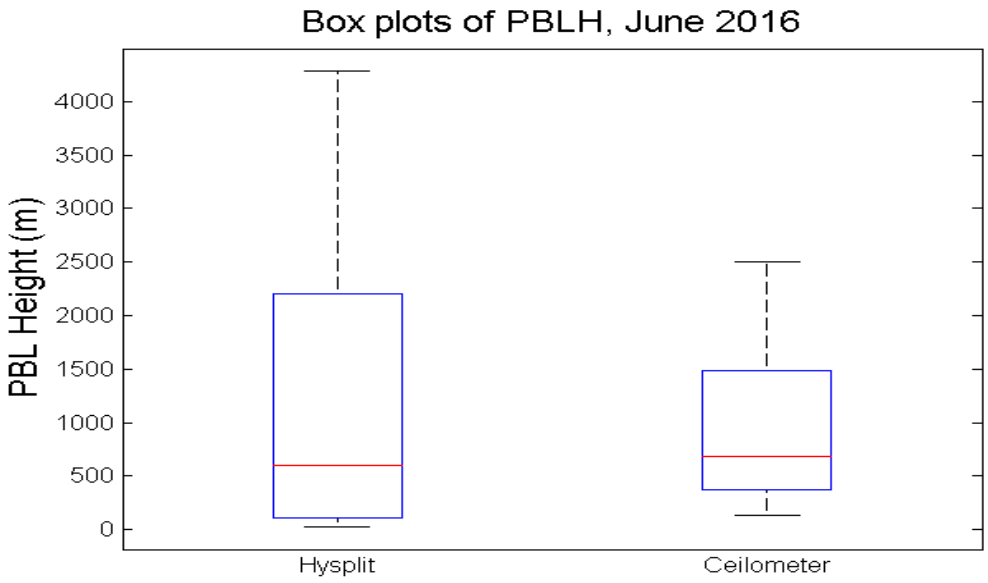


(a)

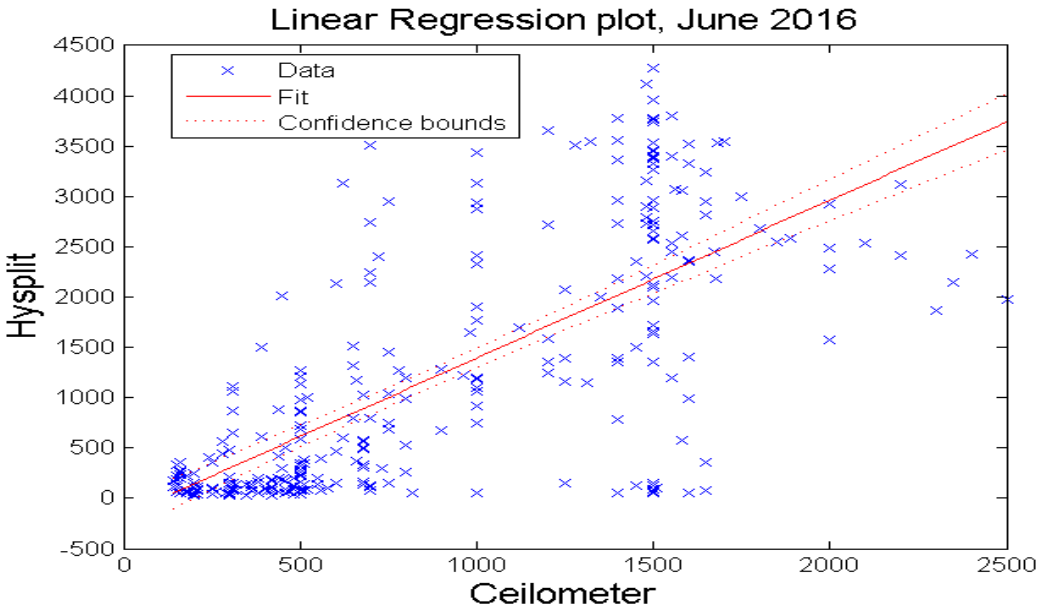


(b)

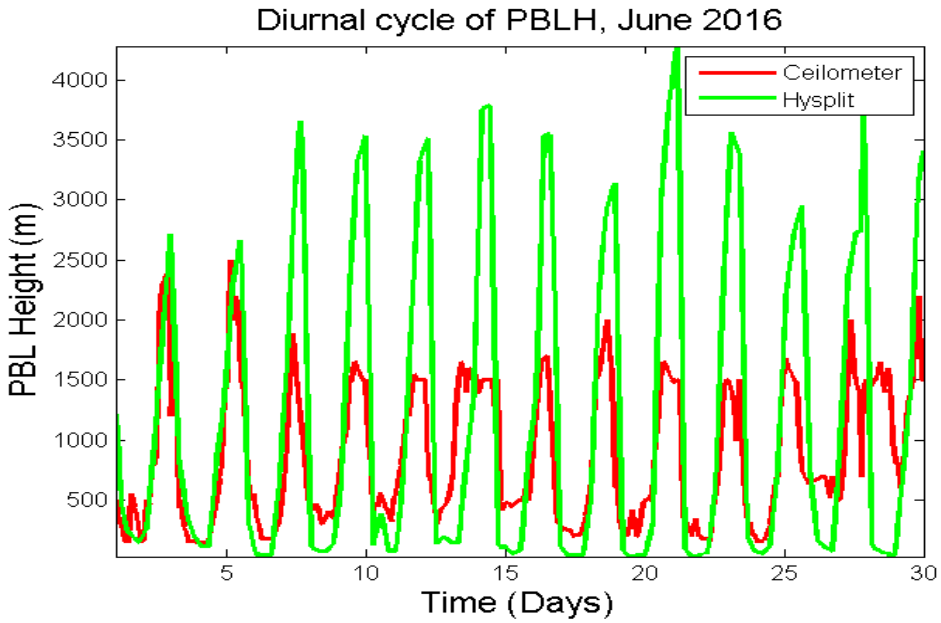


Figure 10. The statistics of the PBLH diurnal cycles over UTEP location: (a) Box plots of the data showing outliers for HYSPLIT; (b) Linear regression plots; (c) Diurnal cycle of the PBLH values throughout the month of June 2016.

**YEAR:2017**

**January 2017:**

Table 19: Descriptive Statistical tests for the January 2017 data retrieved from UTEP.

| | Tests | Ceilometer | HYSPLIT |
|---|---|---|---|
| **Month: January 2017**<br>**Location: UTEP**<br>**Lat and Lon : 31.76 N and -106.5 W** | Mean | 365.70 | 360.62 |
| | Median | 280 | 202.65 |
| | Standard Deviation | 261.13 | 400.90 |
| | Skewness | 1.81 | 1.44 |
| | Maximum | 1700 | 1841.5 |
| | Minimum | 80 | 12.1 |
| | Kurtosis | 7.89 | 4.63 |
| | Variance | 6.81e04 | 1.60e05 |

Both maximum and minimum values of the PBLH are around 1,800 meters due to the winter season. The mean values are also demonstrating similar numerical values.

Table 20: Performance and Error calculation tests for the January 2017 using UTEP data.

| **Test** | **Values** |
|---|---|
| Correlation Coefficient (Pearson) | 0.63 |
| Index of Agreement | 0.63 |
| Mean Absolute Error | 232.95 |
| RMSE | 308.87 |

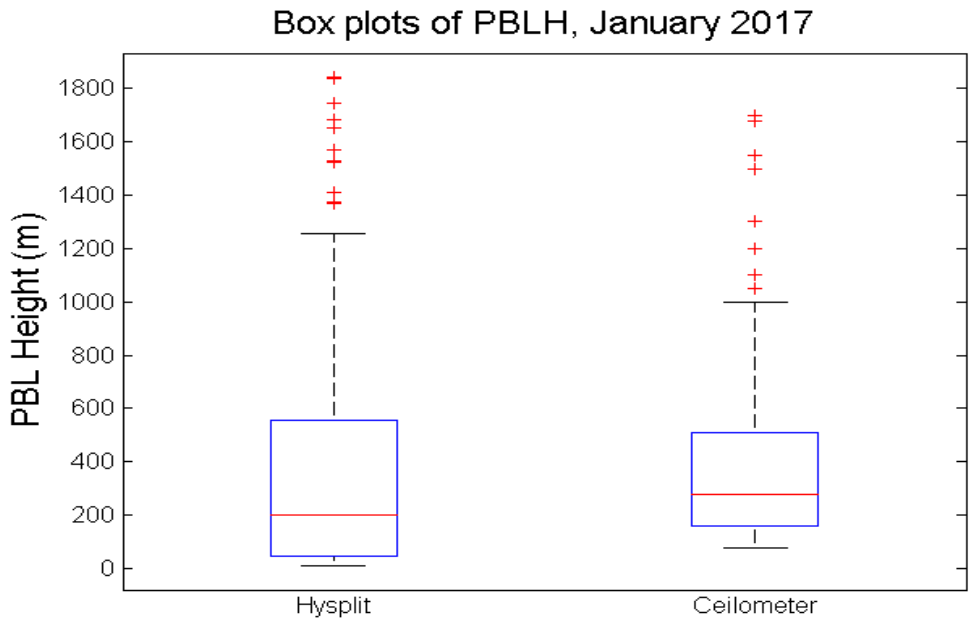
Box plots of PBLH, January 2017
PBL Height (m)
1800
1600
1400
1200
1000
800
600
400
200
0
Hysplit
Ceilometer

(a)

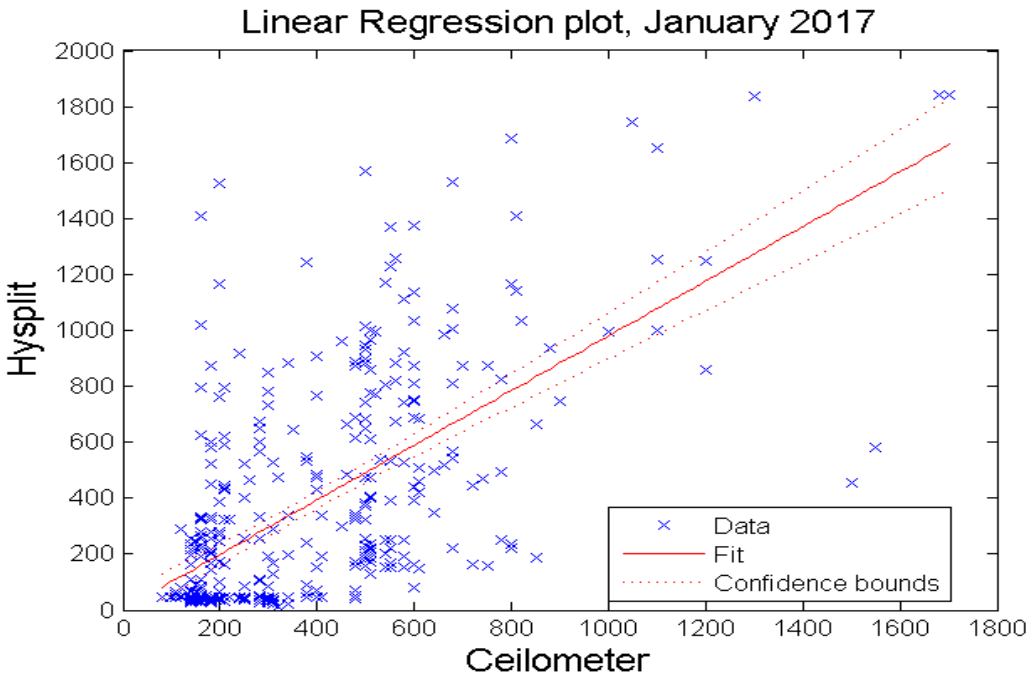
Linear Regression plot, January 2017
Hysplit
Ceilometer
2000
1800
1600
1400
1200
1000
800
600
400
200
0
0
200
400
600
800
1000
1200
1400
1600
1800
Data
Fit
Confidence bounds

(b)

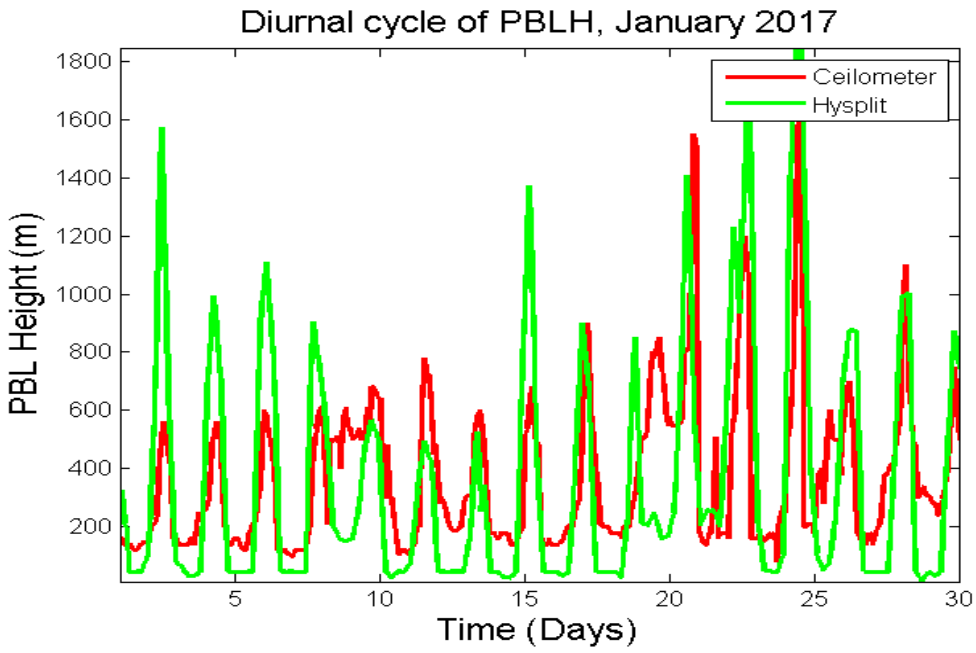


(c)

Figure 11. The statistics of the PBLH diurnal cycles over UTEP location: (a) Box plots of the data showing outliers for HYSPLIT; (b) Linear regression plots; (c) Diurnal cycle of the PBLH values throughout the month of January 2017.

**February 2017:**

Table 21: Descriptive Statistical tests for the February 2017 data retrieved from UTEP.

| | Tests | Ceilometer | HYSPLIT |
|---|---|---|---|
| **Month: February 2017**<br><br>**Location: UTEP**<br><br>**Lat and Lon : 31.76 N and -106.5 W** | Mean | 398.93 | 414.77 |
| | Median | 310 | 106.1 |
| | Standard Deviation | 288.16 | 499.22 |
| | Skewness | 1.41 | 1.11 |
| | Maximum | 1400 | 2139.8 |
| | Minimum | 100 | 9.6 |
| | Kurtosis | 4.67 | 3.13 |
| | Variance | 8.30e04 | 2.49e05 |

February, which is a winter month, typically yields the lower PBLH values in both cases. As it is represented in the above table, the mean value of the PBLH is around 400 meters while the maximum values are around the range of 1,500-2,000 meters.

Table 22: Performance and Error calculation tests for the February 2017 using UTEP data.

| Test | Values |
|---|---|
| Correlation Coefficient (Pearson) | 0.61 |
| Index of Agreement | 0.64 |
| Mean Absolute Error | 301.74 |
| RMSE | 395.11 |

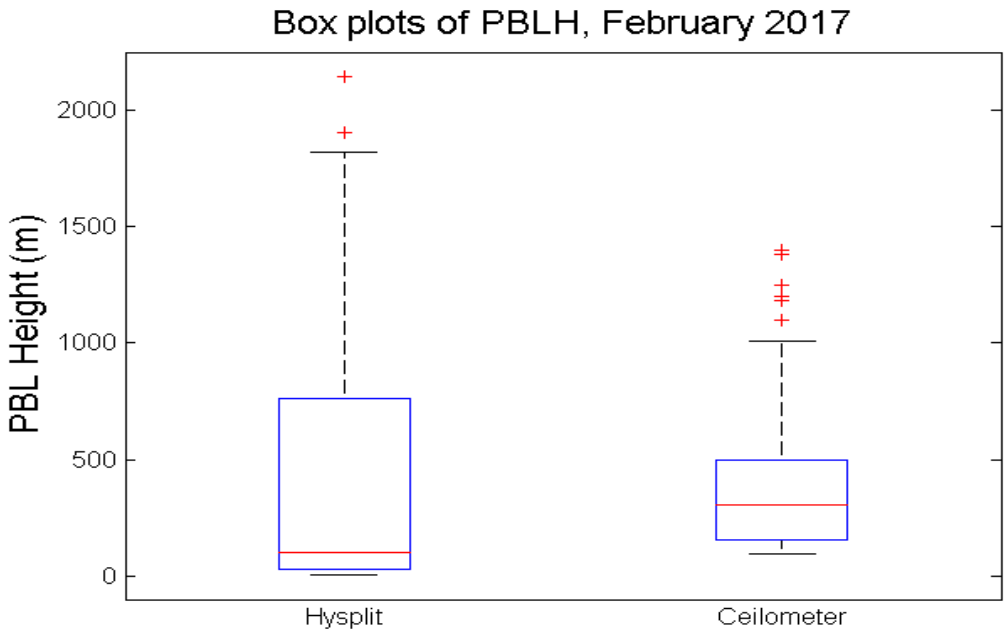


(a)

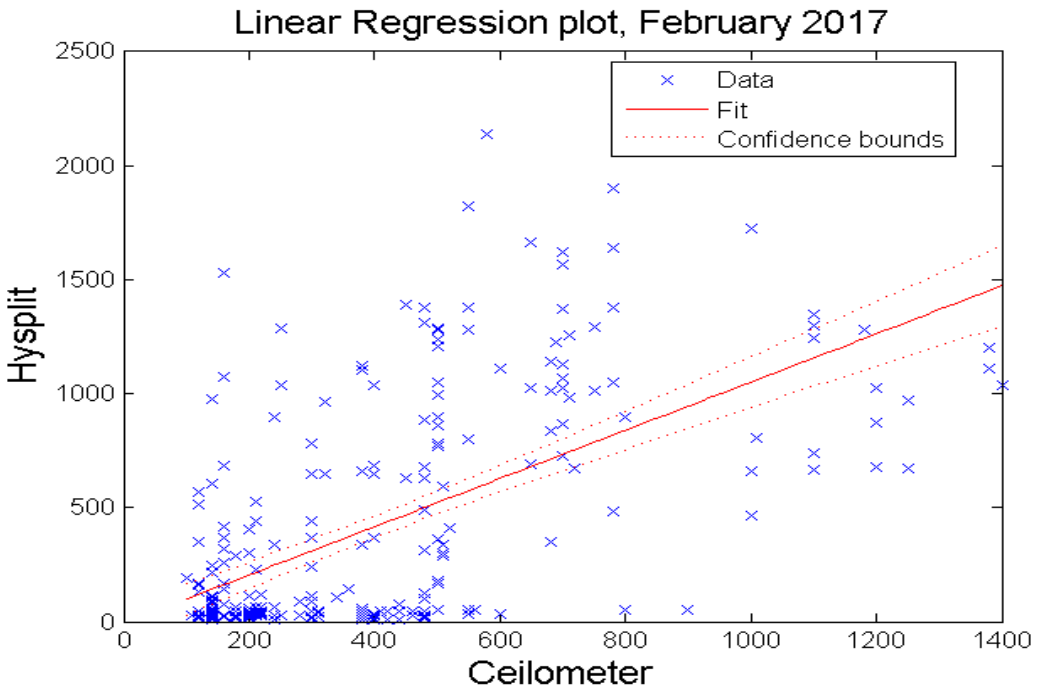


(b)

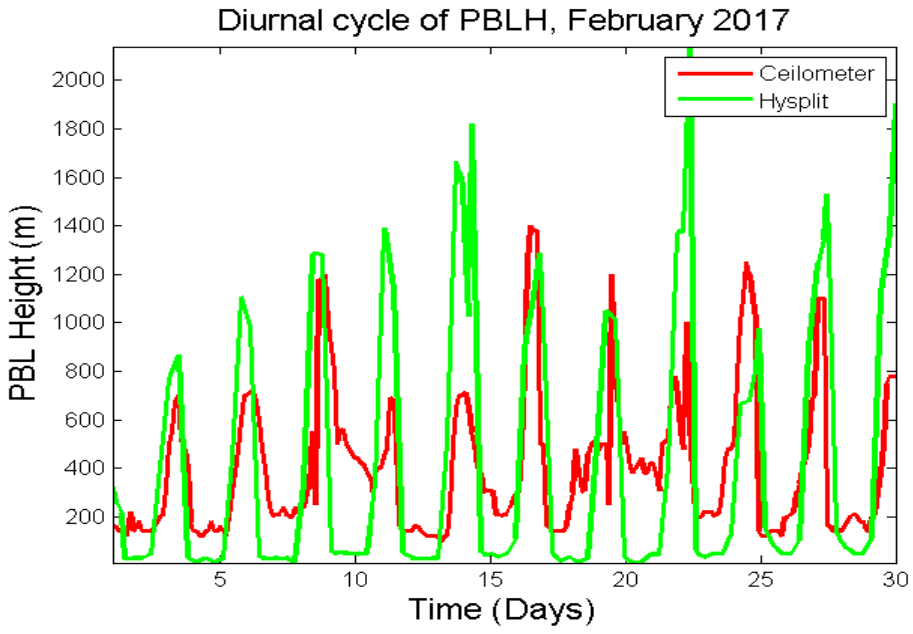


(c)

Figure 12. The statistics of the PBLH diurnal cycles over UTEP location: (a) Box plots of the data showing outliers for HYSPLIT; (b) Linear regression plots; (c) Diurnal cycle of the PBLH values throughout the month of February 2017.

**March 2017:**

Table 23: Descriptive Statistical tests for the March 2017 data retrieved from UTEP.

| | Tests | Ceilometer | HYSPLIT |
|---|---|---|---|
| **Month: March 2017**<br>**Location: UTEP**<br>**Lat and Lon: 31.76 N and -106.5 W** | Mean | 683.98 | 650.80 |
| | Median | 500 | 339.80 |
| | Standard Deviation | 439.75 | 735.91 |
| | Skewness | 0.85 | 1.02 |
| | Maximum | 2000 | 2692.5 |
| | Minimum | 120 | 9.5 |
| | Kurtosis | 2.55 | 2.86 |
| | Variance | 1.93e05 | 5.41e05 |

Temperature increases when spring arrives in March and as a result, the mean, median, and maximum values of the PBLH increase as demonstrated clearly by the above table.

Table 24: Performance and Error calculation tests for the March 2017 using UTEP data.

| **Test** | **Values** |
|---|---|
| Correlation Coefficient (Pearson) | 0.66 |
| Index of Agreement | 0.65 |
| Mean Absolute Error | 433.67 |
| RMSE | 551.19 |

The MAE and RMSE are around 450 and 500 meters correspondingly while the R2 and the IOA values are around 0.65.

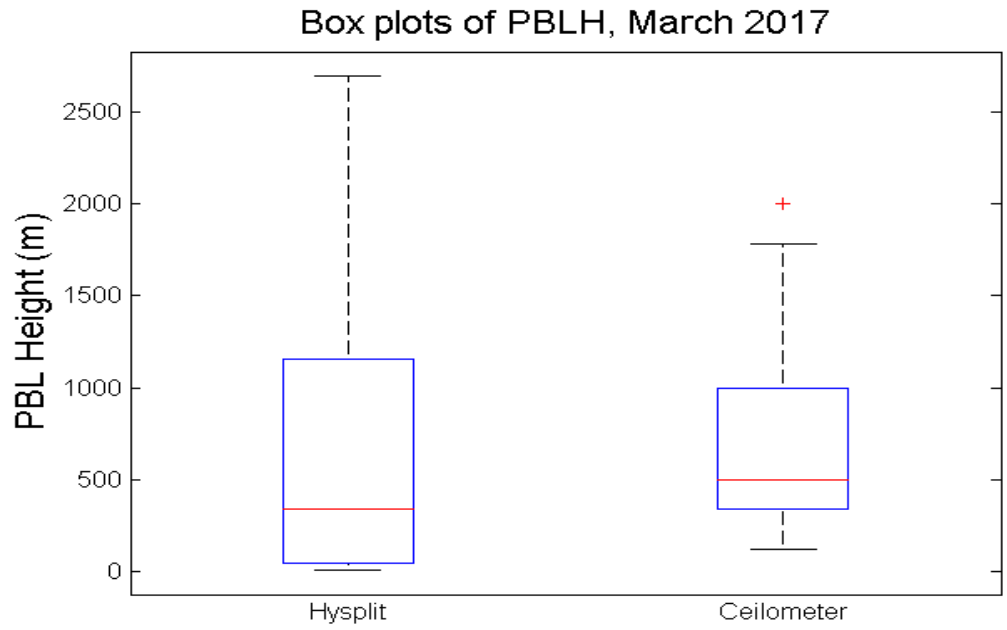
Box plots of PBLH, March 2017
PBL Height (m)
2500
2000
1500
1000
500
0
Hysplit
Ceilometer

(a)

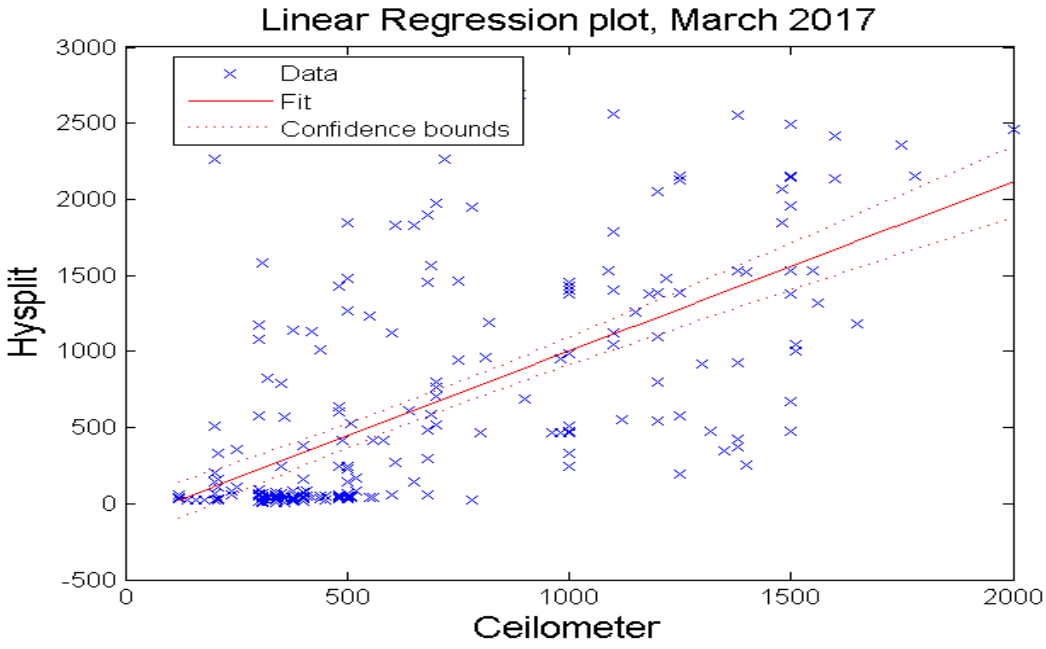
Linear Regression plot, March 2017
Data
Fit
Confidence bounds
Hysplit
Ceilometer
3000
2500
2000
1500
1000
500
0
-500
0
500
1000
1500
2000

(b)

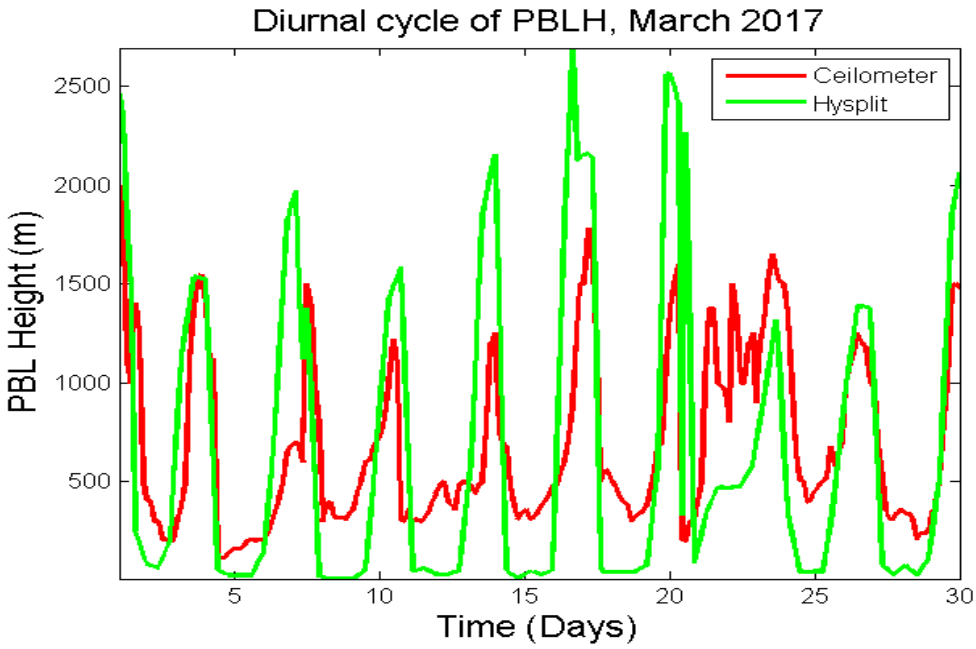


(c)

Figure 13. The statistics of the PBLH diurnal cycles over UTEP location: (a) Box plots of the data showing outliers for HYSPLIT; (b) Linear regression plots; (c) Diurnal cycle of the PBLH values throughout the month of March 2017.

### 3.1 PBL structure during the high and low ozone events

The mixing layer height (MLH) is critical in air pollution modeling because it affects the effective volume of pollutants dispersed [7]. Ozone ($O_3$) is a secondary pollutant produced photochemically in sunshine from nitrogen oxides and volatile organic molecules. The diurnal development of the PBL has a substantial influence on the temporal variation of ground-level $O_3$ levels.

Figure 14 shows the hourly concentration of the ground-level ozone as recorded by CAMS 12 UTEP on 6 June 2016. It can be observed that the eight-hour average ozone concentration during a daytime was above 70 ppbv indicating it was a high ozone event. The ozone concentration starts picking up after 7 am which is obvious since the traffic on the streets also starts picking up around that time. The ozone peak was achieved in the late afternoon around 2 pm. Now, when we compare it with the structure of the PBL as provided by the ceilometer aerosol backscatter profiles,

we can see in figure 15, that early morning the PBLH is shallow. PBLH starts evolving around 1600 UTC which is 10 am Mountain Standard Time (MST). Till then the PBLH is well below 500 m. The maximum PBLH detected that day is around 1700 ± 250 m around 2100 UTC which is around 3 pm local time.

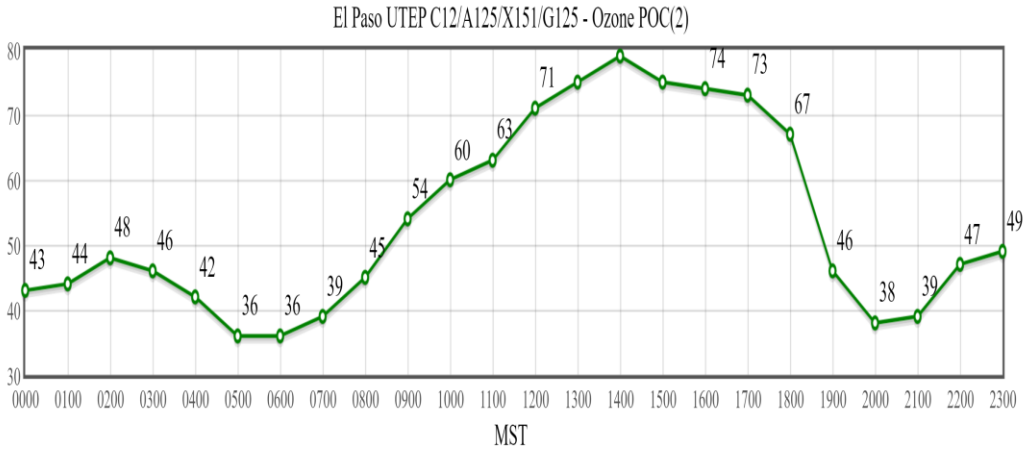

Figure 14. Hourly ozone concentration as recorded by CAMS 12 UTEP on 06 June 2016

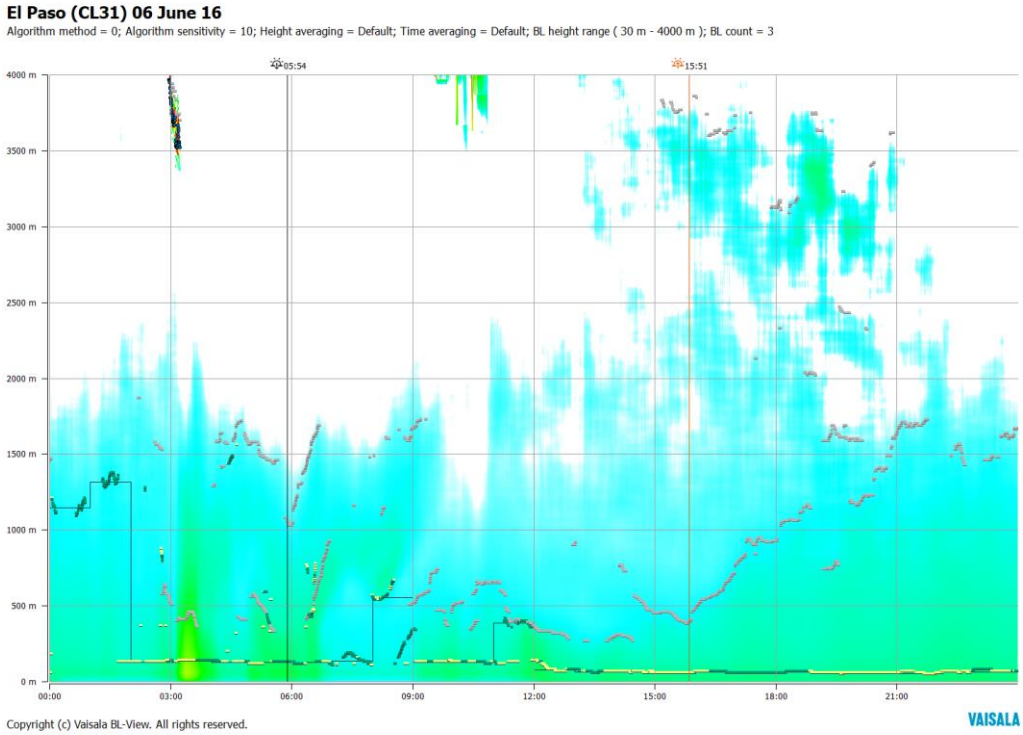


Figure 15. PBLH structure during a high ozone episode 06 June 2016. Time on the x-axis is in UTC.

Figure 16 shows the hourly concentration of the ground-level ozone as recorded by CAMS 12 UTEP on 1 May 2016. It can be observed that the eight-hour average ozone concentration during a daytime was above 50 ppbv and hence it was defined as a low ozone event. The ozone concentration starts increasing after 6 am but plateaus over after 9 am till 5 pm local time. The ozone concentrations are below 43 ppbv throughout this plateau period.

Figure 17 shows the structure of the PBL as provided by the ceilometer aerosol backscatter profiles. The day starts with a higher nocturnal boundary layer height around 400 m before the sunrise and the daytime PBLH starts evolving around 12:00 UTC which is 06 am local time. By 9 am local time PBLH has reached 1,200 m. The maximum PBLH detected that day is around 2,900 ± 250 m around 2200 UTC which is around 4 pm local time.

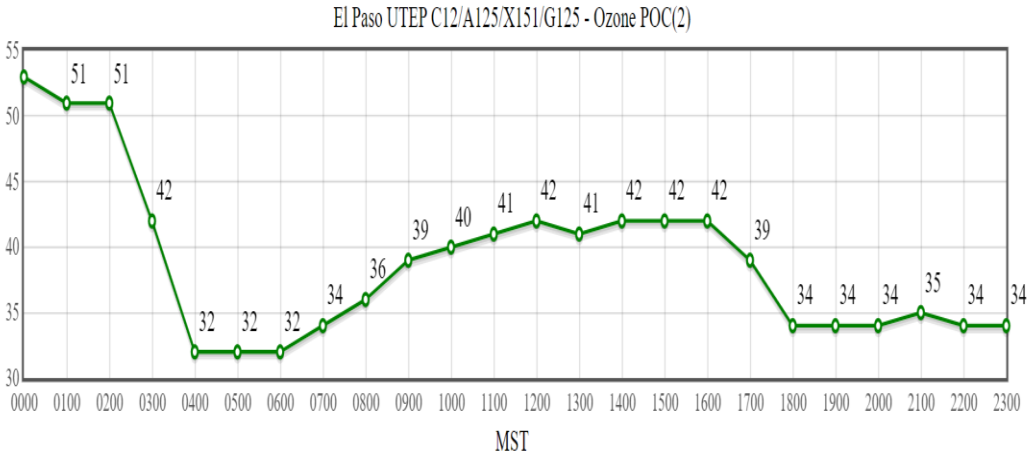


Figure 16. Hourly ozone concentration as recorded by CAMS 12 UTEP on 01 May 2016

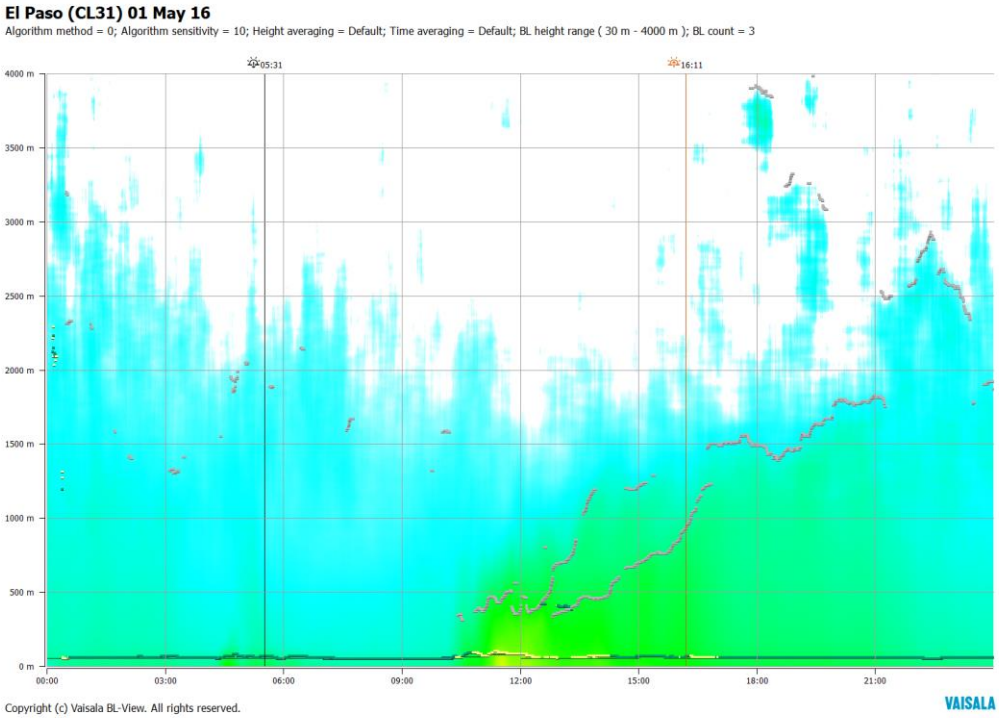


Figure 17. PBL structure on a low ozone day of 01 May 2016.

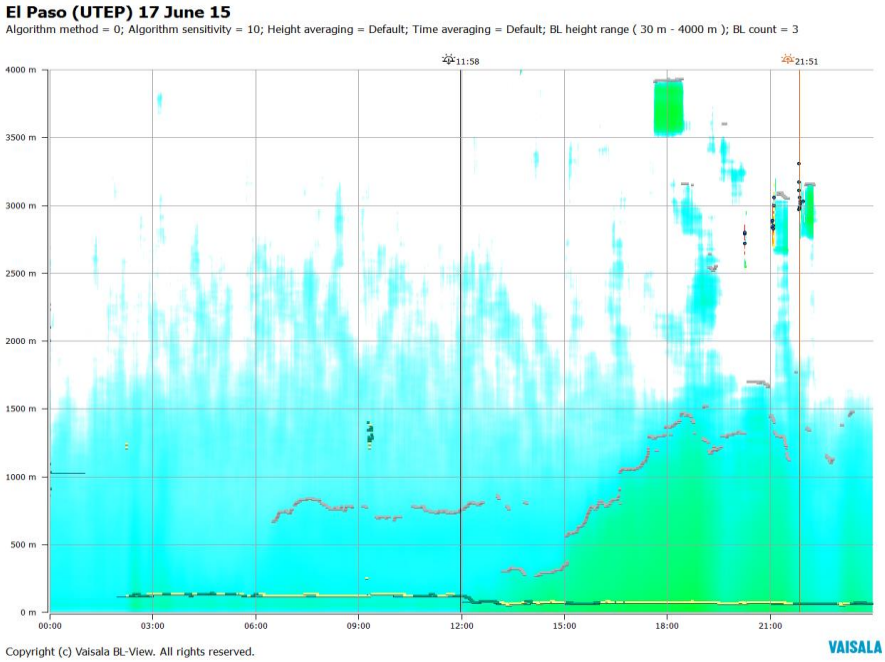


Figure 18. PBL structure during a high ozone episode of 17 June 2015

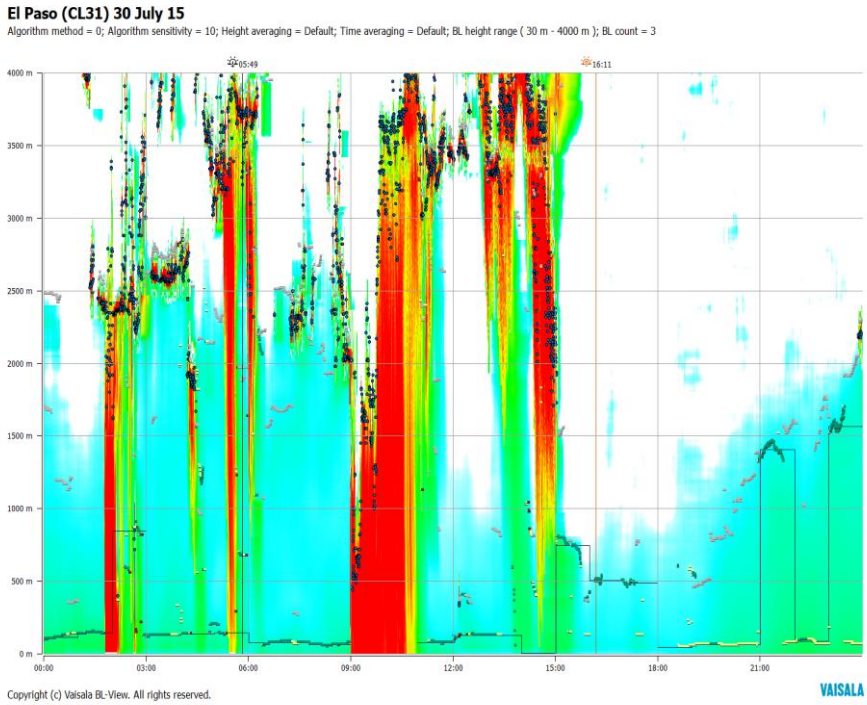


Figure 19. PBL structure during a low ozone episode of 30 July 2015

### 3.2 CONSECUTIVE HIGH AND LOW OZONE EPISODES OF JUNE 2017

In Figure 20a,b the backscatter profiles for both the back-to-back high and low ozone episodes are presented, as well as the estimated MLH. The ceilometer data shows that the MLH rises during the daytime with strong convection in the afternoon for the four successive high ozone episodes, Figure 20a. The figure also shows that there is a residual layer during the nighttime and early morning hours before sunrise. A higher residual layer on top of the elevated nocturnal boundary layer was observed on three successive low ozone days, as seen in Figure 20b. The diurnal variation during the low ozone events was not as clearly visible as compared to the high ozone events. This was due to the horizontal homogeneity of the aerosol layer on 11–13 June 2017. Higher concentrations of PM10 were recorded by CAMS 12 for those three days of the low ozone episodes. Contrary to the PBLH obtained from performing WRF simulations, a distinct difference in the PBL structures during the high and low ozone events was observed. The average MLH from 15–18 L.T. (maximum PBLH in Figure 20a) during the high ozone episodes was shallower (1164 ± 59 m) than the low episode period (1990 ± 79 m) (Figure 20b). The black dots in Figure 20 a, b represent the detection of the cloud base heights by the ceilometer roughly above 4 km. Clouds were detected on 6, 7, and 11 June, respectively, as also confirmed by the intensity of the aerosol backscatter [17].

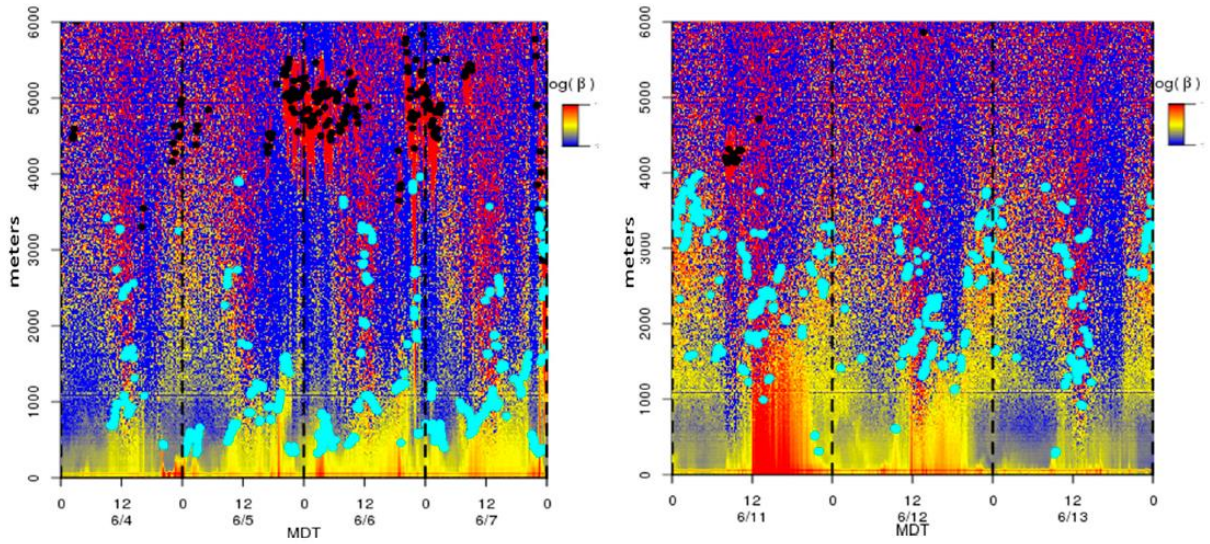


Figure 20. (a) Aerosol backscatter heatmap time series profile for the high ozone episode period. The black dots represent the cloud base detection, and the cyan dots are the aerosol mixing layer height estimated by BL-View; (b) for low ozone days. β represents the aerosol backscatter intensity [17].

# Chapter 4. RWP Operations

## 4.1 Introduction

A Vaisala LAP 3000 radar wind profiler (RWP) in southeast El Paso TX measures winds aloft from approximately 150 meters (m) to 4 kilometers (km) altitude. The RWP station is located at 320 Old Hueco Tanks Road, El Paso, TX 79927, at Latitude 31º 40' 3" North (31.6675º), Longitude 106º 17' 17" West (-106.288º). This station is operated by the Texas Commission on Environmental Quality (TCEQ) and is named the Socorro Hueco CAMS 49 station. The TCEQ also operates a standard 10 m meteorological tower for surface wind speed and direction at this station. Figure 21 shows a photograph of the RWP at the station, and Figure 22 shows a map of the El Paso area with TCEQ monitoring stations and with the Socorro Hueco station shown in the lower center portion of the map, labeled along with the U.S. Environmental Protection Agency (EPA) designation number of 481410057. Data from late 2015 to late in 2018 were available for this work, so that roughly three complete years of recent data are used. The goal of this work is to characterize the upper air winds in El Paso, and to compare upper air winds on high ozone ($O_3$) days to all summer days.

That the RWP at Socorro Hueco can be used to assess upper air winds over the Paso Del Norte area was established by a study in 1996 when two RWPs operated, one in the western part of El Paso and one to the east. Data from both instruments were found to be in general agreement. More information can be provided up request.

The method of operation of the RWP is that a radar pulse is emitted in the vertical direction, and the signal return at specific times can be interpreted for the horizontal speed and direction of air flow at specific altitudes above ground level (AGL). One pulse is emitted and the 25 returns measured at altitudes separated by 57 m shown in Table 25 constitute the first pulse, and 79

seconds later a second pulse is emitted and the 38 returns are measured at altitudes separated by 97 m shown in Table 25. Pairs of pulses are emitted every 30 minutes.

Figure 21 Photograph of the RWP at Socorro Hueco CAMS 49

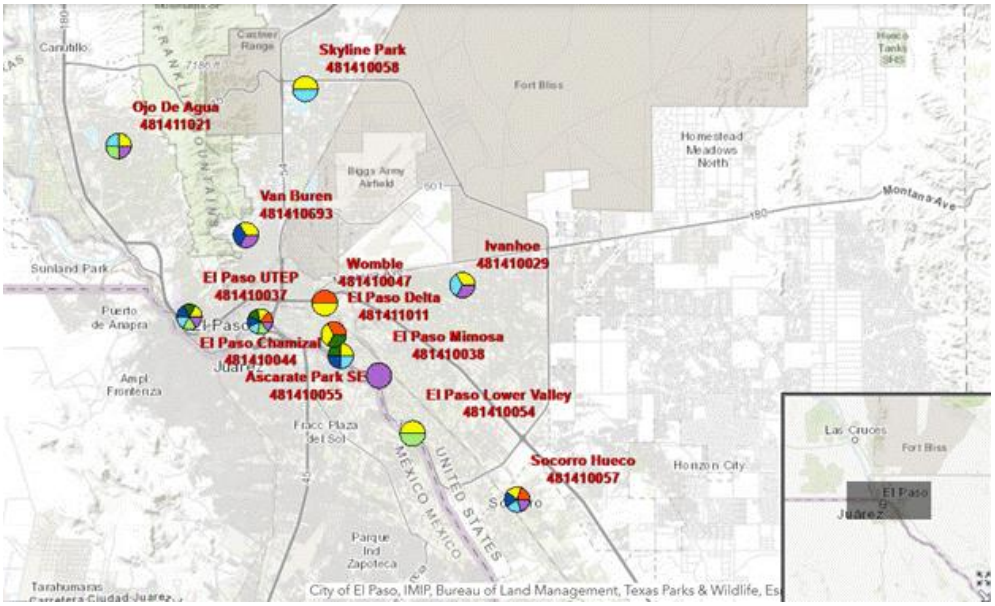


Figure 22. TCEQ Map of Monitoring Stations in the El Paso Region

Table 25: Altitudes in km AGL for the two RWP pulse pairs emitted 79 sec. apart

| First Pulse | Second Pulse |
|---|---|
| 0.146 | 0.206 |
| 0.203 | 0.304 |
| 0.260 | 0.401 |
| 0.317 | 0.498 |
| 0.375 | 0.596 |
| 0.432 | 0.693 |
| 0.489 | 0.790 |
| 0.546 | 0.887 |
| 0.604 | 0.985 |
| 0.661 | 1.082 |
| 0.718 | 1.179 |
| 0.775 | 1.276 |
| 0.832 | 1.374 |
| 0.890 | 1.471 |
| 0.947 | 1.568 |
| 1.004 | 1.665 |
| 1.061 | 1.763 |
| 1.118 | 1.860 |
| 1.176 | 1.957 |
| 1.233 | 2.055 |
| 1.290 | 2.152 |
| 1.347 | 2.249 |
| 1.405 | 2.346 |
| 1.462 | 2.444 |
| 1.519 | 2.541 |
| | 2.638 |
| | 2.735 |
| | 2.833 |
| | 2.930 |
| | 3.027 |
| | 3.124 |
| | 3.222 |
| | 3.319 |
| | 3.416 |
| | 3.514 |
| | 3.611 |
| | 3.708 |
| | 3.805 |

To characterize the upper air winds, the RWP data, with 1,907,049 observations, data records were grouped into bins as follows:

- Altitudes AGL were grouped into six classes. The system measures wind speed and direction at 63 discrete altitudes from 146 m to 3,805 m AGL. The count of the number of records and the grouping of altitudes into six classes is shown in Table 6.

Table 26: Altitude groupings for wind rose bins

| Altitude bins, m | Altitude range, m | Total measurements |
|---|---|---|
| 205 | 146-304 | 216,840 |
| 425 | 317-546 | 301,554 |
| 766 | 596-985 | 472,099 |
| 1,228 | 1,004-1,471 | 452,542 |
| 1,956 | 1,519-2,444 | 282,366 |
| 3,125 | 2,541-3,805 | 181,648 |
| | Grand Total | 1,907,049 |

- Four-hour time blocks: 0:00 – 3:59 MST (0-3 MST), 4:00 – 7:59 MST, 8:00 – 11:59 MST, 12:00 – 15:59 MST, 16:00 – 19:59 MST, 20:00 – 23:59 MST.
- Four wind speed blocks grouped in quartiles: 0 – 2.99 m/s, 3 – 5.99 m/s, 6 – 10 m/s, > 10 m/s. 99% of wind speeds < 22.4 m/s.
- Eight 45 degree (deg) wide wind direction bins: North (N), Northeast (N.E.), East (E), Southeast (S.E.), South (S), Southwest (S.W.), West (W), and Northwest (N.W.)
- In the initial characterization, all data were used, and dates were assigned to 1st quarter (Jan.-Mar.), 2nd quarter (Apr.-Jun.), 3rd quarter (Jul.-Sep.), 4th quarter (Oct.-Dec.) to perform a seasonal assessment. In characterizing high $O_3$ days, the three key months June, July and August were grouped together.

### 4.2 Comparing RWP and Surface Winds

Comparing the low level RWP winds to the surface winds is a very mild quality assurance step in using the RWP data. Figure 23 23 shows the comparison between the lowest measured winds at the Socorro Hueco station at 146 m compared to the 10 m tower also at the station. For this comparison, to avoid the wrap-around from 359 to 0 degrees at dur north, only winds greater than 30 and less than 330 degrees from both instruments were used. Winds were based upon nearly coincident values within each hour, during the months of June through August 2016 – 2018. Winds were filtered for the surface winds to be greater than 5 miles per hour (2.2 m / second (s)). This comparison allowed 3,647 observations to be used, and the results were very significant with slope (0.89) close to 1.0 and $R^2$ (the percent of variation in y explained by the regression) of 76%. Wind speed had relatively poor agreement, with slope close to 1.0 but $R^2$ only 11%.

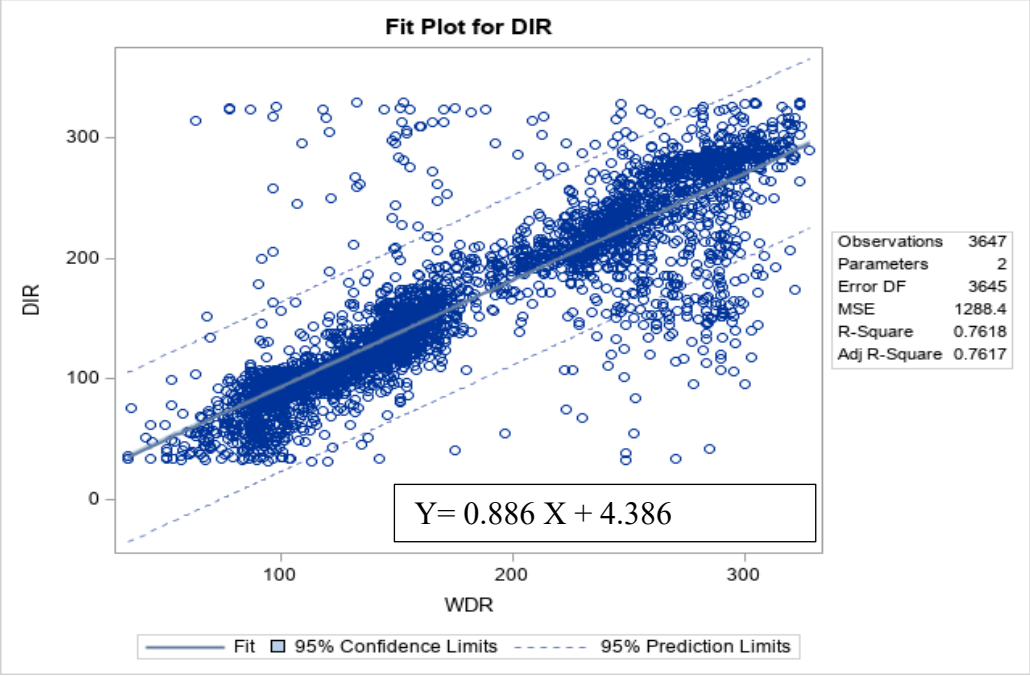


Figure 23. Regression fit to compare low RWP winds with surface meteorology at Socorro Hueco

### 4.3 Wind Speed as a Function of Altitude

In general, wind speed is known to increase with altitude above ground level based on fundamental fluid mechanics. Contact with the surface leads to slow air movement, the effect of which lessens as one moved upward through the fluid boundary layer. At higher altitudes beyond the boundary layer, the rate of change of wind speeds is reduced. Figure 24 shows the graph for the RWP first pulse mean wind speed as a function of altitude AGL and Figure 25 shows the graph for the RWP second pulse mean wind speed as a function of altitude AGL. There are inflection points close to 1 km and 3 km.

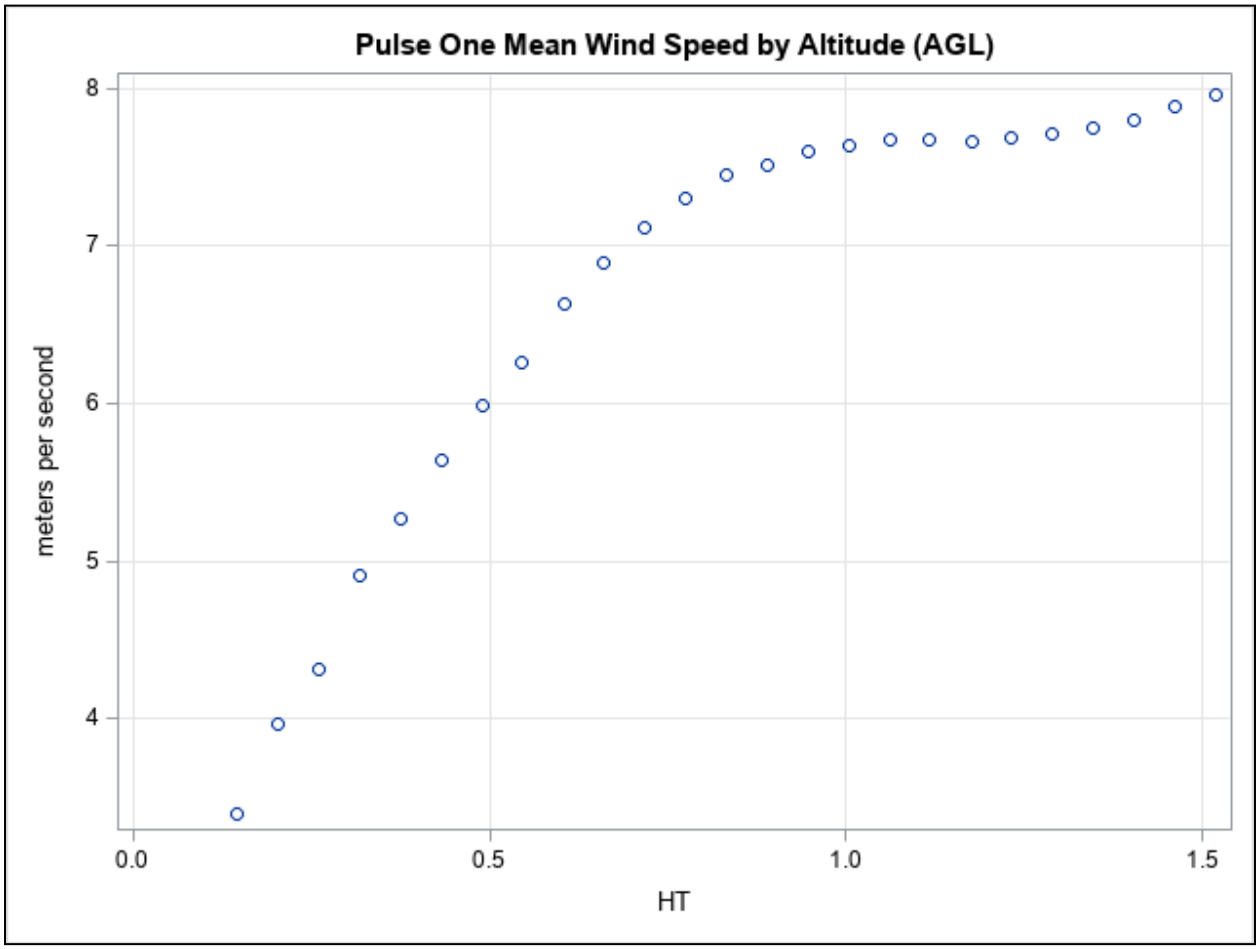


Figure 24. RWP first pulse mean wind speed as a function of height (H.T.) in km AGL

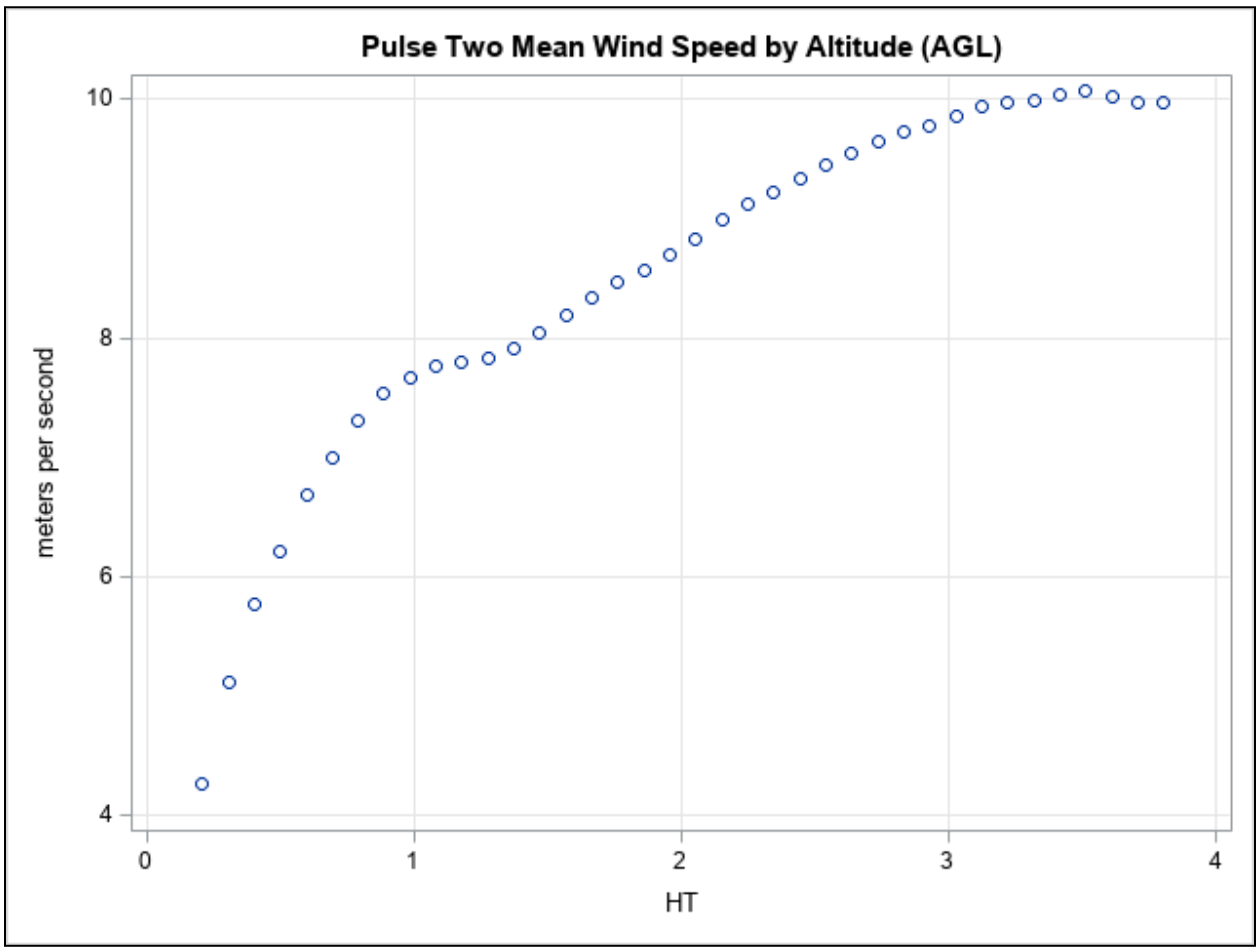

Figure 25. RWP first pulse mean wind speed as a function of height (H.T.) in km AGL

### 4.4 SEASONAL ASSESSMENT

In this section, upper air winds are characterized by looking at the data by season of the year. This was done based on quarters of the calendar year. In a series of 24 wind rose graphs to follow, the frequency of winds by direction and speed are shown for each quarter at six aggregated altitude bins. A broad conclusion in all quarter is that wind speeds increase with altitude, which is an expected result based on atmospheric physics and as illustrated earlier in this report.

A summary of the results by calendar quarter is as follows:

- 1st Quarter – Wider range of wind directions at lower altitudes. For all altitude bins, westerly and southwesterly winds dominate, moving to more southwesterly with higher altitude.
- 2nd Quarter – Wider range of wind directions at lower altitudes, with more easterly winds than in 1st quarter. For all altitude bins, westerly and southwesterly winds dominate, moving to more southwesterly with higher altitude.
- 3rd Quarter – Easterly and southeasterly winds dominate at lower altitudes, moving to near uniform distribution of winds from 1 to 2 km to northeast to southwest peaks at 3 km.
- 4th Quarter – Easterly & westerly peaks at low altitudes, shifting to westerly, then southwesterly at high altitudes.

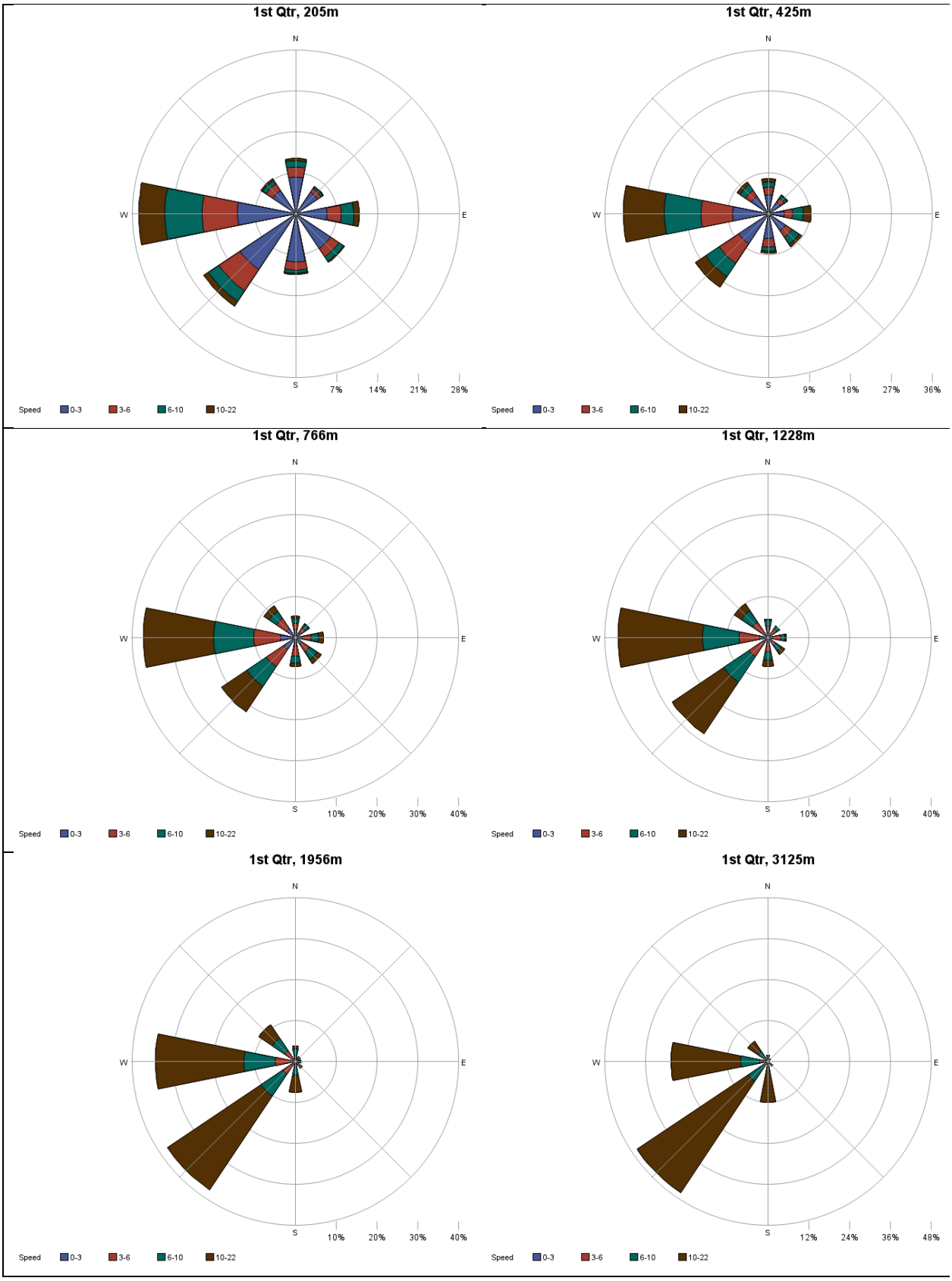
1st Qtr, 205m
N
W
E
S
7%
14%
21%
28%
Speed
0-3
3-6
6-10
10-22
1st Qtr, 425m
N
W
E
S
9%
18%
27%
36%
Speed
0-3
3-6
6-10
10-22
1st Qtr, 766m
N
W
E
S
10%
20%
30%
40%
Speed
0-3
3-6
6-10
10-22
1st Qtr, 1228m
N
W
E
S
10%
20%
30%
40%
Speed
0-3
3-6
6-10
10-22
1st Qtr, 1956m
N
W
E
S
10%
20%
30%
40%
Speed
0-3
3-6
6-10
10-22
1st Qtr, 3125m
N
W
E
S
12%
24%
36%
48%
Speed
0-3
3-6
6-10
10-22

Wind roses

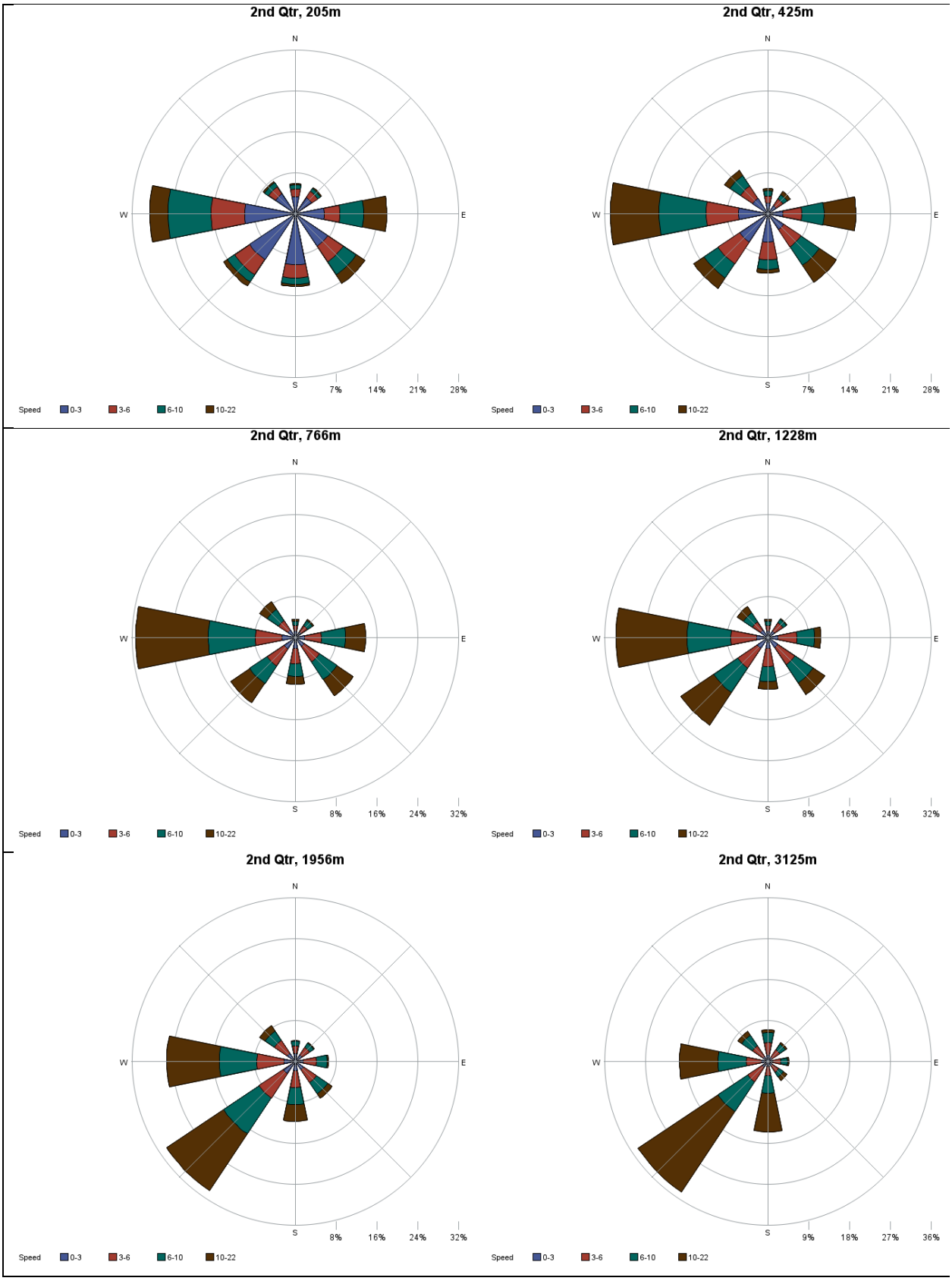
2nd Qtr, 205m
N
W
E
S
7%
14%
21%
28%
Speed
0-3
3-6
6-10
10-22
2nd Qtr, 425m
N
W
E
S
7%
14%
21%
28%
Speed
0-3
3-6
6-10
10-22
2nd Qtr, 766m
N
W
E
S
8%
16%
24%
32%
Speed
0-3
3-6
6-10
10-22
2nd Qtr, 1228m
N
W
E
S
8%
16%
24%
32%
Speed
0-3
3-6
6-10
10-22
2nd Qtr, 1956m
N
W
E
S
8%
16%
24%
32%
Speed
0-3
3-6
6-10
10-22
2nd Qtr, 3125m
N
W
E
S
9%
18%
27%
36%
Speed
0-3
3-6
6-10
10-22

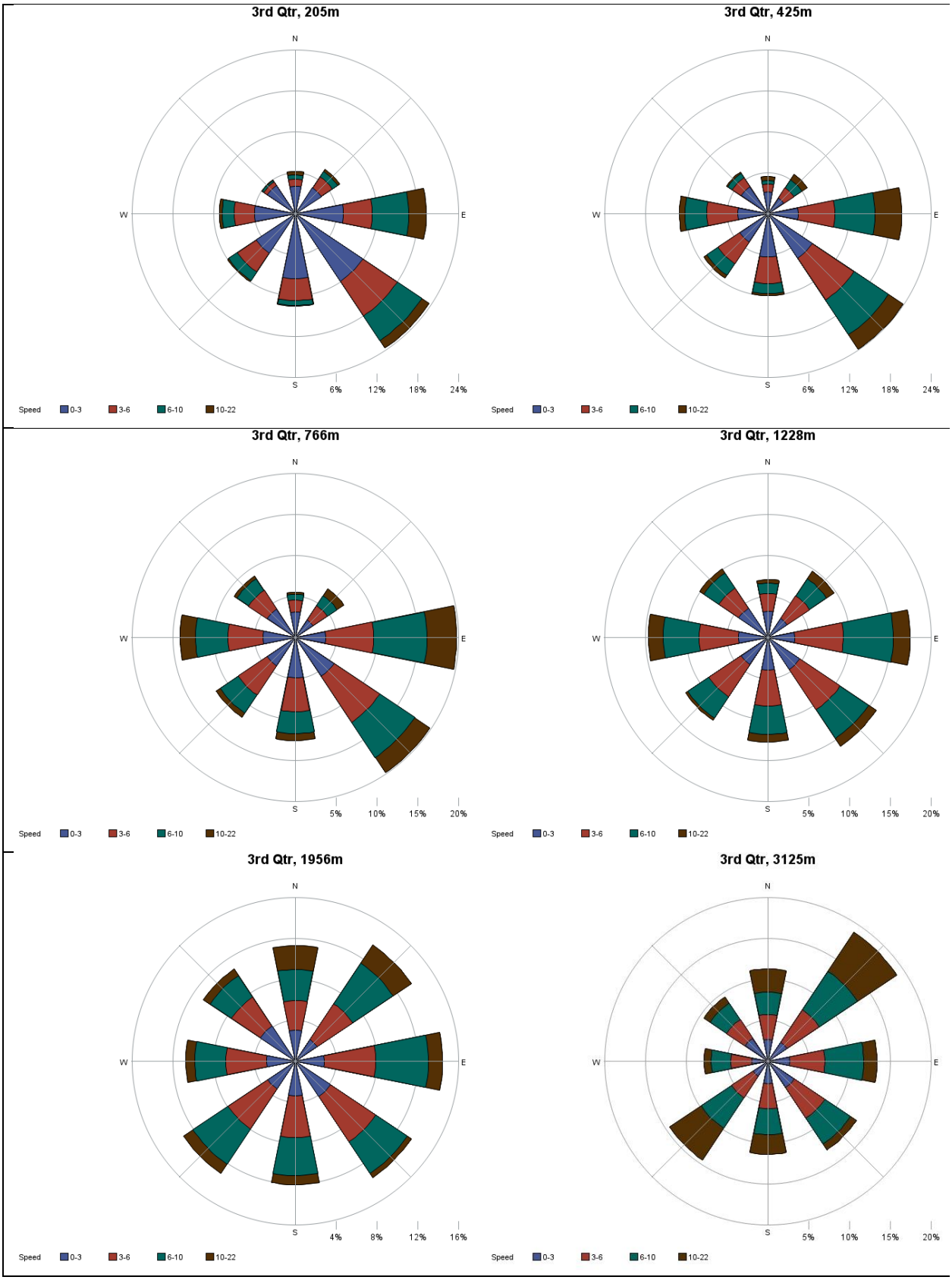
3rd Qtr, 205m
N
W
E
S
6%
12%
18%
24%
Speed
0-3
3-6
6-10
10-22
3rd Qtr, 425m
N
W
E
S
6%
12%
18%
24%
Speed
0-3
3-6
6-10
10-22
3rd Qtr, 766m
N
W
E
S
5%
10%
15%
20%
Speed
0-3
3-6
6-10
10-22
3rd Qtr, 1228m
N
W
E
S
5%
10%
15%
20%
Speed
0-3
3-6
6-10
10-22
3rd Qtr, 1956m
N
W
E
S
4%
8%
12%
16%
Speed
0-3
3-6
6-10
10-22
3rd Qtr, 3125m
N
W
E
S
5%
10%
15%
20%
Speed
0-3
3-6
6-10
10-22

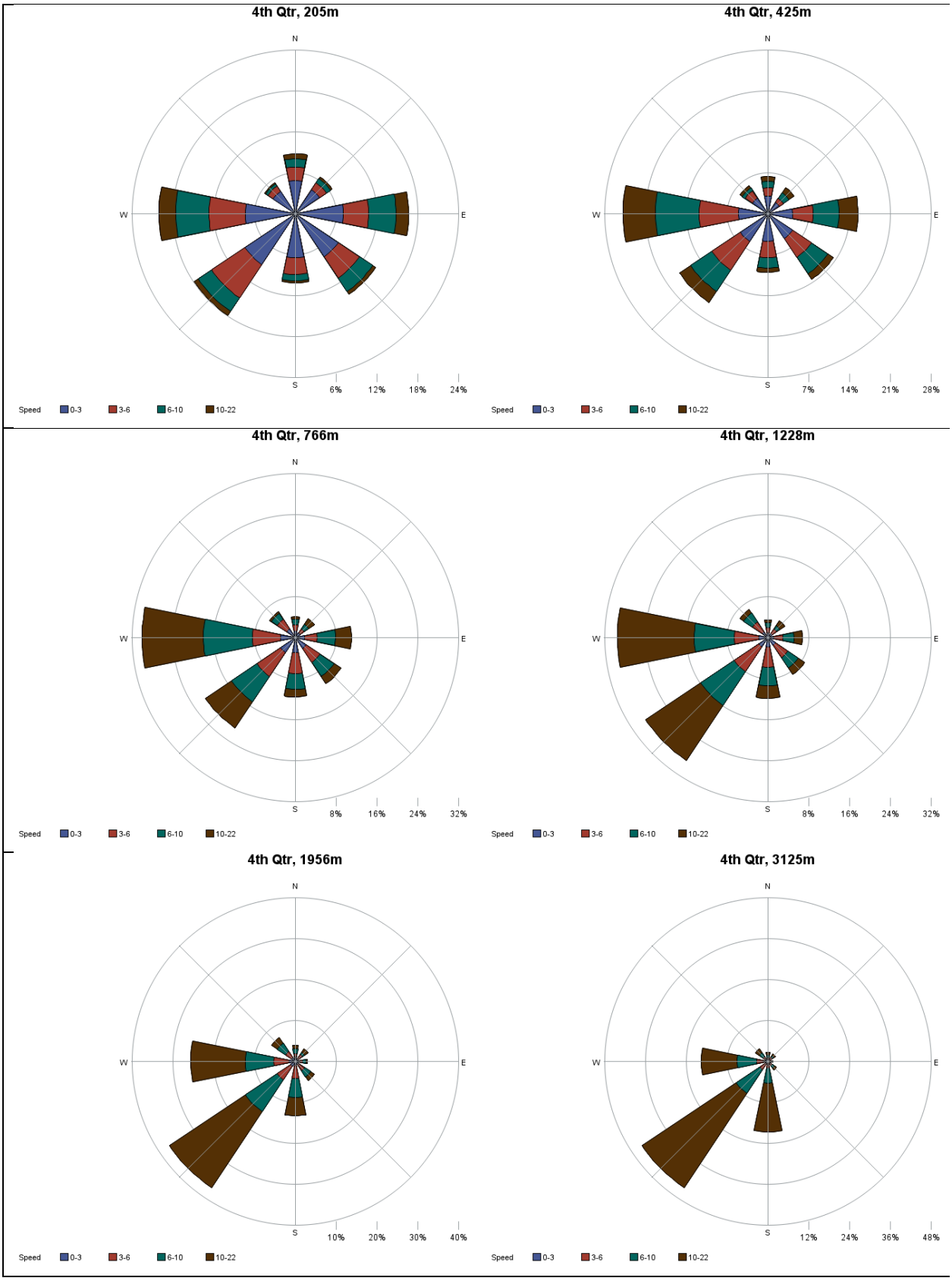
4th Qtr, 205m
N
W
E
S
6%
12%
18%
24%
Speed
0-3
3-6
6-10
10-22
4th Qtr, 425m
N
W
E
S
7%
14%
21%
28%
Speed
0-3
3-6
6-10
10-22
4th Qtr, 766m
N
W
E
S
8%
16%
24%
32%
Speed
0-3
3-6
6-10
10-22
4th Qtr, 1228m
N
W
E
S
8%
16%
24%
32%
Speed
0-3
3-6
6-10
10-22
4th Qtr, 1956m
N
W
E
S
10%
20%
30%
40%
Speed
0-3
3-6
6-10
10-22
4th Qtr, 3125m
N
W
E
S
12%
24%
36%
48%
Speed
0-3
3-6
6-10
10-22

### 4.5 Summer Time of Day Assessment

An assessment of the distribution of high $O_3$ days in El Paso showed that the large majority of days fell in June, July, and August. June is considered a spring month and July and August are summer months. Specifically, over the four-year period of 2015 – 2018, El Paso experienced 37 days with 8-hour $O_3$ exceedances of the National Ambient Air Quality Standard for ozone. All exceedance days occurred between May and September. One way to express the severity of an $O_3$ exceedance day is by counting the number of stations with exceedance on a day. Over this four-year period there were 80 "Monitor-Exceedance Days", so on average two or more monitors had exceedances on exceedance days. A total of 86 percent of exceedance days occurred in June, July, or August, and 90 percent of "Monitor-Exceedance Days" occurred in these three months. The distribution of $O_3$ exceedance days by month from 2015 to 2018 appears in Figure 26.

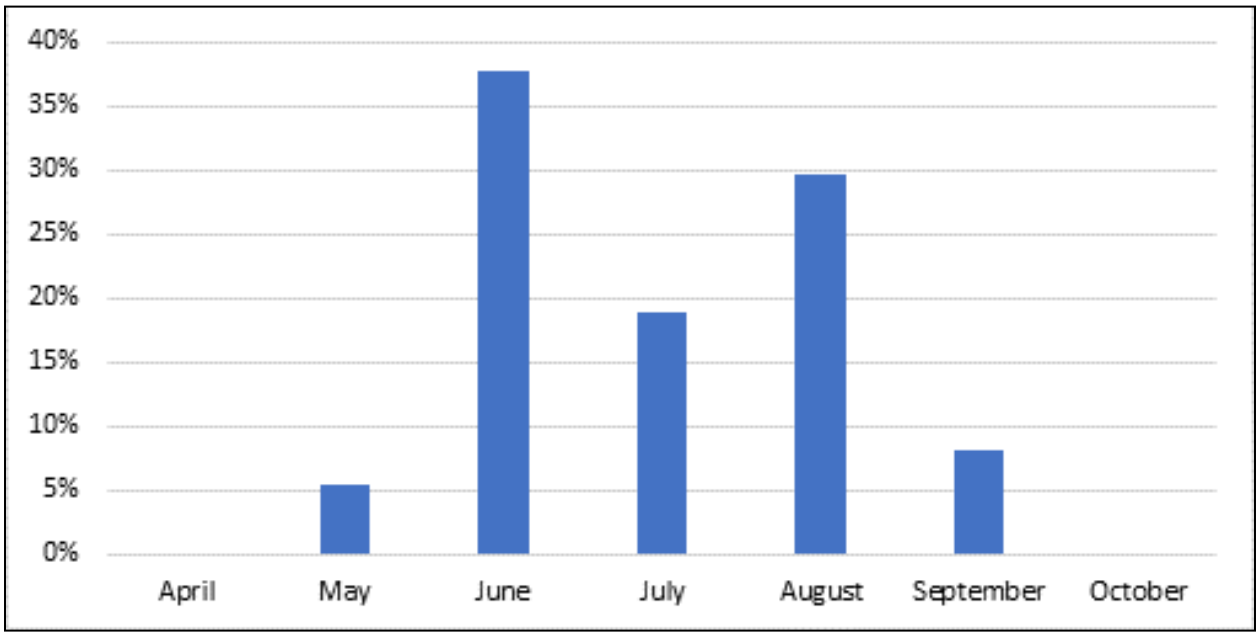


Figure 26. The distribution of El Paso 8-hour O3 exceedance days by month from 2015 to 2018

Based on the major $O_3$ problem being associated with these three months, in this section wind roses are shown for June through August to characterize the winds during these months,

which can be compared to the roses on the high $O_3$ days to look for how high $O_3$ days differ from all ozone season days.

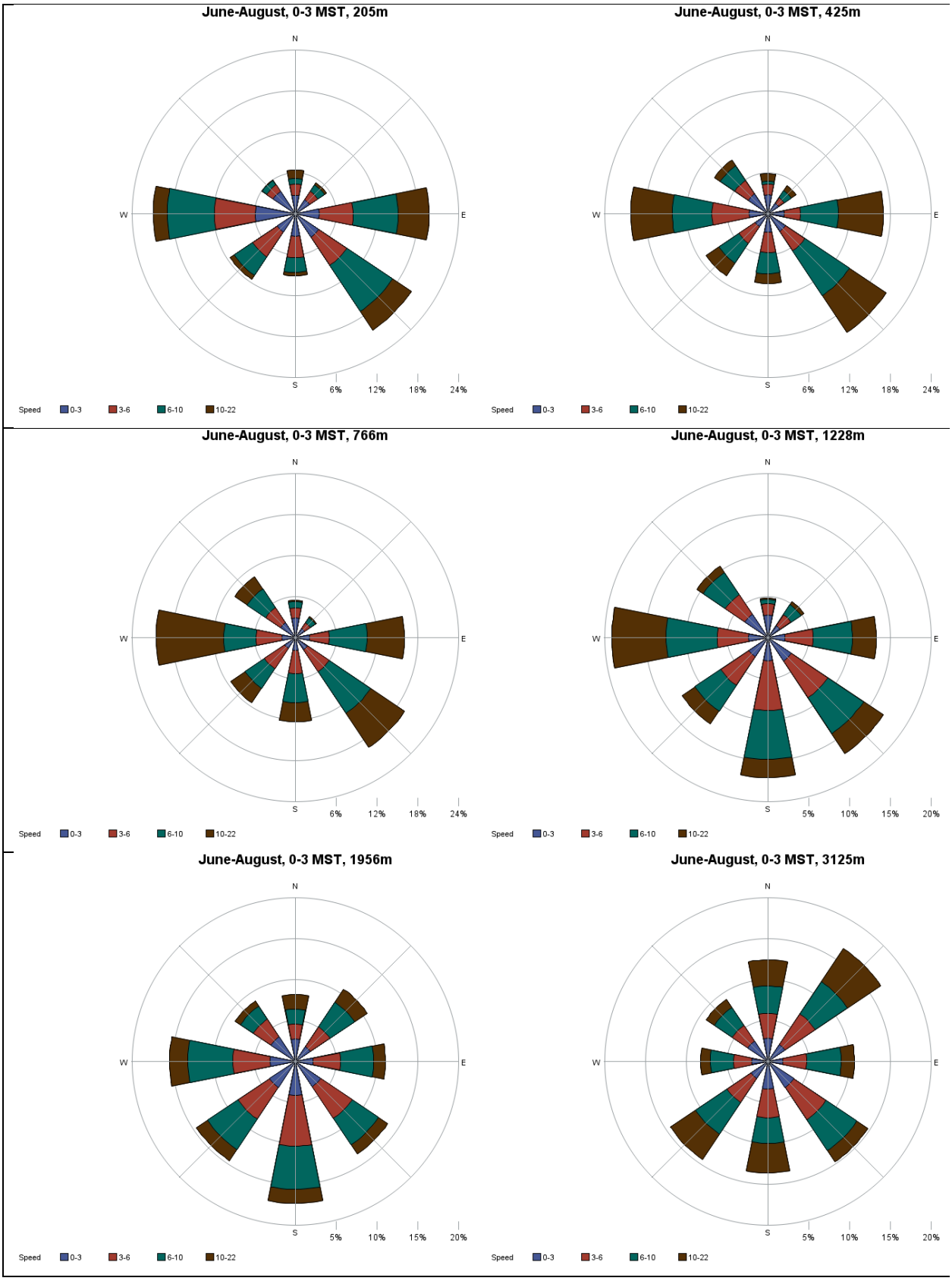
June-August, 0-3 MST, 205m
June-August, 0-3 MST, 425m
June-August, 0-3 MST, 766m
June-August, 0-3 MST, 1228m
June-August, 0-3 MST, 1956m
June-August, 0-3 MST, 3125m
N
E
S
W
6%
12%
18%
24%
5%
10%
15%
20%
Speed
0-3
3-6
6-10
10-22

Wind roses.

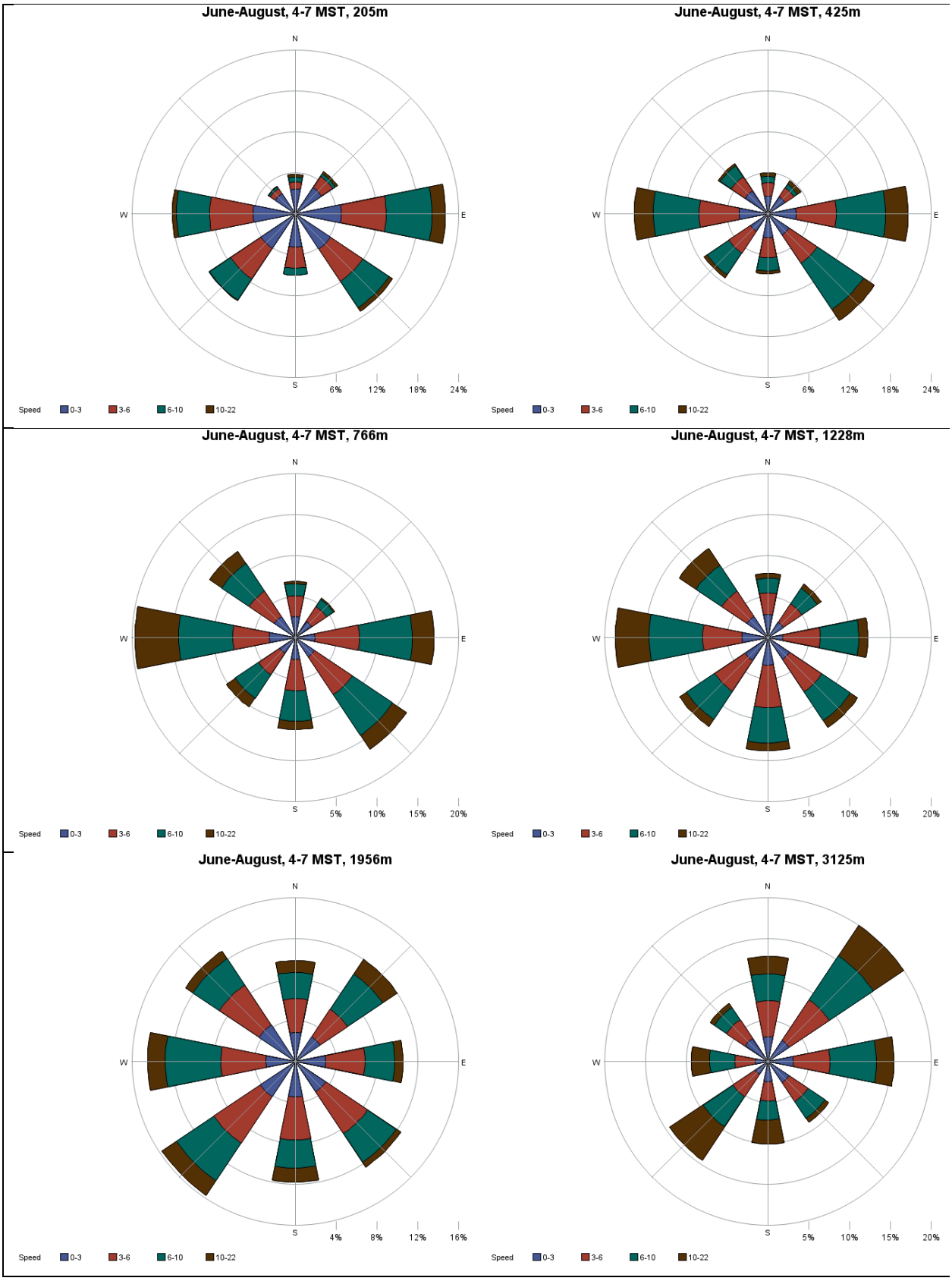
June-August, 4-7 MST, 205m
N
W
E
S
6%
12%
18%
24%
Speed
0-3
3-6
6-10
10-22
June-August, 4-7 MST, 425m
N
W
E
S
6%
12%
18%
24%
Speed
0-3
3-6
6-10
10-22
June-August, 4-7 MST, 766m
N
W
E
S
5%
10%
15%
20%
Speed
0-3
3-6
6-10
10-22
June-August, 4-7 MST, 1228m
N
W
E
S
5%
10%
15%
20%
Speed
0-3
3-6
6-10
10-22
June-August, 4-7 MST, 1956m
N
W
E
S
4%
8%
12%
16%
Speed
0-3
3-6
6-10
10-22
June-August, 4-7 MST, 3125m
N
W
E
S
5%
10%
15%
20%
Speed
0-3
3-6
6-10
10-22

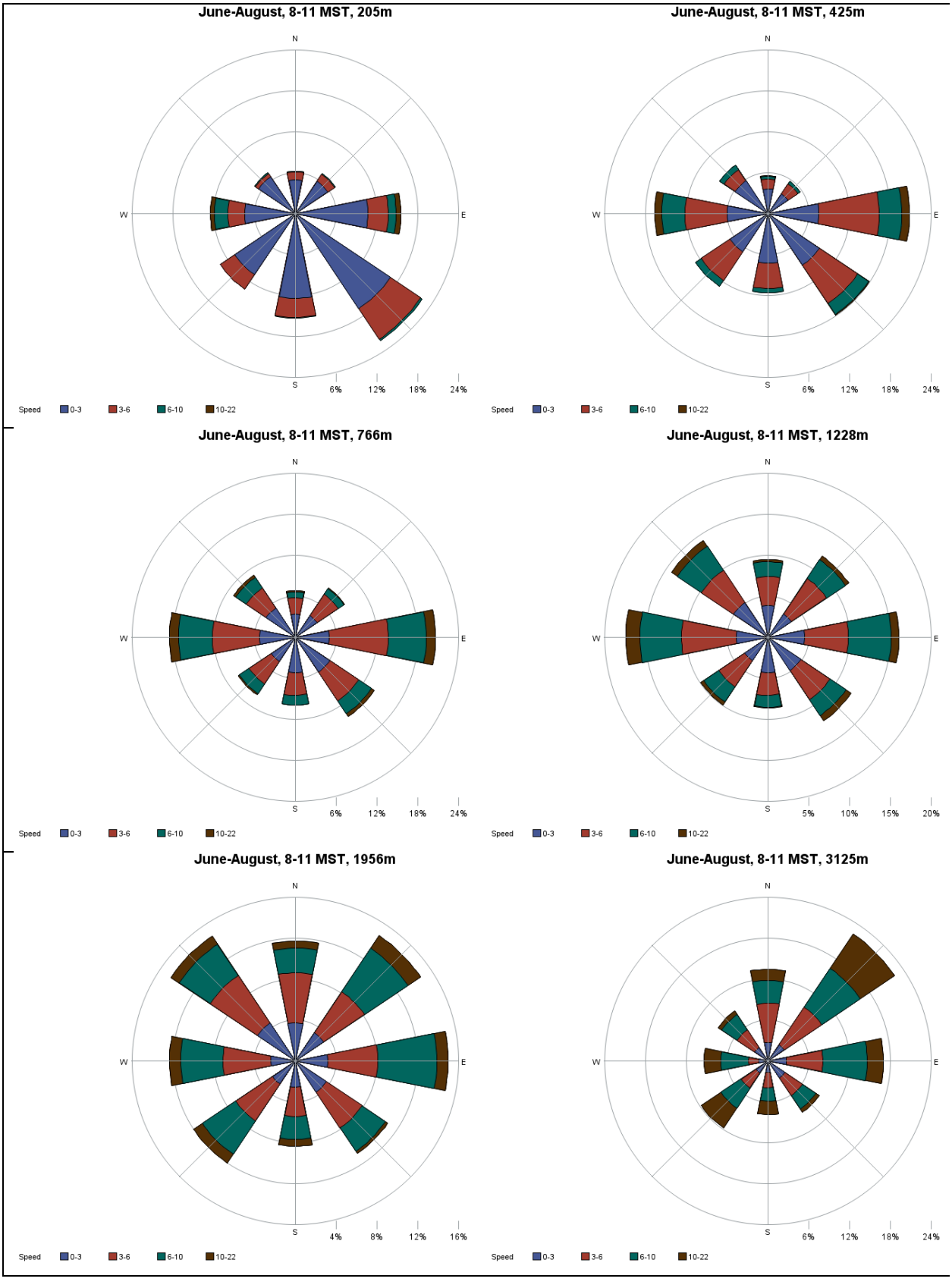
June-August, 8-11 MST, 205m
N
W
E
S
6%
12%
18%
24%
Speed
0-3
3-6
6-10
10-22
June-August, 8-11 MST, 425m
N
W
E
S
6%
12%
18%
24%
Speed
0-3
3-6
6-10
10-22
June-August, 8-11 MST, 766m
N
W
E
S
6%
12%
18%
24%
Speed
0-3
3-6
6-10
10-22
June-August, 8-11 MST, 1228m
N
W
E
S
5%
10%
15%
20%
Speed
0-3
3-6
6-10
10-22
June-August, 8-11 MST, 1956m
N
W
E
S
4%
8%
12%
16%
Speed
0-3
3-6
6-10
10-22
June-August, 8-11 MST, 3125m
N
W
E
S
6%
12%
18%
24%
Speed
0-3
3-6
6-10
10-22

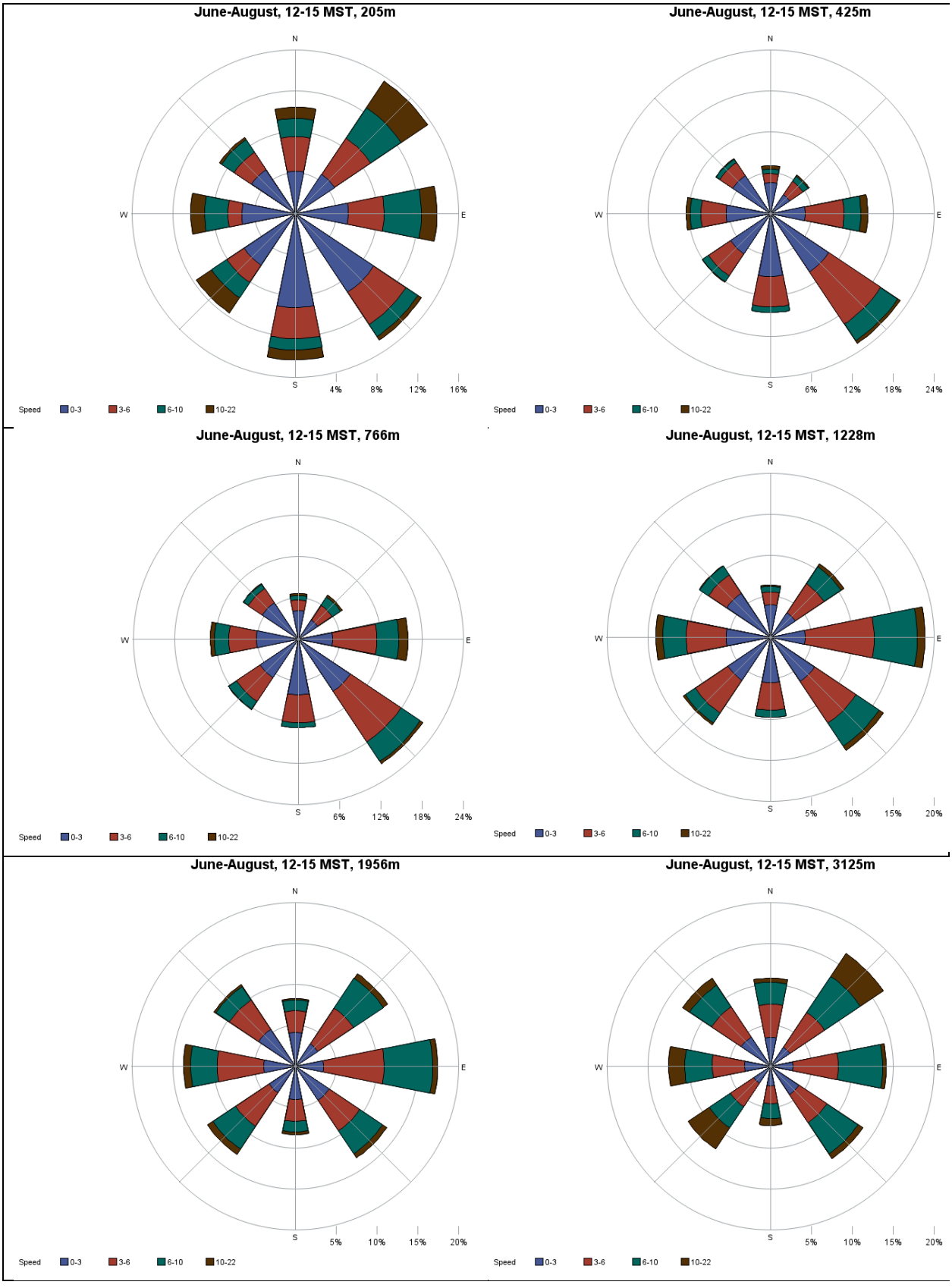
June-August, 12-15 MST, 205m
N
W
E
S
4%
8%
12%
16%
Speed
0-3
3-6
6-10
10-22
June-August, 12-15 MST, 425m
N
W
E
S
6%
12%
18%
24%
Speed
0-3
3-6
6-10
10-22
June-August, 12-15 MST, 766m
N
W
E
S
6%
12%
18%
24%
Speed
0-3
3-6
6-10
10-22
June-August, 12-15 MST, 1228m
N
W
E
S
5%
10%
15%
20%
Speed
0-3
3-6
6-10
10-22
June-August, 12-15 MST, 1956m
N
W
E
S
5%
10%
15%
20%
Speed
0-3
3-6
6-10
10-22
June-August, 12-15 MST, 3125m
N
W
E
S
5%
10%
15%
20%
Speed
0-3
3-6
6-10
10-22

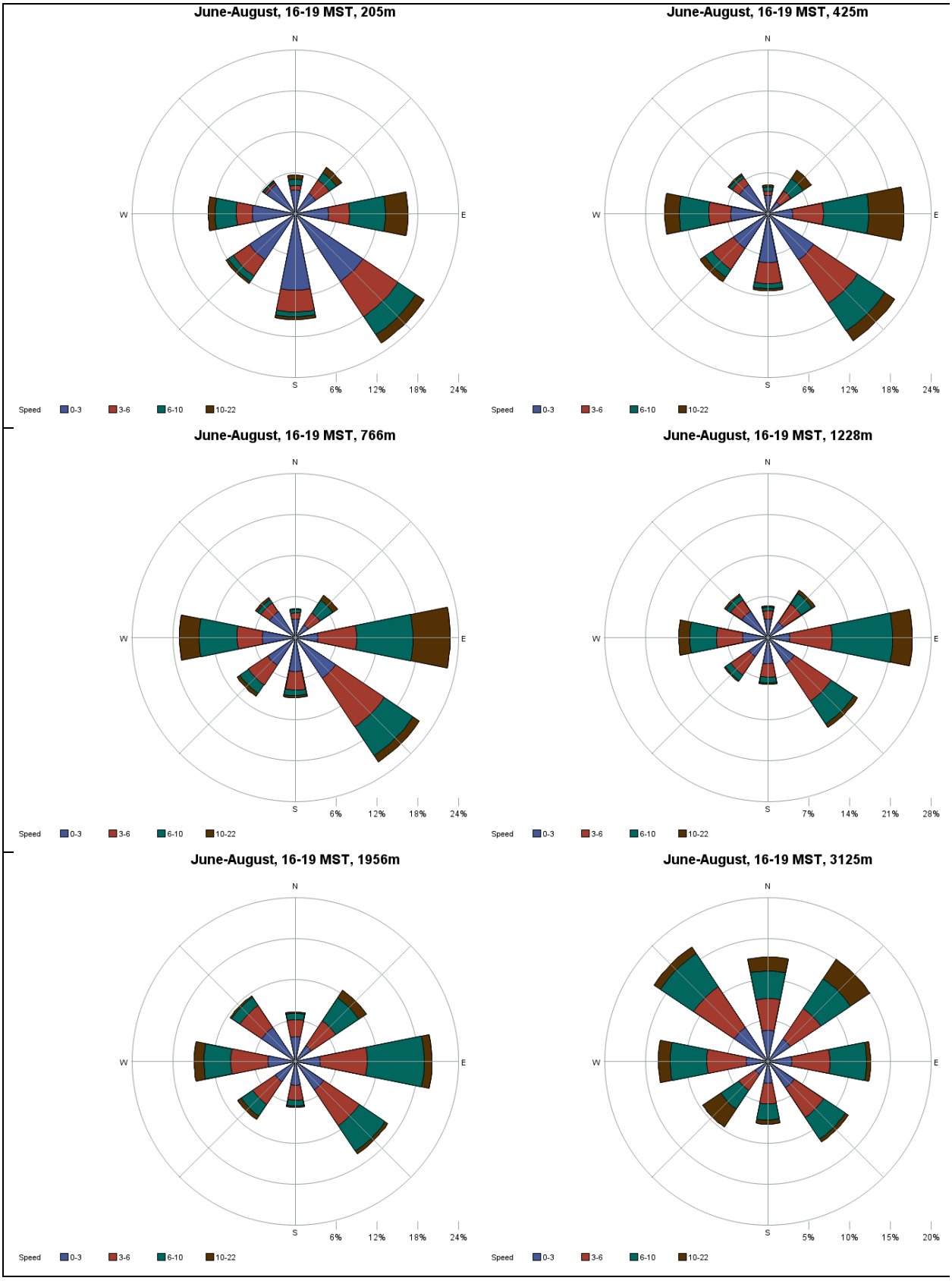
June-August, 16-19 MST, 205m
N
W
E
S
6%
12%
18%
24%
Speed
0-3
3-6
6-10
10-22
June-August, 16-19 MST, 425m
N
W
E
S
6%
12%
18%
24%
Speed
0-3
3-6
6-10
10-22
June-August, 16-19 MST, 766m
N
W
E
S
6%
12%
18%
24%
Speed
0-3
3-6
6-10
10-22
June-August, 16-19 MST, 1228m
N
W
E
S
7%
14%
21%
28%
Speed
0-3
3-6
6-10
10-22
June-August, 16-19 MST, 1956m
N
W
E
S
6%
12%
18%
24%
Speed
0-3
3-6
6-10
10-22
June-August, 16-19 MST, 3125m
N
W
E
S
5%
10%
15%
20%
Speed
0-3
3-6
6-10
10-22

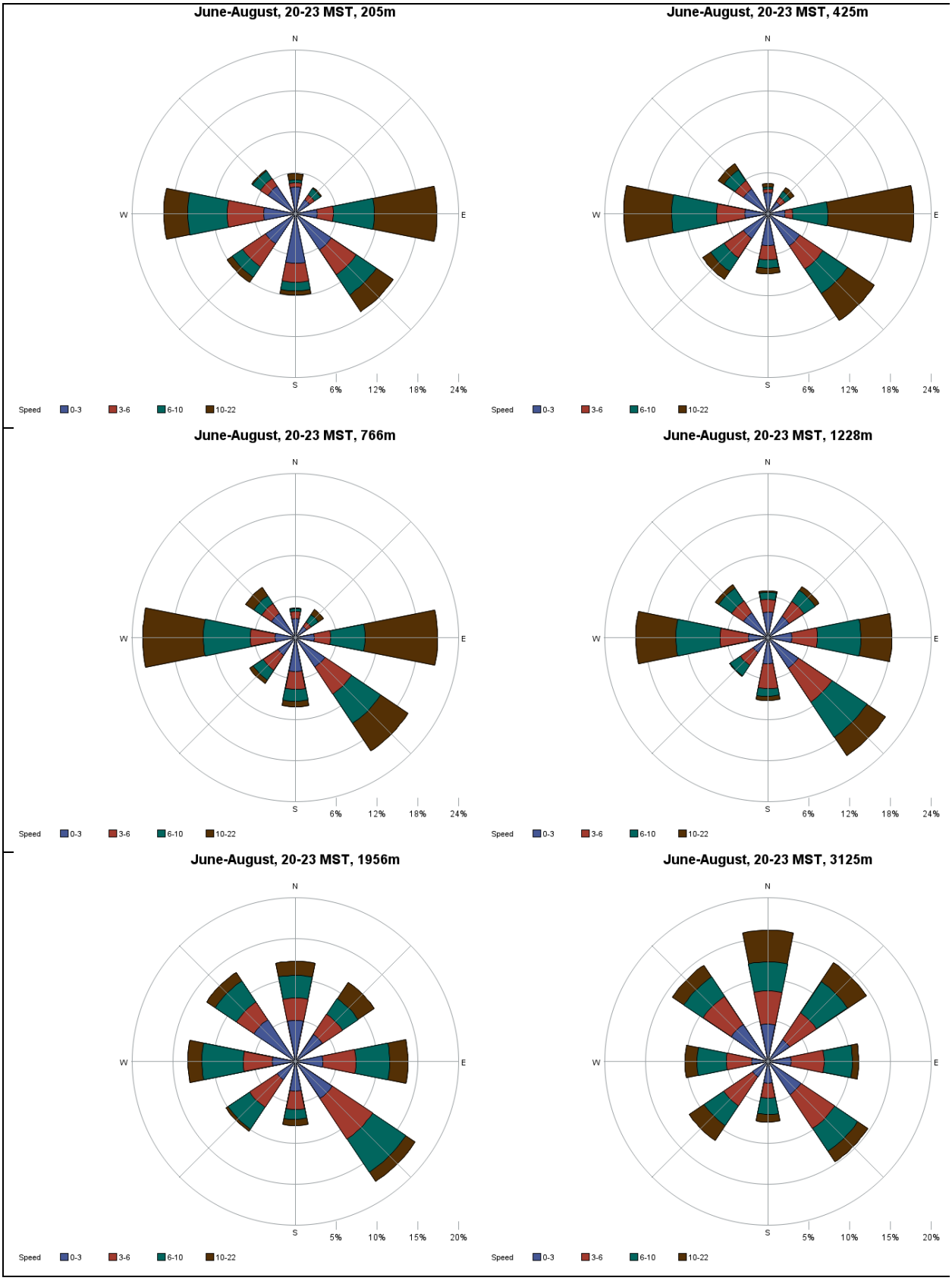
June-August, 20-23 MST, 205m
June-August, 20-23 MST, 425m
June-August, 20-23 MST, 766m
June-August, 20-23 MST, 1228m
June-August, 20-23 MST, 1956m
June-August, 20-23 MST, 3125m
N
E
S
W
6%
12%
18%
24%
5%
10%
15%
20%
Speed
0-3
3-6
6-10
10-22

### 4.6 CHARACTERIZATION OF HIGH OZONE DAYS COMPARED TO JUNE-AUGUST DAYS

As noted earlier, El Paso experienced 37 $O_3$ exceedance days over the 2015 to 2018 period. In this section the wind roses for these days are shown. Since daily highest $O_3$ concentrations are generally 10 MST to 18 MST, only hours 0 – 18 MST have been used in these wind roses. Wind roses from the exceedance days combined are shown next the all June-August days with hours from only hours 0 – 18 MST.

In examining the wind roses, the following observations can be made.

- $O_3$ Exc. Days: more S.E. winds at low altitudes
- $O_3$ Exc. Days: more S winds at 1.2 km
- $O_3$ Exc. Days: more N.W. winds at 2 km
- $O_3$ Exc. Days: more N winds at 3 km

A preliminary conclusion from this comparison could be that emissions from along the Rio Grande / Rio Bravo and from south of the Border with Mexico could contribute to elevated $O_3$ in El Paso based on lower altitude winds, but that also transport from the Continental United States could contribute based on higher altitude winds.

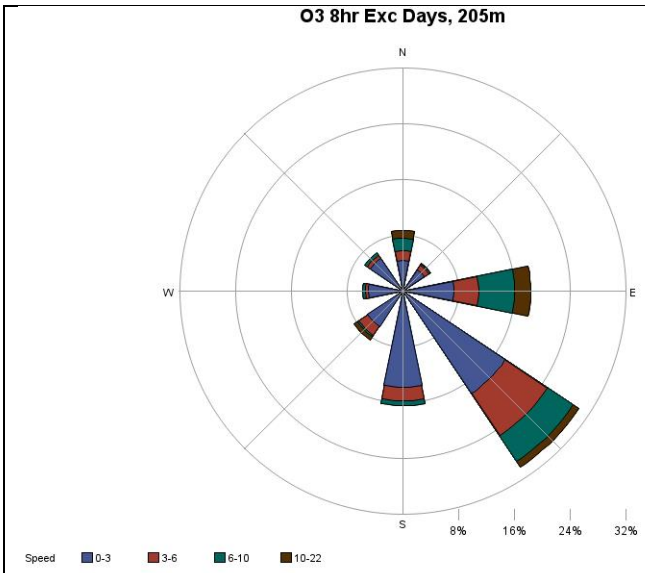
O3 8hr Exc Days, 205m
N
W
E
S
8%
16%
24%
32%
Speed
0-3
3-6
6-10
10-22

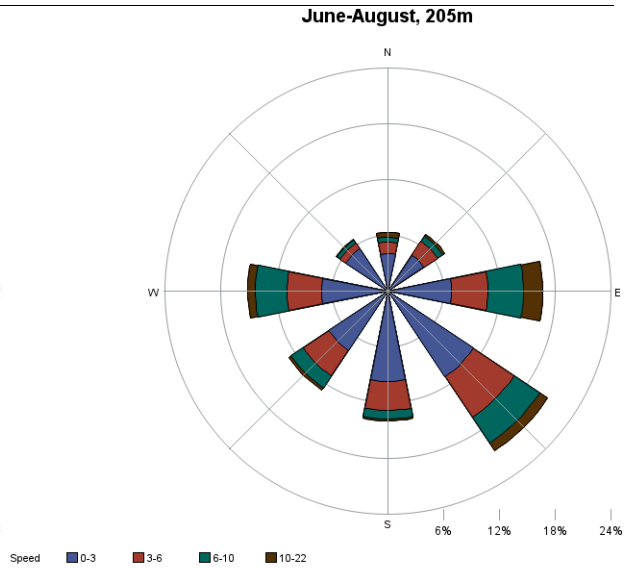
June-August, 205m
N
W
E
S
6%
12%
18%
24%
Speed
0-3
3-6
6-10
10-22

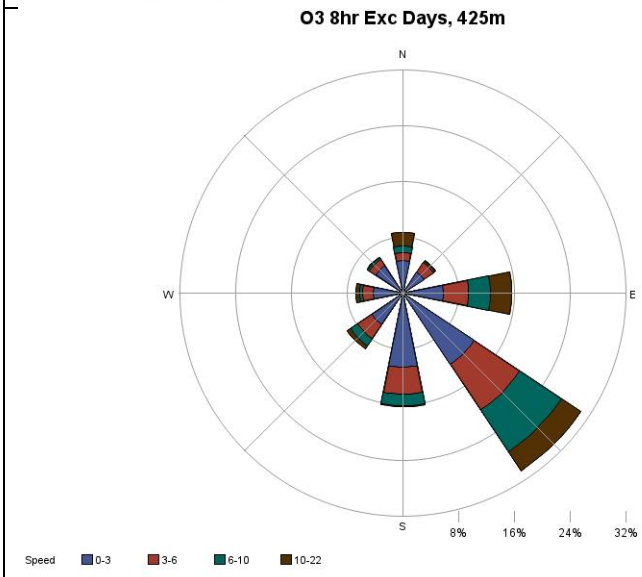
O3 8hr Exc Days, 425m
N
W
E
S
8%
16%
24%
32%
Speed
0-3
3-6
6-10
10-22

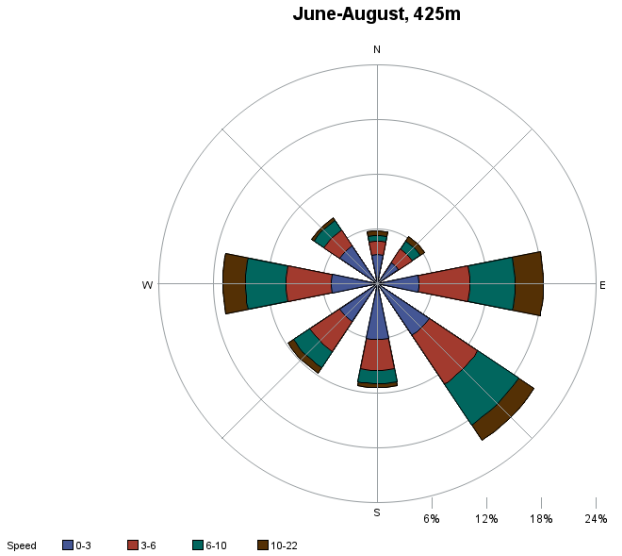
June-August, 425m
N
W
E
S
6%
12%
18%
24%
Speed
0-3
3-6
6-10
10-22

Wind roses

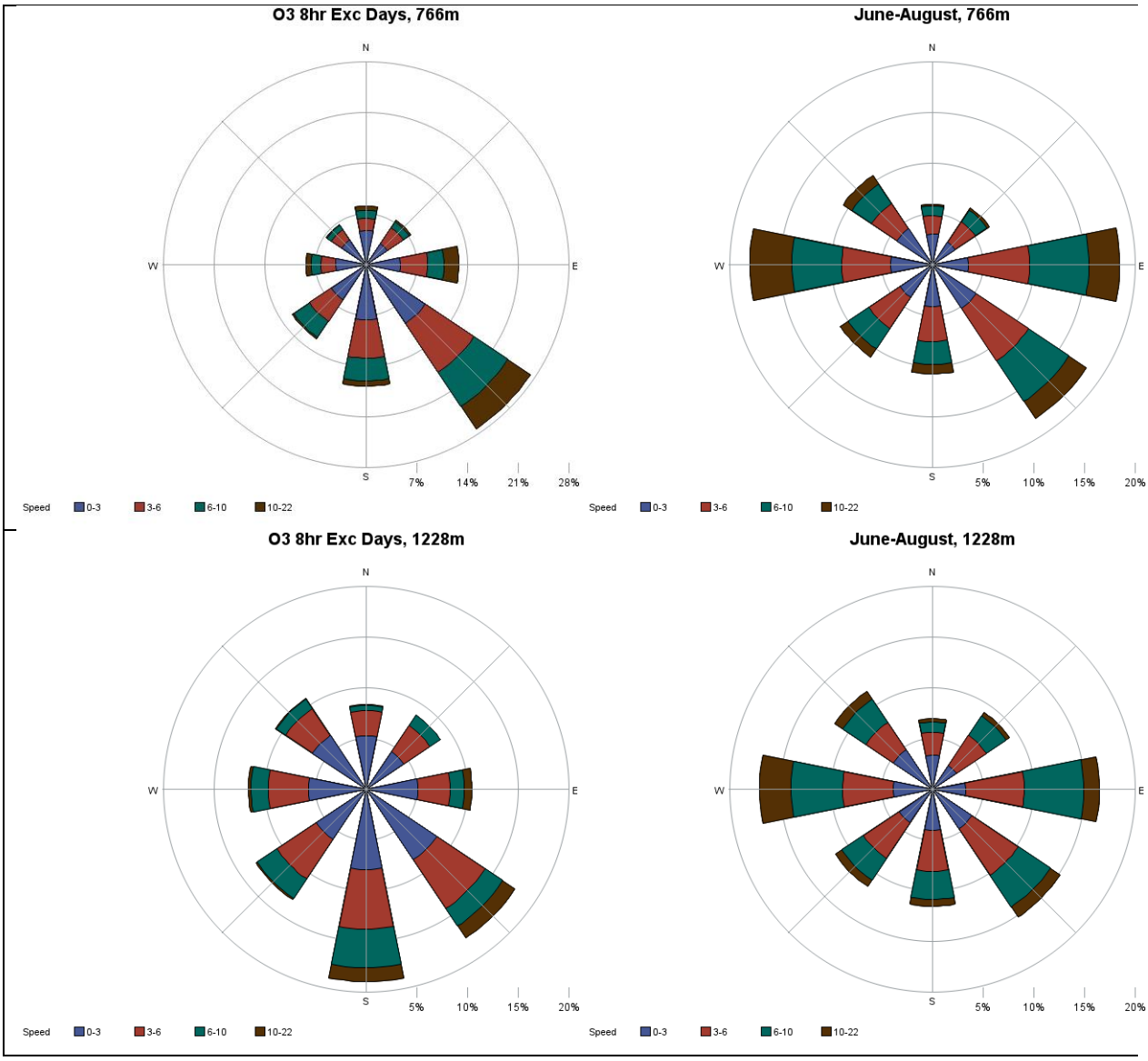
O3 8hr Exc Days, 766m
N
W
E
S
7%
14%
21%
28%
Speed
0-3
3-6
6-10
10-22
June-August, 766m
N
W
E
S
5%
10%
15%
20%
Speed
0-3
3-6
6-10
10-22
O3 8hr Exc Days, 1228m
N
W
E
S
5%
10%
15%
20%
Speed
0-3
3-6
6-10
10-22
June-August, 1228m
N
W
E
S
5%
10%
15%
20%
Speed
0-3
3-6
6-10
10-22

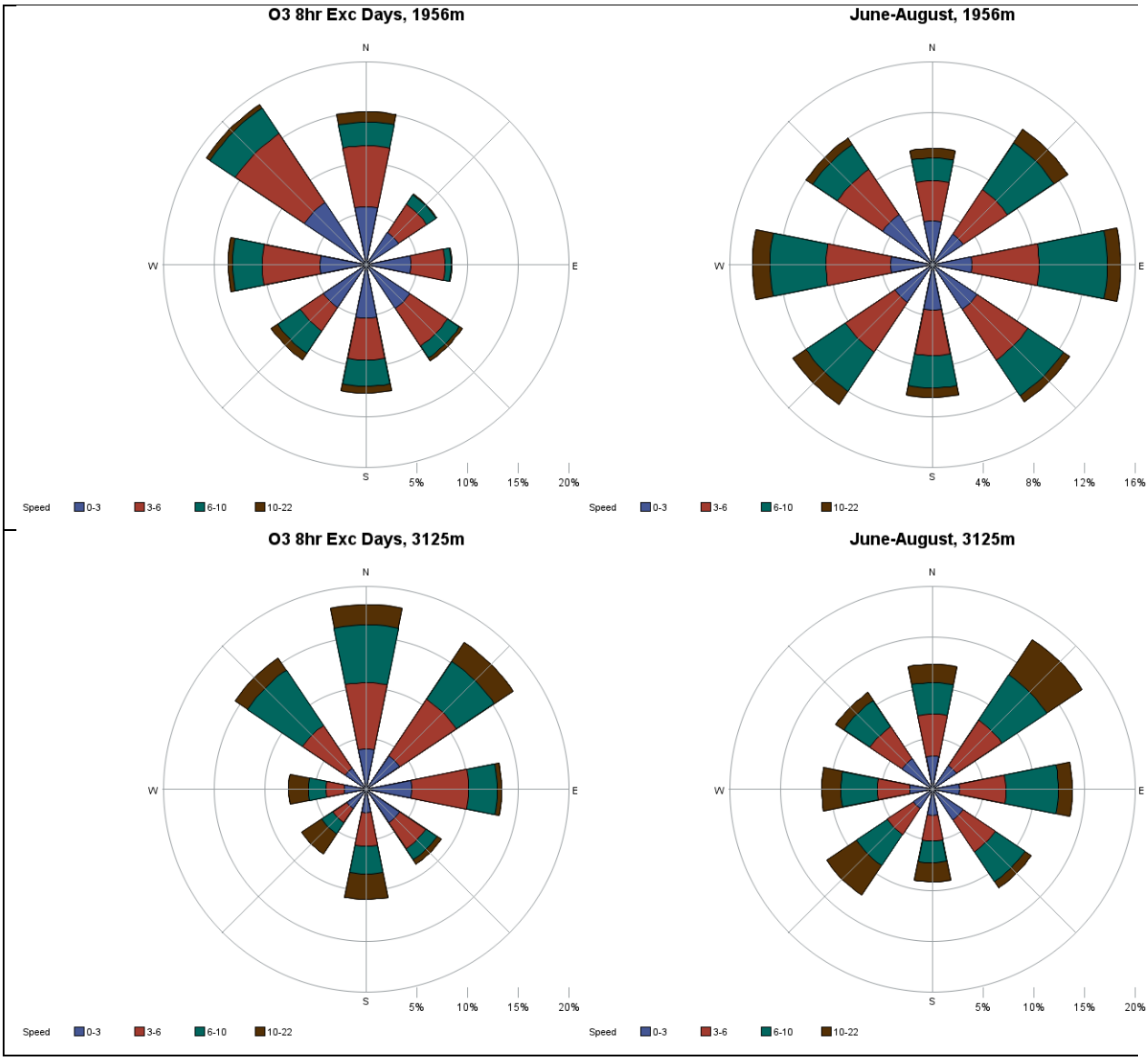
O3 8hr Exc Days, 1956m
June-August, 1956m
O3 8hr Exc Days, 3125m
June-August, 3125m
N
W
E
S
5%
10%
15%
20%
4%
8%
12%
16%
Speed
0-3
3-6
6-10
10-22

## Chapter 5. General Conclusions

This is the first long-term PBL research measurement project and analysis performed in the El Paso-Juarez region. We made long-term diurnal observations regardless of weather conditions with a low-cost Vaisala ceilometer CL31 at UTEP. Vaisala and in-house developed algorithms were used to produce planetary boundary layer heights (PBLH). These measurements were taken over three consecutive years, 2015-17. This study used measurements and modeling to characterize the annual PBL structure of the El Paso-Juarez urban region. The measurements showed the PBLH cycles generally reached greater heights during warm seasons and were reduced during cooler seasons. This is expected due to diurnal and seasonal heating and cooling cycles. However, a diurnal cycle may appear inverted under certain largescale atmospheric conditions.

Another first task for this research was to make a long-term intercomparison between the ceilometer measured PBLH and model simulations. The ceilometer PBLH data for the entire measurement period of three years were sufficiently statistically significant to intercompare with models. The model used was the HYbrid Single- Particle Lagrangian Integrated Trajectory (HYSPLIT) produced and maintained by the National Oceanic and Atmospheric Administration's Air Resources Laboratory (NOAA-ARL). HYSPLIT is a Lagrangian model that utilizes meteorological fields that are input by the user. HYSPLIT examines PBL potential temperature data to characterize the inversion height and to estimate PBLH. The procedures used by HYSPLIT tend to give higher bias to higher PBLHs and to underestimate the effects of shallow stable layers near the ground. This HYSPLIT bias emphases the need for our ceilometer which determines the top of the aerosol layer as a proxy of the PBL height based on aerosol gradient methods that may observe the effects of shallow stable layers better than models. This difference between the model and ceilometer methods in determining the PBLH is a major reason for the discrepancies between the experimental and simulated PBLH we found.

It was observed that the model underestimated the nocturnal boundary layer (NBL) heights almost throughout the year, with NBL height as low as 15 m. Whereas the ceilometer estimated

reasonable NBL heights, and it varied throughout the year based on the season. The lowest ceilometer estimated NBL height was around 120 m, mostly during the winter season. Going by the minimum resolution of the meteorological input data for the HYSPLIT model as described by [18], it will be fair to assume a simulated minimum depth of 250 m, especially in the case of NBL.

A weak agreement of the PBL height on both the day hours and certain days of the season has been found at the research site compared to the ones typically reported globally, most likely due to the complex topography surrounding the monitoring site. The typical diurnal fluctuation of PBL height between the experiment and model was around 1-2 km. This discrepancy in PBL height usually increased in the early hours, peaking about midday. We discovered that the model's PBL height was quite extreme on some days, especially during the summer. The best agreement between the daytime experimental and modeled PBLHs was found during the winter season.

Over the four years of 2015 – 2018, El Paso experienced 37 days with 8-hour $O_3$ exceedances of the National Ambient Air Quality Standard for ozone. All exceedance days Days," so on average, two or more monitors had exceedances on exceedance days. A total of 86 percent of exceedance days occurred in June, July, or August, and 90 percent of "Monitor-Exceedance Days" occurred in these three months. It was observed that during the high ozone event, PBL height was low (shallow), i.e., well below 2 km, and the low ozone days were marked with high PBL, precipitation, and strong winds due to synoptic scale influence. Lower PBLHs implied less volume available for the pollution dispersion and lower vertical mixing. Conversely, deeper PBLH during the low ozone (clean day) leads to precursors' dilution and lower ozone concentration.

A detailed case study regarding the influence of the PBL on ozone events is published by the group in Karle et al. 2020 [reference 9]. Using the case study of the consecutive high and low ozone episodes, we showed that the slow growth in the PBLH in the morning and calm winds during the daytime significantly contributed to high ozone episodes. All the high ozone episodes in the case study had low wind speed, whereas the low ozone events had strong winds. During all the high ozone events, the wind direction was from the East of El Paso. No strong correlation between the modeled daytime PBLH peak and ozone concentration peak was observed during the study.

In addition to the ceilometer and modeling research, this report examined three full years of recent measurements from the RWP operated by the TCEQ in El Paso, TX. The data provide a

means to show the effect of altitude on wind speed, and to depict the behavior of winds during the day, by the time of year. Comparison of upper air winds of high ozone days with all summer days shows that there are differences which may suggest upwind source regions.

Additional work not yet addressed includes using RWP signal to noise ratio data and the rates of wind speed and direction change in relatively short altitude steps to identify boundary layer heights roughly. The RWP research remains in a test-phase and is less accurate than radio acoustic sounding systems (RASS) or the use of ceilometers.

Certain parts of this work was published in the following journal papers:

[reference 9] N. N. Karle, S. Mahmud, R. K. Sakai, R. M. Fitzgerald, V. R. Morris, and W. R. Stockwell, "Investigation of the Successive Ozone Episodes in the El Paso–Juarez Region in the Summer of 2017," Atmosphere (Basel)., vol. 11, no. 5, p. 532, May 2020.

Fitzgerald, R.M., N.N. Karle, J. Polanco, W.R. Stockwell, Optical Measurements of Particulate Matter in the El Paso–Juarez Region: Natural Mineral Dust and Soot, Environmental Manager, Accepted July 29, 2021.

Currently there are 2 manuscripts in preparation, related to some parts of this work.

## References


[1] D. R. Stewart, E. Saunders, R. A. Perea, R. Fitzgerald, D. E. Campbell, and W. R. Stockwell, "Linking Air Quality and Human Health Effects Models: An Application to the Los Angeles Air Basin," *Environ. Health Insights*, vol. 11, p. 1178630217737551, 2017.

[2] R. Pearson and R. Fitzgerald, "Application of a Wind Model for the El Paso-Juarez Airshed," *J. Air Waste Manag. Assoc. J. J. Air Waste Manag. Assoc.*, vol. 51, no. 5, pp. 1096–2247, 2001.

[3] C. Shi, H. J. S. Fernando, and J. Yang, "Contributors to ozone episodes in three U.S./Mexico border twin-cities," *Sci. Total Environ.*, vol. 407, no. 18, pp. 5128–5138, Sep. 2009.

[4] R. Medina, R. M. Fitzgerald, and Q. Min, "Retrieval of the single scattering albedo in the El Paso-Juarez Airshed using the TUV model and a UV-MFRSR radiometer," *Atmos. Environ.*, vol. 46, pp. 430–440, Jan. 2012.

[5] C. P. MacDonald, P. T. Roberts, H. H. Main, T. S. Dye, D. L. Coe, and J. Yarbrough, "The 1996 Paso del Norte Ozone Study: analysis of meteorological and air quality data that influence local ozone concentrations," *Sci. Total Environ.*, vol. 276, no. 1–3, pp. 93–109, Aug. 2001.

[6] R. B. Stull, *An introduction to boundary layer meteorology*. Kluwer Academic Publishers, 1988.

[7] S. Emeis, *Surface-Based Remote Sensing of the Atmospheric Boundary Layer*, vol. 40. Dordrecht: Springer Netherlands, 2011.

[8] G. A. Athanassiadis, S. T. Rao, J.-Y. Ku, and R. D. Clark, "Boundary Layer Evolution

and its Influence on Ground-Level Ozone Concentrations," *Environ. Fluid Mech.*, vol. 2, no. 4, pp. 339–357, 2002.

[9] N. N. Karle, S. Mahmud, R. K. Sakai, R. M. Fitzgerald, V. R. Morris, and W. R. Stockwell, "Investigation of the Successive Ozone Episodes in the El Paso–Juarez Region in the Summer of 2017," *Atmosphere (Basel).*, vol. 11, no. 5, p. 532, May 2020.

[10] N. Karle *et al.*, "Analysis of Regional Meteorology During the Ozone Episodes in the El Paso—Juarez Airshed in the Summer of 2017." AMS, Jan-2019.

[11] R. (Roland) Stull, "Practical Meteorology: an algebra based survey of atmospheric science," *https://www.eoas.ubc.ca/books/Practical_Meteorology/*, 2016.

[12] C. Münkel, N. Eresmaa, J. Räsänen, and A. Karppinen, "Retrieval of mixing height and dust concentration with lidar ceilometer," *Boundary-Layer Meteorol.*, vol. 124, no. 1, pp. 117–128, Jun. 2007.

[13] G. Tsaknakis *et al.*, "Atmospheric Measurement Techniques Inter-comparison of lidar and ceilometer retrievals for aerosol and Planetary Boundary Layer profiling over Athens, Greece," *Atmos. Meas. Tech*, vol. 4, pp. 1261–1273, 2011.

[14] M. Hicks, R. Sakai, and E. Joseph, "The Evaluation of a New Method to Detect Mixing Layer Heights Using Lidar Observations," *J. Atmos. Ocean. Technol.*, vol. 32, no. 11, pp. 2041–2051, Nov. 2015.

[15] J. C. Compton, R. Delgado, T. A. Berkoff, and R. M. Hoff, "Determination of planetary boundary layer height on short spatial and temporal scales: A demonstration of the covariance wavelet transform in ground-based wind profiler and lidar measurements," *J. Atmos. Ocean. Technol.*, vol. 30, no. 7, pp. 1566–1575, 2013.

[16] I. S. Stachlewska, M. Piądłowski, S. Migacz, A. Szkop, A. J. Zielińska, and P. L.

Swaczyna, “Ceilometer observations of the boundary layer over Warsaw, Poland,” *Acta Geophys. 2012 605*, vol. 60, no. 5, pp. 1386–1412, Sep. 2012.

[17] N. N. Karle, S. Mahmud, R. K. Sakai, R. M. Fitzgerald, V. R. Morris, and W. R. Stockwell, “Investigation of the Successive Ozone Episodes in the El Paso–Juarez Region in the Summer of 2017,” *Atmosphere (Basel).*, vol. 11, no. 5, p. 532, May 2020.

[18] R. Draxler, B. Stunder, G. Rolph, A. Stein, and A. Taylor, “HYSPLIT4 USER’s Guide Overview (S000) HYSPLIT4 USER’s GUIDE Version 4-Last Revision: February 2018 1.”

# Appendix

**Mean:** The sum of a list of numbers, divided by the number of elements in the list.

**Mean Absolute Error (MAE):** The mean absolute error of an estimator of a parameter is the expected value of the absolute of the difference between the estimator and the parameter. In symbols, if X is an estimator of the parameter t, then

$MAE(X) = |E((X-t)^2)|$

**Median:** Denoting or relating to a value or quantity lying at the midpoint of a frequency distribution of observed values or quantities, such that there is an equal probability of falling above or below it.

**Kurtosis:** In probability theory and statistics, kurtosis is a measure of the "tailedness" of the probability distribution of a real-valued random variable.

**Skewness:** Skewness is a measure of the asymmetry of the probability distribution of a real-valued random variable about its mean. The skewness value can be positive or negative, or undefined.

**Variance:** The variance of a list is the square of the standard deviation of the list, that is, the average of the squares of the deviations of the numbers in the list from their mean. The variance of a random variable X, Var(X), is the expected value of the squared difference between the variable and its expected value:

$Var(X) = E((X - E(X))2)$.

**Root Mean Square Error:**

The RMSE is the square-root of the mean squared error (MSE) of the estimator.

$Root\ Mean\ Square\ Error = \sqrt{\sum_1^n \frac{(M-0)^2}{n}}$

Where M = Hysplit and O = Ceilometer

**Correlation Coefficient:**

Correlation coefficients are used in statistics to measure how strong a relationship is between two variables. There are several types of correlation coefficient: Pearson's correlation (also called Pearson's R) is a correlation coefficient commonly used in linear regression. We also used Pearson correlation coefficient in this report. So, the mathematical equation of Correlation coefficient as follows:

Correlation = $\frac{1}{n-1}\sum_1^n((O-\bar{O})/\sigma_o) \times (M-\bar{M})/\sigma_m$ )

Where M = Hysplit and O = Ceilometer, $\sigma$ = standard deviation

**Index of Agreement (unit less)**

The Index of Agreement developed by Willmott (1981) as a standardized measure of the degree of model prediction error and varies between 0 and 1. A value of 1 indicates a perfect match, and 0 indicates no agreement at all

Index of Agreement= $(1 - [\ (\sum_1^n(O-M)^2)\ /(\sum_1^n(|M-\bar{O}|) + |O-\bar{O}|^2)\ ]\ )$

Where M = Hysplit and O = Ceilometer